

# A Detailed Analysis of Flavour-changing Decays of Top Quarks as a Probe of New Physics at the LHC

*Debjyoti Bardhan*<sup>a,1</sup>, *Gautam Bhattacharyya*<sup>b,2</sup>, *Diptimoy Ghosh*<sup>c,3</sup>,  
*Monalisa Patra*<sup>d,4</sup> and *Sreerup Raychaudhuri*<sup>a,5</sup>

<sup>a</sup> Department of Theoretical Physics, Tata Institute of Fundamental Research,  
 1 Homi Bhabha Road, Mumbai 400005, India.

<sup>b</sup> Saha Institute of Nuclear Physics,  
 1/AF Bidhan Nagar, Kolkata 700064, India.

<sup>c</sup> Department of Particle Physics and Astrophysics, Weizmann Institute of Science,  
 Rehovot 76100, Israel.

<sup>d</sup> Rudjer Boskovic Institute, Division of Theoretical Physics,  
 Bijeni cka 54, HR-10000 Zagreb, Croatia.

## Abstract

If the LHC should fail to observe direct signals for new physics, it may become necessary to look for new physics effects in rare events such as flavour-changing decays of the top quark, which, in the Standard Model, are predicted to be too small to be observed. We set up the theoretical framework in which experimentally accessible results can be expected in models of new physics, and go on to discuss two models of supersymmetry – one with conserved  $R$ -parity, and one without  $R$ -parity – to illustrate how the flavour-changing signals are predicted in these models. In the latter case, there is a distinct possibility of detecting the rare decay  $t \rightarrow c + Z^0$  at the LHC. We also present a detailed set of very general formulae which can be used to make similar calculations in diverse models of new physics.

Pacs Nos: 11.30.Pb, 12.20.Ds, 12.60.-i, 14.65.Ha

---

<sup>1</sup> debjyoti@theory.tifr.res.in

<sup>2</sup> gautam.bhattacharyya@saha.ac.in

<sup>3</sup> diptimoy.ghosh@weizmann.ac.il

<sup>4</sup> mpatra@irb.hr

<sup>5</sup> sreerup@theory.tifr.res.in

# 1 Introduction : FCNC portal to new physics

The Run-I of the CERN Large Hadron Collider (LHC) has already led to the discovery of the long-sought Higgs boson [1], and, probably, the elusive pentaquark [2] as well. As the LHC has now commenced its crucial Run-II, the eyes of the whole world are focussed on CERN with the hope that there will be startling discoveries at this machine, which is designed to probe an energy regime hitherto inaccessible to terrestrial experiments. Indeed, some hints of this kind [3] have already created considerable excitement [4].

It is natural, at this stage, to inquire into the different possibilities, and ask how sure we are that any such discovery will be made. Unfortunately, it turns out that there is no really *compelling* reason to expect a new discovery at the LHC Run-2 – though it is certainly possible. This is because the whole range of experiments done at low, intermediate and the highest available energies are beautifully explained by the Standard Model (SM), a portmanteau theory which incorporates three or four disparate ideas and holds them together with a set of phenomenological parameters. Ad hoc as it may seem, this clumsy model has been remarkably successful – perhaps too successful – in explaining every known measurement, sometimes to four or five decimal places. Ironically, it is the LHC, in its Run-I, which has put the strongest stamp of authenticity on the SM by discovering the missing Higgs boson, measuring its properties to be consistent with the SM predictions and, at the same time, failing to find any significant deviations from the SM in a host of highly precise measurements. The discovery of the pentaquark is as consistent with the SM as any of the other results.

When we extend our consideration beyond purely terrestrial experiments to the cosmos at large, we immediately realise that the SM fails to explain several outstanding problems. These include the problems of dark matter [5], dark energy [6] and ultra-high energy cosmic rays above the Greisen-Zatsepin-Kuzmin (GZK) bound [7]. In particular, if the Earth is immersed in a distribution of dark matter, as appears to be the case, there must be some way to detect this fact. This is a subject of intense experimental investigation around the world [8–11]. It is also hoped that discoveries at the LHC could shed light on the problem of dark matter, which, if particulate, would appear in a collision as missing energy and momentum. Some of the theoretical deficiencies of the SM are addressed in theories which extend or go beyond it to postulate new structures and symmetries at higher energy scales – these are generically referred to as ‘new physics’. A few of these models also have dark matter candidates. The great hope of the present moment is that unambiguous signals for such new physics will be discovered in Run-II of the LHC.

There are two ways in which new physics can be discovered at the LHC. The first – and simplest – way is to ‘directly’ discover evidence for new particles, which could appear either as resonances or pairs, or be produced in association with SM particles. Denoting a ‘new’ particle by  $P$ , the simplest tree-level processes are:

$$pp \rightarrow P \text{ or } P^* \rightarrow X + Y \qquad pp \rightarrow P + \bar{P} \qquad pp \rightarrow P + X \qquad (1.1)$$

where  $X$  and  $Y$  stand for SM particles. Taking into account the fact that a ‘new’ particle will either decay into SM particles, or, if it is a component of dark matter, lead to missing energy and momentum signals, one can enumerate the possible final states and then analyse the LHC data to see if there is any evidence for such signals. An answer in the affirmative would, of course, be very exciting, and hopefully this is what will occur in the near future.

While we have no wish to pour cold water on optimistic predictions of the above nature, one cannot ignore the possibility that the mass of the ‘new’ particle(s) may very well lie outside the kinematic reach of the LHC. Curiously, the last undiscovered particle for whose mass we had a theoretical *upper* bound was the Higgs boson, and, in fact, the LHC was designed to find it within the entire range of possibilities <sup>1</sup>. For ‘new’ particles, however, all that we have are experimental lower bounds [12–18] – which are more a measure of the failure of experimental searches than a reflection of any physical principle. Thus, future failures to find any signals of new physics can always be explained away as due to higher and higher masses of the ‘new’ particle(s). In such a case, there would arise a serious problem in falsifying the theories in question.

There does, however, exist an escape route, and this happens when we consider the quantum effects of the ‘new’ physics. When we consider, say, tree-level decays of a SM particle which have been mediated by a heavy ‘new’ particle  $P$ , e.g. a decay of the form

$$Q \rightarrow X + P^* \rightarrow X + Y + Z$$

where the  $Q, X, Y, Z$  are all SM particles, then these are generally subject to a propagator suppression by a factor  $M_Q^2/M_P^2$  — which can be quite severe if  $M_Q \ll M_P$ , which is usually the case. However, if, instead of a decaying particle, we have a scattering experiment

$$Q + \bar{X} \rightarrow P^* \rightarrow Y + Z$$

conducted at an energy  $\sqrt{s} < M_P$ , the corresponding ‘suppression’ factor will be  $s/M_P^2$  — which may be orders of magnitude larger than the earlier factor since it is possible to make  $\sqrt{s} \gg M_Q$ . Even then, it could very well be that  $M_P$  is so large that even with the effective values  $\sqrt{s} \sim 1 - 2$  TeV available at the LHC, the propagator suppression will still make the process unobservable at the LHC, especially if there are large backgrounds arising from purely SM production of  $Y + Z$  final states.

What we need to find, therefore, is a process which, for some reason, is severely suppressed in the SM, but, for some equally valid reason, is not so severely suppressed in the new physics sector. Here we are lucky, for there exists a whole class of SM processes which are severely suppressed by the unitarity constraints of the Cabibbo-Kobayashi-Maskawa (CKM) matrix. These are the so-called flavour-changing neutral current (FCNC) processes involving at least two generations of fermions in the initial and final states, and all the generations in the loop.

---

<sup>1</sup>As it happens, the Higgs boson was found rather soon, and that too, near its lower mass bound rather than the upper.

Though this suppression, commonly called the Glashow-Iliopoulos-Maiani (GIM) mechanism [19], is described in any textbook on the SM [20], it is worthwhile to take a quick look at the main argument, since it will form the crux of some of the discussions in this article. The idea is that if we have an initial quark flavour  $q$  and a final quark flavour  $q'$  of the same charge, and the only flavour-changing couplings we have are due to the charged currents coupling to the  $W$ -boson, then the transition amplitude must have the form

$$M_{qq'} = \sum_{i=1}^3 V_{qi}^* V_{q'i} A(x_i, M_W) = \sum_{i=1}^3 \lambda_i A(x_i, M_W) \quad (1.2)$$

where  $x_i \equiv m_i^2/M_W^2$  carries the generation dependence and  $M_W$  sets the mass scale for charged-current interactions. Moreover,  $\lambda_i = V_{qi}^* V_{q'i}$ , and the unitarity of the CKM matrix ensures that if  $q \neq q'$ , then  $\sum_i \lambda_i = 0$ . Obviously, we can expand the  $A(x_i, M_W)$  in a Maclaurin series

$$A(x_i, M_W) = A_0(M_W) + x_i A'_i(M_W) + \frac{1}{2} x_i^2 A''_i(M_W) + \dots \quad (1.3)$$

where

$$A_0(M_W) = A(0, M_W), \quad A'_i(M_W) = \left[ \frac{\partial A}{\partial x_i} \right]_{x_i=0}, \quad A''_i(M_W) = \left[ \frac{\partial^2 A}{\partial x_i^2} \right]_{x_i=0}$$

and so on, where we make the assumption that  $x_i \ll 1$ . The leading term in  $M_{qq'}$  cancels out and what is left is therefore suppressed by  $x_i$ . Obviously, this will work nicely if we take the quarks  $q, q'$  to have charge  $+2/3$ , for then we automatically get a suppression in the probability by  $x_b = (m_b/M_W)^2 \sim 10^{-3}$ , or by even smaller factors for the other generations<sup>2</sup>.

If we now assume that the ‘new’ particle(s)  $P$  make(s) contributions of the form

$$M_{qq'}^{\text{new}} = \sum_{i=1}^3 \lambda_i \eta_i \tilde{A}(y_i, M_P) \quad (1.4)$$

where the  $y_i \equiv m_i^2/M_P^2$  are similar to the  $x_i$  and the  $\eta_i$  are arbitrary flavour-dependent factors, then we immediately see that the leading order contribution stays, for  $\sum_i \lambda_i \eta_i \neq 0$ . Such contributions are unaffected by the GIM suppression, and, therefore, could, in principle, be three orders of magnitude larger than the SM contributions.

The beauty of the above argument lies in the fact that in the above process, all that we need to observe is the transition of a  $t$  quark to a quark of a different flavour but the same charge, i.e. a  $u$  or a  $c$ . There is no requirement to produce heavy ‘new’ particles on-shell. Thus, in the disappointing situation that all direct searches for ‘new’ physics at the LHC fail, one can fall back upon GIM-suppressed processes as a portal through which we can still peer into that otherwise-inaccessible new world.

The major loop-induced FCNC processes involving the top quark which have been studied in the literature are:

---

<sup>2</sup>For FCNC decays of the  $b$  quark, we need to expand about  $x_t$  rather than  $x_i = 0$ , since  $x_t > 1$ . However, this article focusses only on decays of the  $t$  quark.

1. the decays  $t \rightarrow q + S$ , where  $q = u, c$  and  $S$  is a scalar – either the Higgs boson  $H^0$  or its counterpart(s) in new physics models; and
2. the decays  $t \rightarrow q + V$ , where  $q = u, c$  and  $V$  is a vector gauge boson – which can be a photon or a gluon or a  $Z^0$ -boson or any counterpart(s) in new physics models;

In the SM, we have well known results for the branching ratio

$$B(t \rightarrow c + H^0) \sim 10^{-15} \qquad B(t \rightarrow c + Z^0) \sim 10^{-13} \qquad (1.5)$$

These are many, many orders of magnitude too small to be measured at Run-2 of the LHC, where estimates are that at best branching ratios at the level of  $10^{-5}$  may become accessible when enough data are eventually collected (see Figure 8). There have been several predictions in the literature that new physics processes could provide the necessary enhancement and predict branching ratios at this level. The purpose of this article is to investigate these claims critically and try to determine the model requirements which could lead to an actual discovery of new physics at the LHC through the top quark FCNC portal.

Before proceeding further, we address the question of the rare decay  $t \rightarrow q + \gamma$ , which is bound to happen if its counterpart  $t \rightarrow q + Z$  is possible. Electromagnetic gauge invariance demands that  $t \rightarrow q + \gamma$  be mediated only by the magnetic dipole moment operator [21]. This process, however, turns out to be less interesting for two reasons. In the first place, one loop contributions to  $t \rightarrow q + \gamma$  are suppressed by about an order of magnitude compared to the corresponding process with a final-state  $Z$ . This turns out to be essentially because the coupling of a photon to  $d_i$ -quark pairs is suppressed by their fractional charge of  $-1/3$ . A more serious hurdle is that experimental measurement of the rare decay  $t \rightarrow q + \gamma$  is plagued with much larger backgrounds because of the ease with which photons can be radiated at tree-level. For this reason, experiments [22] can only achieve an accuracy for  $t \rightarrow c + \gamma$  which is an order of magnitude poorer than that for  $t \rightarrow c + Z$ . Taken together, these two factors ensure that the search for  $t \rightarrow q + Z$  should clearly take precedence<sup>3</sup> over that for  $t \rightarrow q + \gamma$ . Hence, we do not discuss the latter process further. For similar reasons, we do not consider the process  $t \rightarrow q + g$  either.

This article is organised as follows. In the following section, we consider generic FCNC decays of the top quark [23], taking a toy model, and determine the conditions required to have maximal contributions to an FCNC process like  $t \rightarrow c + B$ , where  $B$  is a scalar or a vector boson. As an example we take up, in the next section, a supersymmetric model which is quite likely to evade direct searches at the LHC. The following section extends this to the case of a supersymmetric model with  $R$ -parity violation, which relies on non-CKM sources of FCNC. Finally we present a summary of our results and a conclusion. In the interests of smooth reading, most of the more cumbersome formulae are relegated to the Appendix.

---

<sup>3</sup>As we will see in the final section, the process  $t \rightarrow c + Z$  is somewhat marginal at the LHC. This makes the case hopeless for  $t \rightarrow c + \gamma$ . Replacing  $c$  by  $u$  leads to even smaller decay widths.

## 2 Generic FCNC Decays of the top quark in a toy model

In this section, we investigate a toy model which could be taken as a prototype for FCNC decays for the top quark. Let us assume there are a pair of charged scalars  $\omega^\pm$  with couplings of the form

$$\begin{aligned} \mathcal{L}_{\text{int}} &= \xi \omega^+ \omega^- H \\ &+ \sum_{i,j=1}^3 (\eta V_{ij} \bar{u}_{iL} d_{jR} \omega^+ + \text{H.c.}) \end{aligned} \quad (2.1)$$

where  $H$  is the SM Higgs boson and  $\xi, \eta$  are unknown couplings. These  $\omega^\pm$ 's are rather like scalar versions of the  $W^\pm$ -bosons. The choice of scalars

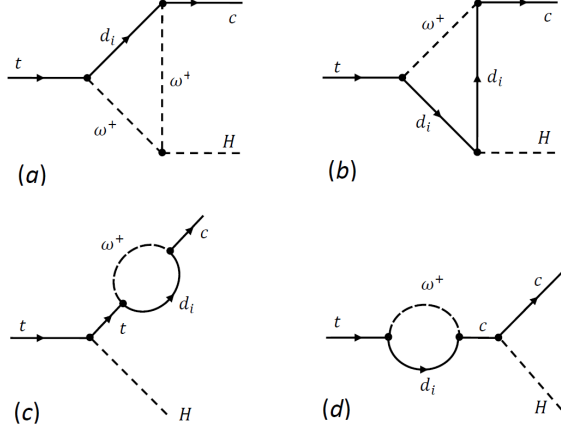


Figure 1: Set of Feynman Diagrams leading to the decay  $t \rightarrow c + H$  in our toy model.

makes the calculation simple and sidesteps complications due to gauge choice which arise with the  $W^\pm$ . For this part we stay within the minimal flavour violation (MFV) paradigm (see for example, Ref. [24]) insofar as the only flavour-changing effects happen through the ‘CKM’ matrix elements  $V_{ij}$ .

Let us now consider the decay  $t \rightarrow c + H$  as predicted in this model. Using the SM Yukawa couplings for the  $H$ -boson and Feynman rules for  $\omega^\pm$  (which can quite easily be read off from the above Lagrangian), we obtain four diagrams, shown in Figure 1. It is then a straightforward matter to calculate the helicity amplitudes for the decay  $t \rightarrow c + H$ . In terms of the  $\lambda_i = V_{ti}^* V_{ci}$ , these can be written in the generic form

$$\mathcal{M}_{h_c h_t} = \sum_{i=1}^3 \lambda_i \mathcal{A}_i(h_c, h_t) \quad (2.2)$$

where  $h_c$  and  $h_t$  are the helicities of the  $c$  and the  $t$  quarks respectively, and  $\lambda_1 + \lambda_2 + \lambda_3 = 0$  by unitarity of the CKM-like matrix  $V$ . Explicit expressions for these in terms of Passarino-Veltman functions [25] are given in Appendix A. We require to calculate only two non-vanishing amplitudes

$$(a) \quad \mathcal{M}_{++} = \sum_{i=1}^3 \lambda_i \mathcal{A}_i(+1, +1) \quad (b) \quad \mathcal{M}_{--} = \sum_{i=1}^3 \lambda_i \mathcal{A}_i(-1, -1) \quad (2.3)$$

which become analogues of the SM amplitudes if we put  $\xi = gM_W$  and  $\eta = g/\sqrt{2}$ . To calculate the branching ratio, we note that the squared and spin-summed/averaged matrix element, in terms of the helicity amplitudes of Eqn. (2.3), is

$$\overline{|\mathcal{M}|^2} = \frac{1}{2} \left[ |\mathcal{M}_{++}|^2 + |\mathcal{M}_{--}|^2 \right] \quad (2.4)$$

The partial width can now be written as

$$\Gamma(t \rightarrow c + H) = \frac{1}{16\pi m_t} \left(1 - \frac{M_H^2}{m_t^2}\right) \overline{|\mathcal{M}|^2} \quad (2.5)$$

and (if necessary) the branching ratio is easily obtained by dividing by the total decay width  $\Gamma_t \simeq 1.29$  GeV.

At this point we pause to make a rough numerical estimate of the above quantities. As may be seen from Eqn. (2.5), the helicity amplitudes must have a mass dimension +1. Since these arise from one-loop computations, and if  $M_\omega$  is close to  $M_W$ , a crude approximation for the amplitude factor will be

$$\overline{|\mathcal{M}|^2} \approx \left(\frac{m_t}{16\pi^2}\right)^2 \quad (2.6)$$

Substituting this into Eqn. (2.5), leads to a numerical estimate

$$\Gamma(t \rightarrow c + H) \approx 5.9 \times 10^{-5} \text{ GeV} \quad (2.7)$$

which is ten orders of magnitude larger than the SM prediction.

It is natural to ask why the SM prediction is so much smaller than what one would naively have expected. The answer is that the SM amplitude is suppressed by a combination of three different effects, each reducing the amplitude by a few orders of magnitude. These are explained below.

1. The first of these suppression effects is, of course, the GIM cancellation, which we have already shown to lead to suppression by a factor

$$\left[\frac{m_b(m_t)}{M_W}\right]^2 = \left[\frac{2.6 \text{ GeV}}{80.4 \text{ GeV}}\right]^2 \simeq 1.0 \times 10^{-3}$$

in the decay amplitude.

2. In this toy model, we have taken the flavour-violating coupling to be  $\eta V_{ij}$  (or  $\eta_i V_{ij}$ ), where the flavour-violation arises exactly as in the SM – from the off-diagonal terms in the ‘CKM’ matrix. This makes it a model with *minimal* flavour violation (MFV). Since the CKM matrix exhibits a strong hierarchy as we move away from the diagonal, this results in a further suppression in all MFV models – which may not hold in a new physics model which deviates from the MFV paradigm. To make matters explicit, we have  $\lambda_i = V_{2i}V_{3i}^*$  for  $i = 1, 2, 3$ . If we choose the  $\eta_i$  as in Eqn. (2.10), the only relevant one is  $\lambda_3 = V_{23}V_{33}^* \simeq V_{23}$  since  $V_{33} \simeq 1$ . Now,  $|V_{23}| \approx 0.04$  [26]. This gives us a suppression by two orders of magnitude.

There is a subtle issue, however. If we consider the flavour mixing in a model of new physics to be arbitrary and of unknown origin, it is perfectly fine to set  $\lambda_3 = 1$  and thereby obtain an enhancement factor of  $1/0.04 = 25$ . In fact, this is what we shall assume in Section 5 of this paper. However, in a large class of non-MFV models, flavour

mixing does arise from mixing effects of the quarks, and there exists some *unitary* matrix  $V'_{ij}$  which is not the measured CKM matrix. To get a maximal value of  $V'_{23}$ , we take

$$V' = \begin{pmatrix} 1 & 0 & 0 \\ 0 & \cos \theta & \sin \theta \\ 0 & -\sin \theta & \cos \theta \end{pmatrix} \quad (2.8)$$

so that  $\lambda'_3 = \sin \theta \cos \theta = \frac{1}{2} \sin 2\theta$ . Obviously, the maximum occurs for  $\theta = \pi/4$  and the corresponding value of  $\lambda_3$  is 0.5 — an enhancement by a factor of 12.5 instead of 25. Thus, what we can achieve by abandoning the MFV paradigm is an enhancement by half of what we would get by discarding the CKM-type mechanism altogether.

3. Finally, in a model of new physics, there is always the possibility that the actual couplings may be enhanced over the SM ones. To see this, we put<sup>4</sup>  $\xi = M_\omega$  instead of  $gM_W$  and  $\eta_3 = 1$  instead of  $g/\sqrt{2}$ , and recalculate the amplitudes, thereby achieving a modest enhancement by a factor of  $2/g^3 \simeq 7.3$ , assuming that  $M_\omega \simeq M_W$ . This means that the ‘SM’ amplitude is suppressed by a factor  $1/7.3 \simeq 0.14$ .

If we now combine the three effects, then the amplitude will have an overall suppression factor

$$(1.0 \times 10^{-3}) \times 0.04 \times 0.14 \simeq 5.6 \times 10^{-6} \quad (2.9)$$

Multiplying the amplitude by this factor and squaring leads to a suppression of the estimated partial decay width in Eqn. (2.7) by ten orders of magnitude to  $1.85 \times 10^{-15}$  — which is in the right ballpark.

Now that we have a clear understanding of the nature of the FCNC suppression in the SM (or a SM-like model), we can remove these effects one by one to see how much the amplitude can be enhanced in a new physics model. In order to predict really significant deviations from the SM branching ratio any new physics model requires to meet the following conditions:

- A. Frustration of the GIM cancellation.
- B. Non-MFV pattern of flavour mixing.
- C. Enhanced couplings.

To illustrate these in a concrete manner, we perform detailed numerical computations of the helicity amplitudes of Eqn. (2.3) using the formulae of Appendix A.1. The loop integrals in these formulae are evaluated using the well-known package FF [27], and our numerical results are given in Figure 2.

The ‘normal case’, when the couplings in Eqn. (2.2) are exactly like those in the SM corresponds to the black curves marked ‘SM’ in Figure 2. The dots correspond to the values  $M_\omega =$

---

<sup>4</sup>Strictly speaking, the couplings can be taken up to  $\sqrt{4\pi} \approx 3.5$ , but then we will have to worry about higher-order effects.



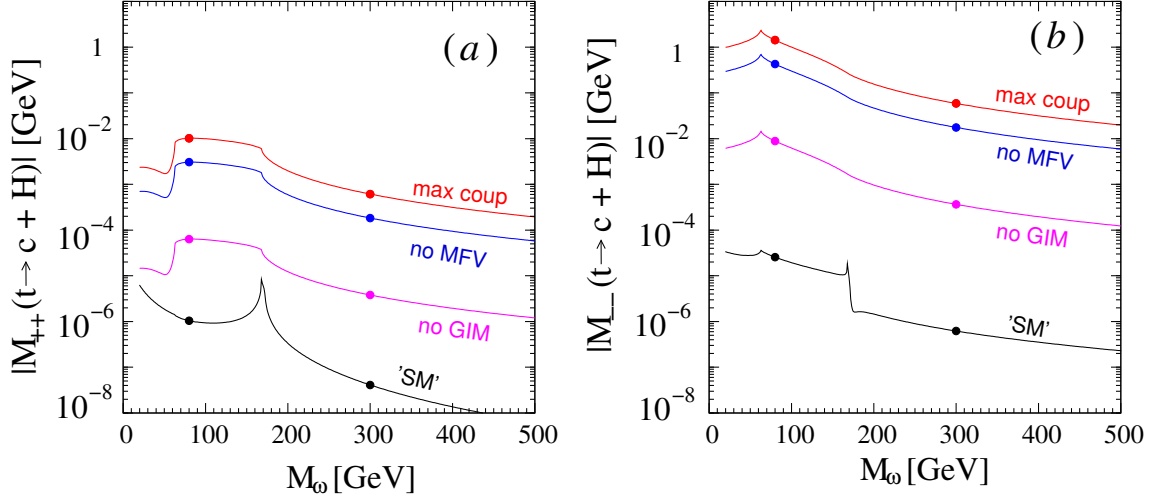


Figure 2: The two non-vanishing helicity amplitudes for the decay  $t \rightarrow c + H$ , as calculated in our toy model as a function of the mass  $M_\omega$  of the scalar field  $\omega$ . The legends next to each curve are explained in the text. The small solid circles indicate the values  $M_\omega = 80, 300$  GeV used in Table 1.

80, 300 GeV (see Table 1). These amplitudes are suppressed due to a combination of all the three effects described above<sup>5</sup> (see below).

We can disrupt the GIM cancellation partially or wholly by replacing the coupling constant  $\eta$  in Eqn. (2.2) by a generation-dependent factor  $\eta_i$ . The maximal effect will be obtained if, for example, we consider

$$\eta_1 = \eta_2 = 0 \quad \eta_3 = \frac{g}{\sqrt{2}} \quad (2.10)$$

The corresponding numerical curves are shown in Figure 2 in magenta, and labelled ‘no GIM’. It is immediately obvious that the amplitude increases by 2 – 3 orders of magnitude, exactly as expected.

Next, we eschew MFV and consider the case  $\lambda_3 = 1$ . This gives an enhancement by a factor of 25. The blue lines marked ‘no MFV’ in Figure 2 represent the case in question. Finally, we set the couplings to the maximal values  $\xi = M_\omega$  and  $\eta_3 = 1$  and obtain a further enhancement illustrated by the curves shown in red in Figure 2 and marked ‘max coup’. This, as predicted, is enhanced by one order of magnitude.

If we consider the combination of all these effects, as we have done in Figure 2, we get an enhancement factor around  $2.04 \times 10^4$  ( $5.43 \times 10^4$ ) for  $|\mathcal{M}_{++}|$  ( $|\mathcal{M}_{--}|$ ) taking  $M_\omega = 80$  GeV. This is a more modest enhancement than estimated in Eqn. (2.9), but that is not surprising, given the fact that the earlier estimate was made under a very crude approximation to the decay amplitude. The actual enhancements available are made explicit in Table 1, where we

<sup>5</sup>It may be seen in Appendix A.1 that the form factors  $F_{1i}^{(b)}$  and  $F_{2i}^{(b)}$  would violate the GIM cancellation. This is indeed true, and arises from the helicity-flipping nature of the scalar  $\omega$  interaction. However, the contributions of  $F_{1i}^{(b)}$  and  $F_{2i}^{(b)}$  are very small, and hence, for all practical purposes, may be ignored in the numerical evaluation.

list the partial widths for  $t \rightarrow c + H$  in the toy model for  $M_\omega = 80, 300$  GeV, for the SM-like case as well as with the three suppression mechanisms successively disabled.

$M_\omega$	‘SM’	$\oplus$ no GIM	$\oplus$ no MFV	$\oplus$ max coup
80	$1.81 \times 10^{-14}$	$2.04 \times 10^{-9}$	$4.74 \times 10^{-6}$	$5.31 \times 10^{-5}$
300	$4.31 \times 10^{-18}$	$5.12 \times 10^{-11}$	$1.19 \times 10^{-7}$	$1.33 \times 10^{-6}$

Table 1: Partial decay widths for the decay  $t \rightarrow c + H$  in the toy model, with successive application of the three enhancement conditions. All numerical values are in units of GeV.

Another process of interest at the LHC is the decay  $t \rightarrow c + Z$ . The diagrams for this are identical to those in Figure 1, except that the scalar  $H$  line must be replaced by a wiggly  $Z$  line. We do not exhibit these diagrams in the interest of brevity, though we keep the same configuration and numbering. In this case, the computation is rendered a little more complicated because of the vector nature of the  $Z$  boson. The toy Lagrangian will be

$$\mathcal{L}_{\text{int}} = i\xi\omega^+\overleftrightarrow{\partial}_\mu\omega^-Z^\mu + \sum_{i,j=1}^3 (\eta V_{ij} \bar{u}_{iL} d_{jR} \omega^+ + \text{H.c.}) \quad (2.11)$$

where  $\xi, \eta$  are unknown couplings, as before. We can now compute the partial width for the decay  $t \rightarrow c + Z$ . The Feynman amplitude will assume the form

$$\mathcal{M}_{h_ch_t}^{(h_Z)} = \sum_{i=1}^3 \lambda_i \mathcal{A}_i(h_Z; h_c, h_t) \quad (2.12)$$

where the sum over  $h_Z$  runs over the longitudinal polarisation  $\varepsilon_L = \varepsilon(h_Z)|_{h_Z=0}$  and the transverse polarisations  $\varepsilon_T^\pm = \varepsilon(h_Z)|_{h_Z=\pm 1}$ . The only non-vanishing amplitudes are

$$\begin{aligned} (a) \quad \mathcal{M}_{-+}^{(+)} &= \sum_{i=1}^3 \lambda_i \mathcal{A}_i(+1; -1, +1) & (b) \quad \mathcal{M}_{+-}^{(-)} &= \sum_{i=1}^3 \lambda_i \mathcal{A}_i(-1; +1, -1) \\ (c) \quad \mathcal{M}_{++}^{(0)} &= \sum_{i=1}^3 \lambda_i \mathcal{A}_i(0; +1, +1) & (d) \quad \mathcal{M}_{--}^{(0)} &= \sum_{i=1}^3 \lambda_i \mathcal{A}_i(0; -1, -1) \end{aligned} \quad (2.13)$$

and these may be regarded as ‘SM’ amplitudes, if we take  $\xi = gM_\omega$  and  $\eta = g/\sqrt{2}$  as before. Once again, we plot these amplitudes in Figure 3 as a function of  $M_\omega$  and relegate the detailed formulae to Appendix A.

In Figure 3, the four panels marked (a)–(d) correspond to the four amplitudes (a)–(d) indicated in Eqn. (2.13). The colour coding and conventions for this figure are identical to those in Figure 2. It is not difficult to see that once again, we get enhancement factors for these amplitudes which are very similar to those for the  $t \rightarrow c + H$  case, when we successively (a) relax the GIM cancellation, (b) abandon the minimal flavour-violation paradigm and (c) enhance the couplings. This enables us to predict much larger partial widths, as shown in Table 2.

For this calculation, we require the squared and spin-summed/averaged matrix element, which is

$$\overline{|\mathcal{M}|^2} = \frac{1}{2} \left[ \left| \mathcal{M}_{-+}^{(+)} \right|^2 + \left| \mathcal{M}_{+-}^{(-)} \right|^2 + \left| \mathcal{M}_{++}^{(0)} \right|^2 + \left| \mathcal{M}_{--}^{(0)} \right|^2 \right] \quad (2.14)$$

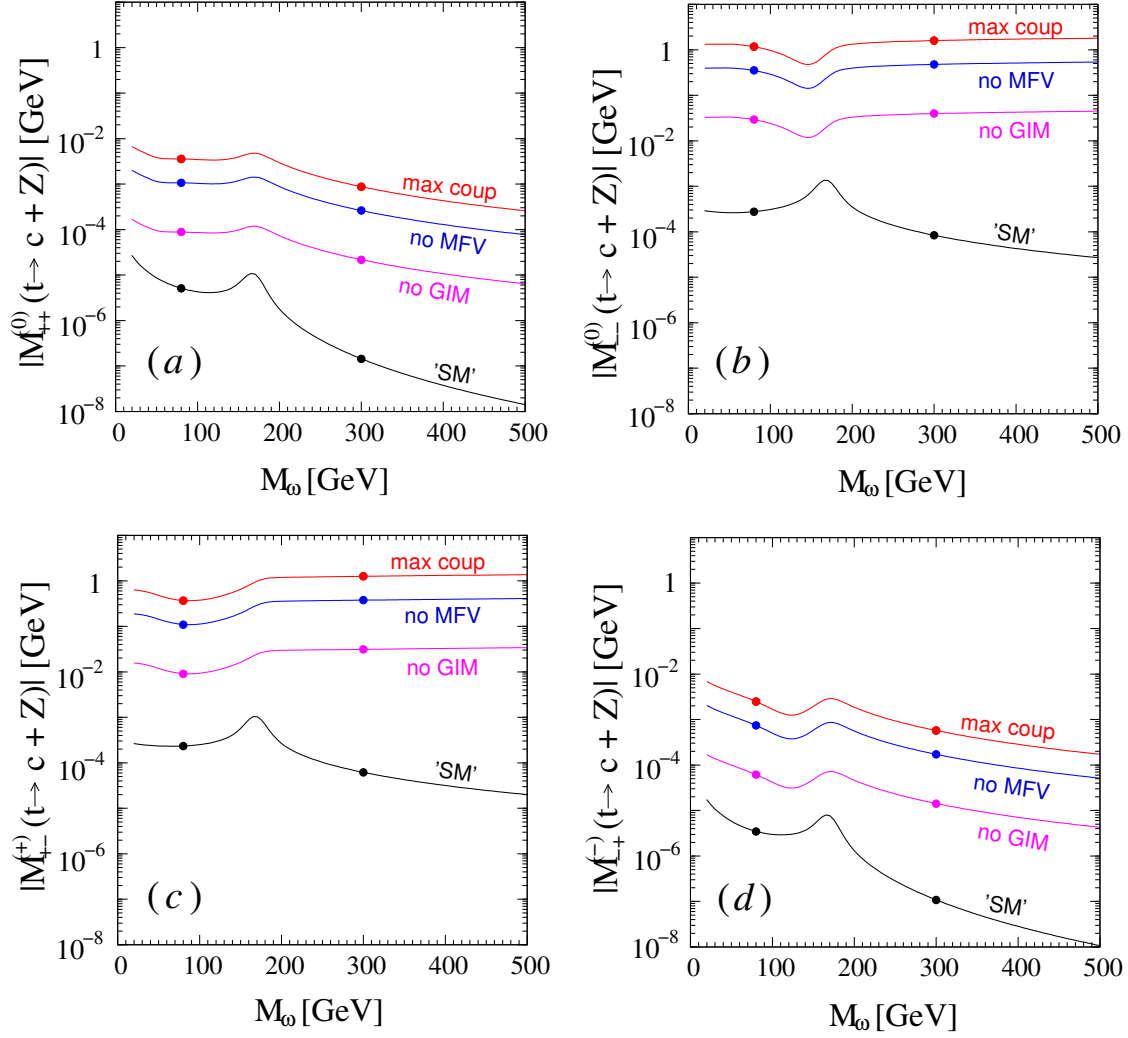


Figure 3: Helicity amplitudes for the decay  $t \rightarrow c + Z$  in our toy model. The notations and conventions follow those of Figure 2.

in terms of the helicity amplitudes of Eqn. (2.13). The partial width can now be written

$$\Gamma(t \rightarrow c + Z) = \frac{1}{16\pi m_t} \left( 1 - \frac{M_Z^2}{m_t^2} \right) |\overline{\mathcal{M}}|^2 \quad (2.15)$$

as before, with  $M_Z$  replacing  $M_H$ . In this case, of course, the partial width in more enhanced cases far exceeds the measured top quark width of 1.29 GeV, but this is not a serious matter, since this is, after all, a toy model. The enhancement in this case due to, successively, frustration of the GIM mechanism, saturation of the flavour off-diagonal terms and saturation of the coupling constant, have the same magnitudes as in the case of the top decaying through a scalar  $H$  boson. We may, therefore, apply the same insights to both cases.

In general, the summed amplitudes for the decay  $t \rightarrow c + Z^0$  are about an order of magnitude larger than the similar summed amplitudes for the decay  $t \rightarrow c + H^0$ . This is principally because a major contribution comes from the diagram with a  $\omega^+\omega^-Z$  or  $\omega^+\omega^-Z$  vertex, which are proportional to  $g \cos \theta_W$  and  $\lambda$  respectively, other factors being equal or similar. Since the

measurement of the Higgs boson mass tells us that  $\lambda \simeq 0.12$  it follows that  $g \cos \theta_W / \lambda \simeq 5$ . A further factor of around 2 is obtained because of the four non-vanishing helicity amplitudes for  $t \rightarrow c + Z^0$  as opposed to the two obtained for  $t \rightarrow c + H^0$ . Thus, we get an enhancement of around 10, which becomes around  $10^2$  when we consider the partial decay width. As this is a generic feature of the SM and most new physics models, it is obvious that the decay mode  $t \rightarrow c + Z^0$  is more promising for discovery than the  $t \rightarrow c + H^0$  mode.

$M_\omega$	'SM'	no GIM	no MFV	max coup
80	$4.23 \times 10^{-11}$	$3.55 \times 10^{-4}$	$5.15 \times 10^{-2}$	0.58
300	$8.16 \times 10^{-12}$	$8.32 \times 10^{-3}$	1.21	13.5

Table 2: Partial widths for the decay  $t \rightarrow c + Z$  in the toy model, with successive application (L to R) of the three enhancement conditions. All numerical values are in units of GeV.

### 3 FCNC decays of the top quark in the SM

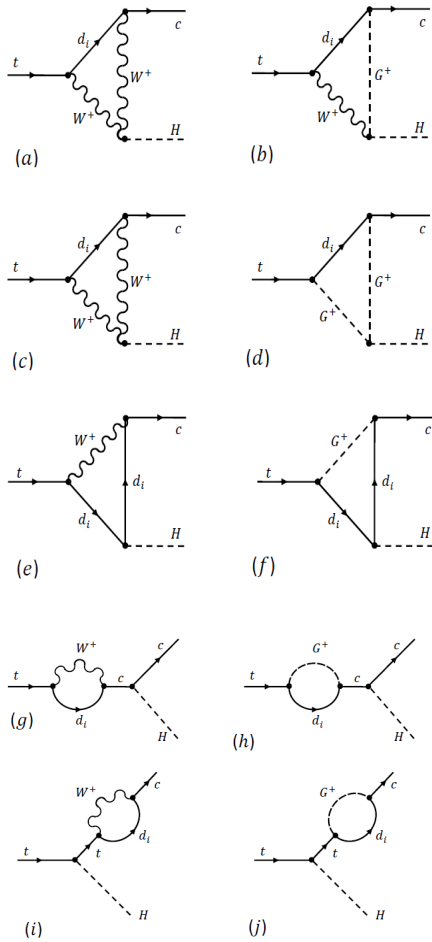


Figure 4: Feynman Diagrams leading to the decay  $t \rightarrow c + H$  in the SM.

We are now in a position to explore the decays  $t \rightarrow c + H$  and  $t \rightarrow c + Z$  in the Standard Model, using insights from the toy model in the previous section. We start with  $t \rightarrow c + H$ . This time, of course, we have to take into account the exchange of the weak gauge bosons  $W^\pm$  in the loops, and this requires a choice of gauge in which to work. For loop diagrams, it is convenient to choose the 'tHooft-Feynman gauge, since that keeps the ultraviolet divergences at a manageable level. Of course, this comes at the cost of having extra diagrams with unphysical Higgs bosons, and hence, in the SM, the four diagram topologies of Figure 1 become the ten diagrams in Figure 4.

There is a small catch in using the 'tHooft-Feynman gauge, however, and that lies in the appearance of the unphysical Higgs bosons. The couplings of these to quarks depend on the  $d$ -quark masses  $m_i$ , and hence, would apparently lead to frustration of the GIM mechanism. However, these contributions cancel out when all the diagrams are added, as may be expected, since after all, they constitute a gauge artefact. The largest contributions to the amplitudes from individual diagrams (once the singularities are isolated) are of the order of  $10^{-3}$  – this already

contains the suppression of one order due to the electroweak couplings and the factor  $1/16\pi^2$  which appears in all loop diagrams. When all the contributions are summed-up, the GIM cancellation becomes manifest, and there is a reduction by  $\mathcal{O}(m_b^2/m_t^2) \approx 6 \times 10^{-4}$ . This brings down the amplitude to  $\mathcal{O}(10^{-7})$  and hence, its square to  $\mathcal{O}(10^{-14})$ . Another order is lost in kinematics, and thus we get the final result  $5.8 \times 10^{-15}$ , as quoted in Eq. (1.5).

When we turn to the decay  $t \rightarrow c + Z$ , we have a situation similar to the toy model in the previous section. The Feynman diagrams for this can be obtained from those of Fig. 4 by replacing the dashed lines for  $H$  by wiggly lines for  $Z$  and changing the labels accordingly.

We then go on to calculate the helicity amplitudes of Eqn. (2.13) in terms of four form factors, which are given in Appendix B. Most of the arguments given in the case of  $t \rightarrow c + H$  above hold for this case as well, except that the presence of four separate helicity amplitudes leads to a somewhat larger branching ratio,  $\mathcal{O}(10^{-13})$  as quoted in Eq. (1.5).

The most important thing we learn from this exercise has already been stated in the Introduction – the branching ratios for flavour-changing  $t$ -quark decays in the SM are severely suppressed, being far too small to be detected at the LHC, or even the most ambitious futuristic machine that can be conceived. This has the effect of making these decays a very sensitive probe of new physics, for any enhancement to measurable levels must arise from new physics beyond the SM.

## 4 FCNC decays of the top quark in the cMSSM

When we turn to new physics beyond the SM, the very first option must be the one which has captivated the imagination of high energy physicists for the last few decades, viz., supersymmetry (SUSY). The merits and demerits of SUSY have been exhaustively discussed in the literature [28] and do not require to be repeated here. Instead, we focus on the effects of SUSY on the flavour-changing processes  $t \rightarrow c + H$  and  $t \rightarrow c + Z$  which are the subject of this work.

Apart from the fact that every SM field has a supersymmetric partner differing from it in spin by one half, one of the most significant new features of SUSY models is the fact that they all require the existence of two scalar Higgs doublets. Thus, after the electroweak symmetry-breaking, these models contain five physical scalar fields, viz. a pair of charged Higgs bosons  $H^\pm$  and a triplet of neutral Higgs bosons, of which two ( $h^0, H^0$ ) are even under  $CP$  and one ( $A^0$ ) is odd under  $CP$ . The lighter one  $h^0$  of the  $CP$ -even pair can be identified with the near-125 GeV scalar state found at the LHC in recent times. All the other states,  $H^\pm$ ,  $H^0$  and  $A^0$ , are presumed to be heavier, and, in fact, too heavy to have been detected in any experiments so far, including the LHC. As we shall see, it is likely that these states are all heavier than the  $t$ -quark, and hence, the only kinematically-permitted decay will be  $t \rightarrow c + h^0$ , which is analogous to the SM decay.

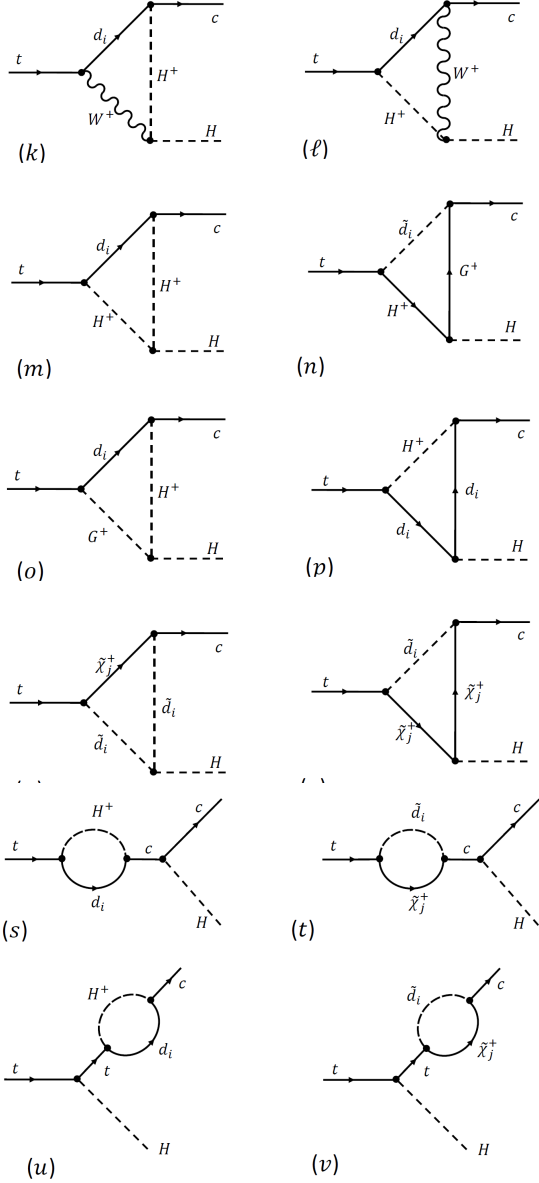


Figure 5: Additional Feynman diagrams leading to the decay  $t \rightarrow c + H$  in the cMSSM.

the SUSY model which is most constrained by experiment. However, since a light Higgs boson  $h^0$  is a common feature of all SUSY models, including the cMSSM, the only features which will be affected will be the couplings and the super-partner masses. As we have seen, this is not too serious a constraint on loop-induced processes, so it is sensible to use the cMSSM as a paradigm case for FCNC processes in SUSY. This is adopted in our work and it fixes the particle content and the vertex factors, though there will be large variations in the latter as the model parameters change.

In the cMSSM, the process  $t \rightarrow c + h^0$  will be mediated by the 10 diagrams of the SM listed earlier in Fig. 4 as well as the 12 additional one-loop diagrams listed in Fig. 5. These diagrams have not only charged Higgs bosons but also charginos and squarks in the loops. The details for

The more important difference from the SM in SUSY models arises because of the contributions of new particles in the loops. The most important of these are the contributions due to the charged Higgs bosons  $H^\pm$ , which have flavour-changing coupling like the  $W$ -boson. However, since these couplings originate from the Yukawa sector, they are proportional to the quark masses and hence will frustrate the GIM mechanism. Then there are contributions where the SM particles are replaced by their SUSY partners, viz. squarks and charginos. Here the flavour-changing effects will arise from the mixing matrices for squarks. In the so-called minimal flavour violation (MFV) models, the squark mixing matrices are aligned with the quark mixing matrix, i.e. the CKM matrix. This is the paradigm we shall adopt in the present study. Non-MFV models have been studied in the literature and we shall have occasion to discuss them in the final section.

Though there are many SUSY versions of the SM and its extensions, the minimal version of this is the so-called constrained minimal supersymmetric SM, or cMSSM [28]. This is the SUSY model which has the minimum number of extra parameters (four parameters and a sign), when compared with all the others. Not surprisingly, it is also

calculating all these 22 diagrams are given in Appendix B, in terms of the usual form factors. Numerical evaluation of these form factors, and hence the branching ratio, is not, however, very simple.

gauginos :	$\tilde{\chi}_1^\pm$	$\tilde{\chi}_2^\pm$	$\tilde{\chi}_1^0$	$\tilde{\chi}_2^0$	$\tilde{\chi}_3^0$	$\tilde{\chi}_4^0$	$\tilde{g}$	
mass bound (GeV) :	94	94	46	63	100	116	520	
squarks :	$\tilde{u}_1$	$\tilde{u}_2$	$\tilde{d}_1$	$\tilde{d}_2$	$\tilde{t}_1$	$\tilde{t}_2$	$\tilde{b}_1$	$\tilde{b}_2$
mass bound (GeV) :	1100	1100	1100	1100	96	96	89	247
gauginos :	$\tilde{e}_1$	$\tilde{e}_2$	$\tilde{\tau}_1$	$\tilde{\tau}_2$	$\tilde{\nu}_e$	$\tilde{\nu}_{\tau 1}$		
mass bound (GeV) :	82	82	73	94	94	94		
Higgs bosons :	$H^0$	$A^0$	$H^\pm$					
mass bound (GeV) :	500	0	80					

Table 3: Experimental lower bounds on new particle masses relevant to SUSY models. The results for the second generation of quarks and leptons are the same as those shown for the first generation. The most conservative bounds have been taken. The numbers shown in this Table correspond to the case when  $R$ -parity is conserved, but they do not change very much when  $R$ -parity is violated.

The problem here is that we cannot make *any* random choice of the four parameters and one sign in the cMSSM, for large ranges of these have been ruled out by experimental data on a variety of measured processes. We, therefore, must evaluate the branching ratio for  $t \rightarrow c + h^0$  *only* for points in the parameter space which are permitted by all the experimental constraints [29]. At a first glance, this is a daunting prospect, given the wide range and diverse nature of experimental data which impact the cMSSM, but the task is made much easier by the presence of public domain software which do most of the computation automatically. We have, therefore, made free use of these software to constrain the cMSSM parameter space. The exact procedure followed is described below.

1. A set of random choices is made of the four parameters of the cMSSM, viz. the universal scalar mass  $m_0$ , the universal fermion mass  $m_{1/2}$ , the universal trilinear coupling  $A_0$  and the ratio of Higgs boson vevs  $\tan \beta$ , within the ranges

$$\begin{aligned}
100 \text{ GeV} \leq m_0 \leq 10 \text{ TeV} & & 100 \text{ GeV} \leq m_{1/2} \leq 10 \text{ TeV} \\
-10 \text{ TeV} \leq A_0 \leq 10 \text{ TeV} & & 2 \leq \tan \beta \leq 50
\end{aligned}$$

The sign of the  $\mu$  parameter is chosen positive, since it is known that the negative sign is disfavoured by measurements of the muon anomalous magnetic moment.

2. Given a choice of the above parameters, we find the low-energy cMSSM mass spectrum by using the software SUSPECT [30], which takes these values at the scale of grand unification and uses the renormalisation group equations to evolve them down to the electroweak scale, and also calculates mixing induced by the electroweak symmetry-breaking.

3. We eliminate parameter sets which are inconsistent with the observed  $h^0$  mass  $125 \pm 2$  GeV. This turns out to be a very severe constraint for low values of  $m_0$ ,  $m_{1/2}$  and  $A_0$ .
4. Of the surviving parameter sets, we eliminate those that are inconsistent with the results of direct searches for SUSY, i.e. which yield masses for the SUSY particles which are smaller than the experimental lower bounds given in Table 3 below [12–18, 26, 31].
5. With the remaining parameter sets, we calculate a clutch of low-energy variables measured in  $K$  and  $B$  decays, using the software SUPERISO [32]. We then eliminate parameter sets which are inconsistent with the 95% C.L. experimental data on these variables, as given in Table 4.

The most restrictive of these are the branching ratios  $\mathcal{B}(B \rightarrow X_s \gamma)$  and  $\mathcal{B}(B_s \rightarrow \mu^+ \mu^-)$ . The former is known to be highly sensitive to low values of the charged Higgs boson mass and the latter is important for precluding very large values of  $\tan \beta$ . Once a parameter set survives all the above filters, we consider it acceptable and use it to evaluate the  $t \rightarrow c + h^0$  branching ratio. Our results are then set out in Figure 6.

Variable	Lower Bound	Upper Bound
$\mathcal{B}(B \rightarrow X_s \gamma)$	$2.766 \times 10^{-4}$	$4.094 \times 10^{-4}$
$\Delta_0(B \rightarrow K^* \gamma)$	$-3.8 \times 10^{-2}$	$1.0 \times 10^{-1}$
$\mathcal{B}(B_s \rightarrow \mu^+ \mu^-)$	$7.261 \times 10^{-10}$	$6.173 \times 10^{-9}$
$\mathcal{B}(B_d \rightarrow \mu^+ \mu^-)$	$4.0 \times 10^{-11}$	$6.8 \times 10^{-10}$
$\mathcal{B}(B \rightarrow X_s \mu^+ \mu^-)$ (low $Q^2$ )	$2.4 \times 10^{-7}$	$2.96 \times 10^{-6}$
$\mathcal{B}(B \rightarrow X_s \mu^+ \mu^-)$ (high $Q^2$ )	$1.48 \times 10^{-7}$	$6.88 \times 10^{-7}$
$\mathcal{B}(B \rightarrow \tau^+ \nu_\tau)$	$7.388 \times 10^{-5}$	$2.993 \times 10^{-4}$
$R[\mathcal{B}(B \rightarrow \tau^+ \nu_\tau)]$	$5.5 \times 10^{-1}$	2.71
$\mathcal{B}(B \rightarrow D \tau \nu)$	$5.2 \times 10^{-3}$	$1.02 \times 10^{-2}$
$\mathcal{B}(D_s \rightarrow \tau \nu)$	$5.06 \times 10^{-2}$	$5.7 \times 10^{-2}$
$\mathcal{B}(D_s \rightarrow \mu \nu)$	$4.95 \times 10^{-3}$	$6.67 \times 10^{-3}$
$\mathcal{B}(D \rightarrow \mu^+ \mu^-)$	$3.49 \times 10^{-4}$	$4.15 \times 10^{-4}$
$R[\mathcal{B}(K \rightarrow \mu \nu)]$	$6.325 \times 10^{-1}$	$6.391 \times 10^{-1}$
$R_\mu^{23}$	$9.92 \times 10^{-1}$	1.006
$\delta(a_\mu)$	$-6.5 \times 10^{-10}$	$5.75 \times 10^{-9}$

Table 4: Experimental bounds [32–41] at 95% C.L. on low energy parameters calculable in the software SUPERISO. For detailed definitions, see [32].

The left panel in Figure 6 shows a scatter plot indicating the allowed regions in the  $m_0$ – $m_{1/2}$  plane, which is probably the best way to indicate constraints on the cMSSM. We note that every point on this plane corresponds to all possible random choices of the other parameters in the model, which accounts for the fuzziness in shapes. The black regions are disallowed by ‘theory’ constraints, which include the proper shape of the electroweak potential [42, 43] and the requirement that the lightest supersymmetric particle – a prime dark matter candidate – should be electrically neutral and have no colour quantum numbers. The extensive region in blue is ruled out by a combination of the  $h^0$  mass constraint and the direct searches for supersymmetry, while the comparatively limited red regions are ruled out by constraints from



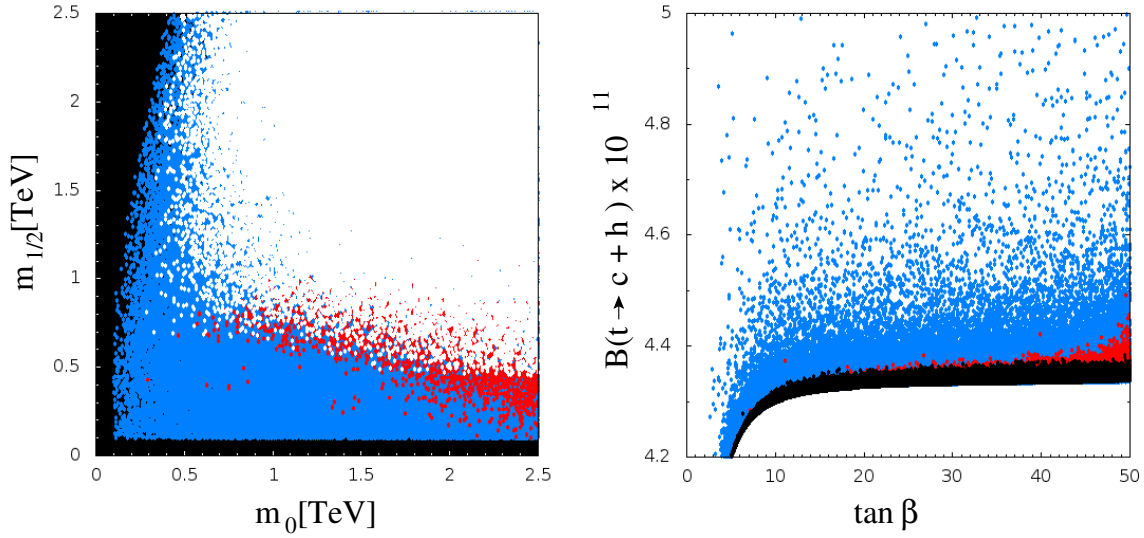


Figure 6: The panel on the left shows the parts of the  $m_0$ - $m_{1/2}$  plane in the cMSSM which are ruled out for all chosen values of  $A_0$  and  $\tan\beta$ . In the left panel, the black region is ruled out by theory constraints, the blue dots by the Higgs boson mass constraints, and the red dots by all low-energy constraints. In the right panel, blue and red dots follow the same convention as in the left panel, while the black dots are *allowed* by all constraints.

low-energy measurements. Points falling in the white region are all allowed, and it is for these that we can legitimately try to evaluate top FCNC processes. It is important to note that almost the entire region for  $m_0$  and  $m_{1/2}$  within a TeV is ruled out – this is another way of stating that there are no light squarks, unless we consider the third generation, where a seesaw-type mechanism can give us one lighter squark state.

The panel on the right in Figure 6 contains our actual results. The scale on the  $y$ -axis, where we have plotted the branching ratio of  $t \rightarrow c + h^0$  immediately tells that this always comes of the order of  $10^{-11}$ , which is just two-orders of magnitude above the SM prediction. On the  $x$ -axis we have plotted the  $\tan\beta$  variable, even though the actual branching ratio is not a very sensitive function of this, except when  $\tan\beta$  is around 5. As before, the blue points are ruled out by Higgs mass constraints and direct constraints, and the red points are ruled out by low-energy measurements. Unlike the left panel, however, the *black* points are the ones which represent the allowed parameter sets. It is immediately obvious, therefore, that the cMSSM prediction for  $B(t \rightarrow c + h)$  is around  $4.3 \times 10^{-11}$ , and this holds for almost all the points in the allowed parameter space.

Why is this branching ratio so small in the cMSSM, when there exist charged Higgs bosons to frustrate the GIM mechanism, as well as a wide range of possible couplings? The reason is quite simple. We do indeed have contributions which frustrate the GIM mechanism. This raises the branching ratio from the SM value of  $\mathcal{O}(10^{-15})$  to  $\mathcal{O}(10^{-11})$ . However, if the factor had been as large as  $m_W^2/m_b^2 \simeq 5 \times 10^5$ , we should have expected the prediction to be one order larger. That this does not happen is a phenomenon rather peculiar to the cMSSM, which

is more constrained than other SUSY models. The requirement of a light Higgs boson with a mass as high as 125 GeV above the tree-level value, which is  $M_Z$ , requires most of the SUSY partners in this model to be very heavy, and this, being essentially a logarithmic effect, leads to the additional suppression of one order of magnitude in the  $t \rightarrow c + Z$  branching ratio. Once this is understood, we cannot get the other enhancements, since (a) we have adopted the MFV paradigm, and (b) the couplings in SUSY closely resemble the gauge couplings. The Yukawa couplings of the charged Higgs boson are, indeed, dependent on  $\tan \beta$ , but they are proportional to

$$\frac{m_t}{M_W} \cot \beta + \frac{m_b}{M_W} \tan \beta$$

and hence do not grow very large in the range  $3 \leq \tan \beta \leq 50$ .

As shown in the right panel in Figure 6, the application of the Higgs mass and direct search constraints pushes the branching ratio down by a factor around 3, which is expected since these are known to push up the SUSY partner masses from the 100 GeV to the TeV range. The application of low-energy constraints (especially  $B_s \rightarrow \mu^+ \mu^-$ ) further kills the feeble enhancement due to large  $\tan \beta$ , leading to the somewhat disappointing prediction of  $4.3 \times 10^{-11}$ .

When we come to the process  $t \rightarrow c + Z^0$ , this will be mediated by the whole set of diagrams in Figures 4 and 5 where, as in the previous case, the  $h^0$  is replaced by the  $Z^0$  and the corresponding broken line by a wiggly line. As in the previous section, we can calculate the four helicity amplitudes in terms of  $F_1$ – $F_4$  form factors which are listed in Appendix B.2 and make a numerical evaluation. As in the case of the toy model, we predict branching ratios which are about two orders of magnitude greater than the branching ratios for  $t \rightarrow c + h^0$ , i.e. we get  $\mathcal{B}(t \rightarrow c + Z^0) \sim 10^{-9}$ , which is still far too small to be accessed by experiment. The reason is, of course, the same – breakdown of the GIM mechanism leads to a value about four orders of magnitude greater than the SM prediction, but so long as we stay within the MFV paradigm and have couplings which are not significantly greater than gauge coupling, no further enhancements will be obtained.

We see, therefore, that not only does the cMSSM fail to produce enough enhancement of the top FCNC decays for observation, but this will be a generic feature of any MSSM variant which follows the MFV paradigm. Not much can be gained, therefore, by relaxing the universality constraints on the SUSY-breaking parameters, as is done in, for example, the so-called phenomenological MSSM or pMSSM models. However, it is possible to break the MFV paradigm by choosing squark mixing matrices which are not aligned with the CKM matrix [44]. This provides some enhancement of the branching ratios for top FCNC decay, but only to the level of about  $10^{-7}$ , partly because the squarks are already constrained to be rather heavy.

## 5 Beyond the MFV paradigm : R-parity violation

In the preceding section we have discussed how the cMSSM and its variants fail to produce top FCNC effects at a measurable level. Within SUSY, however, there exists another scenario which can provide the necessary enhancements, and that is the scenario when  $R$ -parity is violated. It is well-known that the conservation of the  $Z_2$  quantum number  $R = (-1)^{L+2S+3B}$ , where  $L$ ,  $S$  and  $B$  stand for lepton number, spin and baryon number of a particle, is a condition which must be imposed by hand on all SUSY models if we want the lightest SUSY particle, or LSP, to be a candidate for cold dark matter. Thus, when we consider a scenario in which the  $R$ -parity is not conserved, we abandon the idea of explaining dark matter in a SUSY model – a feature which has contributed to making such models far less popular than the opposite variant. It is important to note, however, that  $R$ -parity conservation is not demanded by SUSY at all – it is an add-on which was originally believed to be necessary to explain the long lifetime of the proton [45]. However, ever since it was pointed out that this can be done by separately conserving either lepton number  $L$  or baryon number  $B$ , it has been known that one can easily have  $R$ -parity violating models which are consistent with both exact and broken SUSY. In that case,  $R$ -parity loses its special position, for the way in which  $R$ -parity produces a dark matter candidate is no different from any other  $Z_2$  symmetry imposed by hand on a new physics model, such as, for example, the KK-parity imposed in models with a universal extra dimension [46] and the  $T$ -parity imposed in the littlest Higgs models [47]. Thus, at the cost of decoupling SUSY from the search for an explanation of dark matter in terms of new particles, it is legitimate to consider models where  $R$ -parity is violated.

Once we allow  $R$ -parity violation, it is straightforward to write down the extra interactions allowed. These will arise from a superpotential term [48]

$$\widehat{W}_R = \sum_{i,j,k=1}^3 \left( \frac{1}{2} \lambda_{ijk} \widehat{L}_i \widehat{L}_j \widehat{E}_k^c + \lambda'_{ijk} \widehat{L}_i \widehat{Q}_j \widehat{D}_k^c + \frac{1}{2} \lambda''_{ijk} \widehat{U}_i^c \widehat{D}_j^c \widehat{D}_k^c \right) \quad (5.1)$$

where the  $\widehat{L}$  and  $\widehat{Q}$  superfields are SU(2) doublets (suitably combined) and the  $\widehat{E}^c$ ,  $\widehat{U}^c$  and  $\widehat{D}^c$  are SU(2) singlets. The indices  $i$ ,  $j$  and  $k$  run over the three matter generations. It is immediately clear that the  $\lambda_{ijk}$  are antisymmetric in  $i$  and  $j$ , i.e. there are 9 independent  $\lambda_{ijk}$ 's and the  $\lambda''_{ijk}$  are antisymmetric in  $j$  and  $k$ , i.e. there are 9 independent  $\lambda''_{ijk}$ 's. The  $\lambda'_{ijk}$  have no such symmetry properties and hence there will be 27 independent  $\lambda'_{ijk}$ 's, bringing the total number of independent parameters to 45. However, to avoid fast proton decay, we must either conserve lepton number and set all the  $\lambda_{ijk}$ 's and  $\lambda'_{ijk}$ 's to zero, or conserve baryon number and set all the  $\lambda''_{ijk}$ 's to zero. Either alternative leads to FCNC processes, including, when the third generation is considered, the top quark. In this work, all RPV couplings will be considered real.

Constraints on the  $R$ -parity violating couplings from various low-energy FCNC processes have been industriously studied in the literature [48–54] and a first look would lead to the conclusion that the  $\lambda$ ,  $\lambda'$  and  $\lambda''$  couplings must be rather small. Such constraints depend, however, on two crucial assumptions, viz.,

- Only one (or at most two) of the  $R$ -parity couplings are substantial and all the others are zero or of negligible value. This makes a phenomenological analysis simple, but its virtue ends there. The oft-repeated analogy with a similar pattern observed in the SM Yukawa couplings is not a very convincing argument.
- Most of the bounds used to be presented with scaling factors depending on the mass of the exchanged squark, which was assumed to be around 100 GeV. Today, most of the lower bounds on the squark masses (at least in the first two generations) are an order of magnitude higher, leading to considerable relaxation in the constraints on the  $R$ -parity violating couplings.

Once we realise that the  $R$ -parity violating couplings can, in fact, be very large, we also note that they have no need to be aligned with the CKM matrix or even satisfy unitarity constraints, for these are parameters of the Lagrangian, and do not arise from the mixing of

	Strongest Constraint arises from	Scales as mass of	Scaling Exponent	Upper bound (100 GeV)	Sfermion mass (GeV)	Current upper bound
$\lambda'_{121}$	Atomic Parity Violation [49]	$\tilde{q}_L$	1	0.035	1350 [56]	0.473
$\lambda'_{122}$	$\nu_e$ mass bound [57]	$\tilde{d}_R$	$1/2$	0.004	1100 [26]	0.013
$\lambda'_{123}$	CC Universality [49]	$\tilde{b}_1$	$1/2$	0.02	620 [58]	0.05
$\lambda'_{131}$	Atomic parity violation [73]	$\tilde{t}_L$	1	0.019	300 [59]	0.057
$\lambda'_{132}$	FB asymmetry ( $e^+e^-$ ) [73] [48]	$\tilde{t}_L$	1	0.28	300 [59]	0.84
$\lambda'_{133}$	$\nu_e$ mass bound [57]	$\tilde{b}_1$	$1/2$	0.0002	620 [58]	0.0005
$\lambda'_{221}$	Bounds on $R_{\mu e}$ [60]	$\tilde{d}_R$	1	0.18	1100 [26]	1.98
$\lambda'_{222}$	$\nu_\mu$ mass bound [57]	$\tilde{d}_R$	$1/2$	0.015	1100 [26]	0.05
$\lambda'_{223}$	$D_s$ meson decay [60]	$\tilde{b}_1$	1	0.18	620 [58]	1.1
$\lambda'_{231}$	$\nu_\mu$ DIS [48, 49]	$\tilde{\nu}_\tau$	1	0.22	1700 [61]	2.00
$\lambda'_{232}$	Bounds on $R_\mu(Z)$ [62, 63]	$\tilde{s}$	1	0.39	1000 [26]	2.00
		$\tilde{\mu}$	-1		100 [26]	
$\lambda'_{233}$	$\nu_\mu$ mass bound [57]	$\tilde{d}_R$	$1/2$	0.001	1100 [26]	0.003
$\lambda'_{321}$	$D_s$ decays [48]	$\tilde{d}_R$	1	0.52	1100 [26]	0.66
$\lambda'_{322}$	$\nu_\tau$ mass bound [57]	$\tilde{d}_R$	$1/2$	0.02	1100 [26]	0.07
$\lambda'_{323}$	$D_s$ decay [48]	$\tilde{b}_1$	1	0.52	620 [58]	2.00
$\lambda'_{331}$	Bounds on $R_\tau(Z)$ [62]	$\tilde{d}$	1,	0.22	1000 [26]	2.00
$\lambda'_{332}$		$\tilde{\tau}$	-1	0.22	100 [26]	2.00
$\lambda'_{333}$	$\nu_\tau$ mass bound [57]	$\tilde{b}_1$	$1/2$	0.001	620 [58]	0.003

Table 5: Showing the experimental constraints on the  $R$ -parity-violating couplings  $\lambda'_{i2j}$  and  $\lambda'_{i3j}$  relevant for FCNC decays of the top quark. The abbreviations used in the second column are as follows: charged current (CC), forward-backward (FB), deep inelastic scattering (DIS), branching ratio (BR). The upper bounds on the  $\lambda'$  and  $\lambda''$  couplings scale as the masses of the sfermions listed in the third column, raised to the powers given in the fourth column. The fifth column records the upper bounds when these masses are uniformly set to 100 GeV (except for the gluino, whose mass is set to 1000 GeV). The sixth column gives the current lower bound on the relevant sparticle masses and the last column gives the corresponding (scaled) upper bound on the  $R$ -parity-violating couplings.

fields. The  $R$ -parity violating scenario, therefore, can satisfy all the conditions required for FCNC enhancement, viz. frustration of the GIM mechanism, non-MFV mixing terms and almost unconstrained coupling constants. We therefore choose, in this section, the  $R$ -parity violating model (RPV-MSSM) as a paradigm to illustrate how large top FCNC effects can be obtained.

As a first step to this study, we note that the  $\lambda_{ijk}$ , while interesting enough in their own right, are not relevant for the processes of interest in this article, since they do not appear with operators involving quark fields. We do not discuss them further in this article. The couplings of interest are the  $\lambda'_{ijk}$  or the  $\lambda''_{ijk}$  – but obviously not both. We therefore list, in Table 5 below, the constraints on the  $R$ -parity violating couplings relevant for the processes under consideration, taking into account the current constraints on the masses of the sleptons and squarks. These, of course, still assume that one (or at most two) coupling(s) at a time is dominant.

Strongest Constraint arises from	Scales		Upper bound (100 GeV)	Sfermion mass (GeV)	Current upper bound
	as mass of	Scaling Exponent			
$\lambda''_{212}$ $\lambda''_{213}$ $\lambda''_{223}$	Perturbativity [64]	–	–	–	1.24
$\lambda''_{312}$ $\lambda''_{313}$	$n - \bar{n}$ oscillation [65, 66]	$\tilde{d}_R$ $\tilde{g}$	2 $1/2$	$10^{-3}$ 1100 [26] 1000 [31]	0.1 0.1
$\lambda''_{323}$	Bounds on $R_b(Z)$ [67]	$\tilde{b}$ $\tilde{\tau}$	1 -1	1.89 1.89 500 [58] 80 [26]	1.89

Table 6: Showing the experimental constraints on the  $R$ -parity-violating couplings  $\lambda''_{2jk}$  and  $\lambda''_{3jk}$  relevant for FCNC decays of the top quark. The notations and abbreviations follow the conventions of Table 5.

A glance at the last column of Tables 5 and 6 will make it clear that with the current values of sfermion masses, the constraints on most of the  $R$ -parity-violating couplings are very weak. These couplings can be as large as gauge couplings, or, in specific cases, much larger. Top FCNC processes will typically involve

1. the products  $\lambda'_{i2k}\lambda'_{i3k}$  for the decays  $t \rightarrow c + h^0/Z$ , where  $i$  denotes the leptonic flavour in the loop and  $k$  denotes the  $d$ -type quark flavour in the loop. For decays to  $t \rightarrow u + h^0/Z$ , we would get the products  $\lambda'_{i1k}\lambda'_{i3k}$ , but these have not been considered in this work.
2. the products  $\lambda''_{2jk}\lambda''_{3jk}$  for the decays  $t \rightarrow c + h^0/Z$ , where  $j$  denotes a quark flavour of the  $u$ -type and  $k$  denotes a  $d$ -type quark flavour. As in the previous case, for the decays  $t \rightarrow u + h^0/Z$ , we would get products like  $\lambda''_{1jk}\lambda''_{3jk}$ , which are not considered in this work.

$\lambda'_{121}\lambda'_{131}$	$\lambda'_{122}\lambda'_{132}$	$\lambda'_{123}\lambda'_{133}$	$\lambda'_{221}\lambda'_{231}$	$\lambda'_{222}\lambda'_{232}$	$\lambda'_{223}\lambda'_{233}$
0.0269	0.0109	$2.5 \times 10^{-5}$	3.96	0.1	0.0033
$\tilde{e}_L, \tilde{d}_R$	$\tilde{e}_L, \tilde{s}_R$	$\tilde{e}_L, \tilde{b}_R$	$\tilde{\mu}_L, \tilde{d}_R$	$\tilde{\mu}_L, \tilde{s}_R$	$\tilde{\mu}_L, \tilde{b}_R$
$\lambda'_{321}\lambda'_{331}$	$\lambda'_{322}\lambda'_{332}$	$\lambda'_{323}\lambda'_{333}$	$\lambda''_{212}\lambda''_{312}$	$\lambda''_{213}\lambda''_{313}$	$\lambda''_{223}\lambda''_{323}$
1.32	0.14	0.006	0.124	0.124	2.3436
$\tilde{\tau}_L, \tilde{d}_R$	$\tilde{\tau}_L, \tilde{s}_R$	$\tilde{\tau}_L, \tilde{b}_R$	$\tilde{s}_R$	$\tilde{b}_R$	$\tilde{b}_R$

Table 7: Showing upper limits on the products of pairs of  $R$ -parity-violating couplings relevant for the decays  $t \rightarrow c + h^0/Z$ , as well as the sparticles exchanged in the loops for each combination.

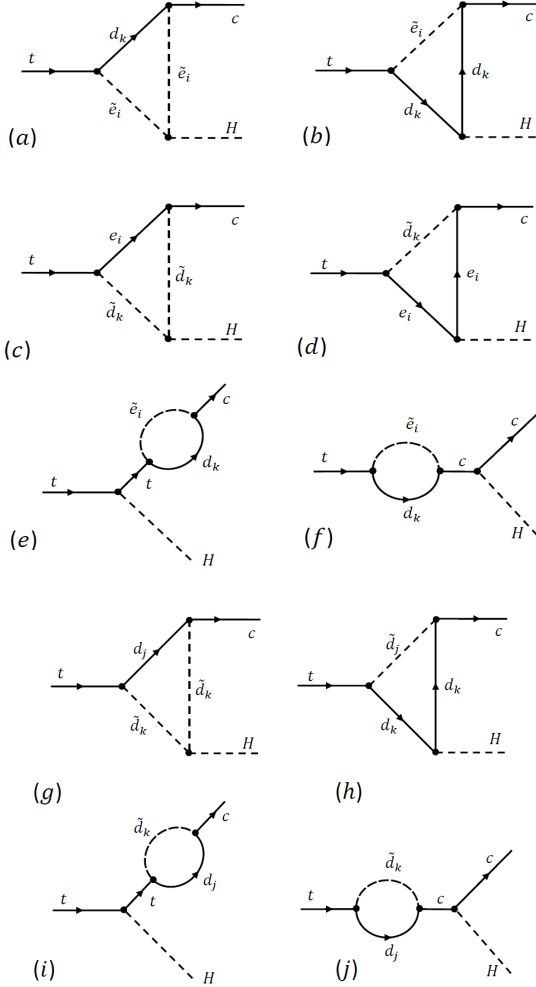


Figure 7: Further Feynman Diagrams leading to the decay  $t \rightarrow c + H$  in the RPV MSSM.

As before, the details of the calculation are given in Appendix C. It is important to note that we have presented the diagrams mediated by  $\lambda'$  couplings and the diagrams mediated by  $\lambda''$  couplings in the same framework. The former include diagrams labelled (a)–(f), while the latter are labelled (g)–(j). The corresponding amplitudes will be added, as described in Appendix C. However, there is no harm done, so long as we keep all the  $\lambda''$  zero when the  $\lambda'$  are non-zero, and vice versa. The variation of the branching ratios for  $t \rightarrow c + h^0$  and  $t \rightarrow c + Z$  as a function of the sfermion mass are given in Figure 8. The panels on the left, carrying the header LQ $\bar{D}$ , correspond to the  $\lambda'$  couplings and show values proportional to  $(\lambda'_{i2k}\lambda'_{i3k})^2$ . The relevant values of  $ik$  are marked alongside each curve. To illustrate the variation with the sfermion masses, we have set these couplings to the experimental upper bounds in the last column of Table 5, and consequently, the products to the values in Table 7. These, of course,

In Table 7, we list the pairs of  $R$ -parity-violating couplings which can lead to top FCNC processes, together with their maximum values corresponding to the last column of Tables 5 and 6. Some of the products are rather large, though staying well within the perturbative limit of  $4\pi$ .

The Feynman diagrams which contribute to the FCNC decay  $t \rightarrow c + h^0$  in the RPV-MSSM have been listed in Fig. 7. Of course, since the  $R$ -parity violating superpotential is added to the MSSM terms, we will also have contributions from all the diagrams in Figs. 4 and 5. However, these are always small – as we have seen – and hence the dominant contribution will arise from  $R$ -parity-violating terms alone.

As before, the details of the calculation are given in Appendix C. It is important to note that we have presented the diagrams mediated by  $\lambda'$  couplings and the diagrams mediated by  $\lambda''$  couplings in the same framework. The former include diagrams labelled (a)–(f), while the latter are labelled (g)–(j). The corresponding amplitudes will be added, as described in Appendix C. However, there is no harm done, so long as we keep all the  $\lambda''$  zero when the  $\lambda'$  are non-zero, and vice versa.

will be relaxed further if the concerned sfermion masses are taken higher, and would lead to even greater branching ratios, as may be imagined. However, we have chosen to keep the couplings fixed to the values given in Table 7. In a similar way, the panels on the right, carrying the header  $U\bar{D}\bar{D}$ , correspond to the  $\lambda''$  couplings, and show values proportional to the products  $(\lambda''_{2jk}\lambda''_{3jk})^2$ . Here, too, we have marked the values of  $jk$  next to the relevant curves.

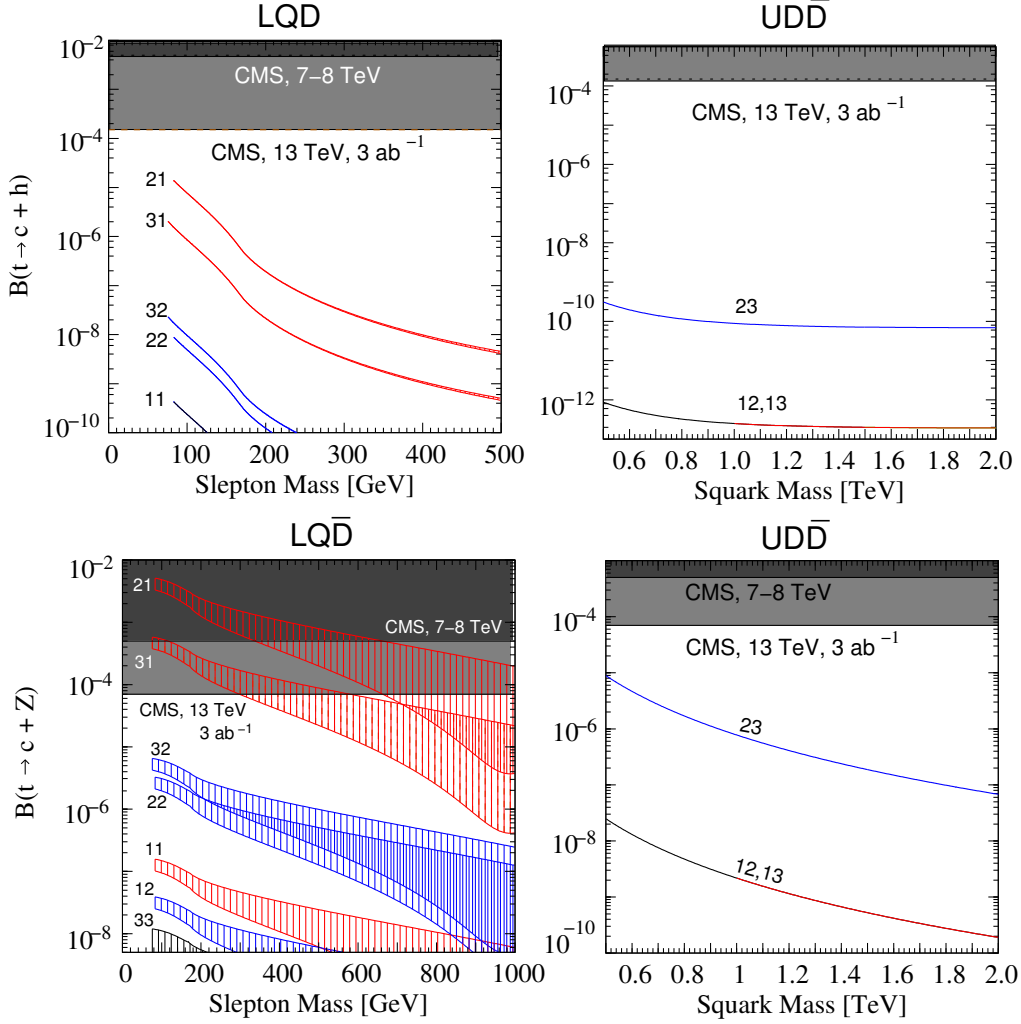


Figure 8: Illustrating the variation in the branching ratios  $\mathcal{B}(t \rightarrow c + h^0)$  (upper panels) and  $\mathcal{B}(t \rightarrow c + Z^0)$  (lower panels) with increase in the sfermion masses. For the panels on the left, which show branching ratios proportional to  $(\lambda'_{i2k}\lambda'_{i3k})^2$  with the values of  $ik$  marked next to each curve, the mass of the slepton  $\tilde{e}_{Li}$  is plotted along the abscissa, and the mass of the squark  $\tilde{d}_{Rk}$  is responsible for the thickness of the lines in the upper panel and the hatched region in the lower panel. For the panels on the right, which show branching ratios proportional to  $(\lambda''_{2jk}\lambda''_{3jk})^2$  with the values of  $jk$  marked next to each curve, the mass of the squark  $\tilde{d}_{Rk}$  is plotted along the abscissa. The dark (light) grey shaded regions represent the experimental bounds (discovery limits) from the LHC, operating at 7–8 TeV (13 TeV, projected).

In Figure 8, the left panels illustrate the behaviour of the respective branching ratios with respect to variations in the mass of the slepton  $\tilde{e}_{Li}$ . Each curve starts on the left from the current lower bound on the mass of this slepton and goes up to a TeV. The variation of the branching ratio as the mass of the squark  $\tilde{d}_{Rk}$  varies from 1 – 2 TeV is represented by the

thickness of the lines in the upper panel, and by the hatched regions on the lower panel (with the upper boundary indicating a squark mass of 1 TeV). Quite obviously, the branching ratio  $\mathcal{B}(t \rightarrow c + h^0)$  is hardly affected by changes in the squark mass, whereas the branching ratio  $\mathcal{B}(t \rightarrow c + Z^0)$  can vary by as much as an order of magnitude as the squark grows heavier.

The panels on the right in Figure 8 illustrate the variation in the respective branching ratios with change in the mass of the squark  $\tilde{d}_{Rk}$ , which is the  $b$ -squark for  $jk = 13, 23$  and the  $c$ -squark for  $jk = 12$ . The black and blue curves correspond to the former two cases and the red curves to the latter. In all the panels, the upper region shaded dark grey corresponds to bounds on the relevant branching ratios as set by the CMS Collaboration [68], while the regions shaded light grey corresponds to the projected discovery limits at the 13 TeV LHC, assuming an integrated luminosity of  $3000 \text{ fb}^{-1}$ . It is immediately obvious, that even with all the enhancements available to us in a model with  $R$ -parity violation, the FCNC branching ratios of the  $t$ -quark are rather small. For  $\lambda''$  couplings, in fact, these are hopelessly small – in fact, so small, that even if we take the couplings to their perturbative limits, detection at the LHC will become a touch-and-go affair. The situation is better for  $\lambda'$  couplings, largely because the sleptons can still be quite light. However, as the sleptons become heavier, the FCNC branching ratios fall rather fast and become unobservable. The best case arises for  $\mathcal{B}(t \rightarrow c + Z^0)$  when we have the couplings  $\lambda'_{221}\lambda'_{231}$  and  $\lambda'_{321}\lambda'_{331}$ , with exchange of  $\tilde{\mu}_L$  or  $\tilde{\tau}_L$  in the loops. In the former case, the data already available from the LHC constrains the slepton mass to be greater than about 350 GeV. In either case, a discovery at the 13 TeV run is possible for a wide range of slepton and squark masses. For other combinations of the  $\lambda'$  couplings, the branching ratios are too small to be accessible at the LHC, even at the end of its run.

Before concluding this section, we may take up the issue mentioned before, that if the experimental bounds on the sfermion masses increase, the upper bounds on the  $R$ -parity-violating couplings can be relaxed still further. This may lead to higher values of the branching ratios is question, if the sfermion in the FCNC loop is not the same one which leads to relaxation of the bound. However, if we consider the only products which lead to sizable results as shown in Figure 8, viz.  $\lambda'_{221}\lambda'_{231}$ ,  $\lambda'_{321}\lambda'_{331}$  and  $\lambda''_{223}\lambda''_{323}$ , we can see from Table 7 that the values are, respectively, 3.96, 1.32 and 2.34. The maximum value that we can push these to is, of course,  $4\pi$ , and that would provide enhancements in the branching ratios at the level of one or two orders of magnitude. This might just make it possible to observe the decay  $t \rightarrow c + Z$  if it is mediated by  $\lambda''_{223}\lambda''_{323}$ , with more optimistic results for the  $\lambda'$  couplings. However, only if some sign of  $R$ -parity-violating SUSY is found at the LHC will it be worthwhile to investigate further details in this regard.



## 6 Summary and Conclusions

This work was undertaken with a definite view, viz. to investigate FCNC decays of the  $t$  quark which involve heavy particles that cannot be discovered directly at the LHC. Several such claims exist in the literature, but the results obtained are not always mutually consistent (see Table 8 below). By starting with a toy model which closely resembles the SM, we have shown that the extremely low values of FCNC branching ratios of the  $t$ -quark in the SM arise from three different sources. These are (i) the GIM cancellation between one-loop diagrams with different  $d$ -type quarks in the loop, (ii) the MFV paradigm, i.e. the choice of the hierarchical CKM matrix as the only source of flavour violation, and (iii) the choice of gauge couplings or their equivalent for the new particles. These result in suppression factors of the order  $10^{-5}$ ,  $10^{-4}$  and  $10^{-1}$  respectively, driving the loop-induced branching ratios from their naive values around  $10^{-4}$  to tiny values in the neighbourhood of  $10^{-14}$ . It follows, therefore, that a new physics model will be able to predict enhanced rates of these FCNC decays only to the extent that one or more of these conditions is violated. We then illustrate this set of conditions by considering (a) the cMSSM – a model where GIM cancellation is frustrated, but MFV holds and the couplings can be modestly enhanced, and (b) the  $R$ -parity-violating extension of the cMSSM, where all three conditions can be broken. In vindication of the general principles enunciated above, the branching ratios in the cMSSM do not exceed  $10^{-10}$  for  $t \rightarrow c + h^0$  and  $10^{-8}$  for  $t \rightarrow c + Z^0$ , whereas, for the case when  $R$ -parity is violated, we can predict them to be as large as  $10^{-5}$  and  $10^{-3}$  respectively. The last-mentioned values are well within the range of accessibility at the LHC, as illustrated in Figure 8 above.

Reference	Model	GIM	MFV	g	$t \rightarrow ch^0$	$t \rightarrow cZ^0$
T.-J. Gao <i>et al.</i> [69]	$\mathcal{B}, \mathcal{L}$	×	×	×	$10^{-4(5)}$	–
J.-J. Cao <i>et al.</i> [70]	MSSM	×	✓	×	$10^{-5(9)}$	$10^{-6(7)}$
B. Mele [71]	MSSM	×	✓	×	$10^{-5(9)}$	$10^{-8(7)}$
S. Bejar <i>et al.</i> [72]	2HDM Type-II	×	✓	×	$10^{-4(9)}$	–
G. Eilam <i>et al.</i> [73]	$\mathcal{R}$ SUSY	×	×	✓	$10^{-5(5)}$	–
C. Yue <i>et al.</i> [74]	Non-universal $Z'$	×	×	×	–	$10^{-6(4)}$
I. Baum <i>et al.</i> [75]	$t$ -quark 2HDM	×	✓	×	$10^{-6(6)}$	–
A. Dedes <i>et al.</i> [44]	SUSY	×	×	×	$10^{-7(7)}$	–

Table 8: A few of the earlier calculations of FCNC decays of the top quark. Some of the results are in agreement with our predictions, given in parentheses. Those which are not are generally due to choice of vastly different parameters, which were allowed when these calculations were performed.

The utility of identifying the three suppression principles is well illustrated in Table 8, where some of the different models considered in the literature are classified according to the conditions which hold (✓) or are violated (×). It is, then, easy to utilise the suppression levels quoted above to understand/criticise the branching ratios predicted by these authors. Moreover, we now have a quick rule of thumb to predict the branching ratios for FCNC decays of the top quark for *any* new physics model, for all that we need is to ask ourselves is which of

these three conditions are applicable.

The appendices of this article present a collection of the formulae needed to perform the computations given in the text, in an explicit and user-friendly form, using the 'tHooft-Veltman and Passarino-Veltman formalism for one-loop integrals. The formulae are given in terms of certain generic couplings, so as to be easily usable to carry out similar computations in almost any new model of physics beyond the SM.

Finally, a word about the phenomenological implications of this work. It turns out that the use of the FCNC decays of the top quark is not such a ready handle to new physics at the LHC (and other high energy machines) as one might naively think, since the corresponding branching ratios are generally rather small. Even when we deviate almost completely from the SM, as exemplified in the  $R$ -parity-violating couplings, we require to be lucky to have just the right masses and pairing(s) of couplings in order to predict an observable effect. This is something which only the future can tell, and it is certain that the eyes of the entire high energy community will be turned to the results of the LHC, as they slowly unfold over the years to come.

*Acknowledgments:* The authors are grateful to A. Dighe and T.S. Roy for discussions and to D. Bhatia and T. Samui for help in computation. Thanks are also due to P.S. Bhupal Dev and D.K. Ghosh for pointing out an error in Table 5. The work of SR is partially supported under project no. 2013/37C/37/BRNS by the Board of Research in Nuclear Studies, Government of India.

## Appendix A Toy model amplitudes

### A.1 The decay $t \rightarrow c + H$

We consider the decay  $t(k) \rightarrow c(p) + H(q)$ . In the rest frame of the  $t$  quark, we have  $k = (m_t, \vec{0})$  and

$$u(k, h_t) = \sqrt{\frac{m_t}{2}} \begin{pmatrix} 1 + h_t & 1 - h_t & 0 & 0 \end{pmatrix}^T \quad (\text{A.1})$$

where  $h_t = \pm 1$  is the helicity of the  $t$  quark. Now, the three-momenta  $\vec{p}$  and  $\vec{q}$  will be back-to-back, and we can choose this as the  $z$ -axis. In this case, we can write

$$p = \begin{pmatrix} E_c & 0 & 0 & |\vec{p}| \end{pmatrix} \quad q = \begin{pmatrix} E_H & 0 & 0 & -|\vec{p}| \end{pmatrix} \quad (\text{A.2})$$

where

$$|\vec{p}| \simeq E_c \simeq \frac{m_t^2 - M_H^2}{2m_t} \quad E_H \simeq \frac{m_t^2 + M_H^2}{2m_t} \quad (\text{A.3})$$

taking  $m_c \ll m_t, M_H$ . In the approximation, the  $c$ -quark wave function is

$$u(p, h_c) \simeq \sqrt{\frac{m_t^2 - M_H^2}{8m_t}} \begin{pmatrix} 1 + h_c & 1 - h_c & 1 + h_c & -1 + h_c \end{pmatrix}^T \quad (\text{A.4})$$

The helicity amplitudes  $\mathcal{M}(h_c, h_t)$  now have the explicit form

$$\mathcal{M}(h_c, h_t) = \sum_{i=1}^3 \lambda_i \mathcal{A}_i(h_c, h_t) \quad (\text{A.5})$$

where  $i$  runs over the three  $d$ -type quarks in the loop,  $\lambda_i = V_{2i} V_{3i}^*$ , and we parametrise

$$\mathcal{A}_i(h_c, h_t) = \bar{u}(p, h_c) i (F_{1i} P_L + F_{2i} P_R) u(k, h_t) \quad (\text{A.6})$$

where  $P_L, P_R$  are the chiral projection operators

$$P_L = \frac{1}{2} (1 - \gamma_5) \quad P_R = \frac{1}{2} (1 + \gamma_5) \quad (\text{A.7})$$

and  $F_{1i}$  and  $F_{2i}$  are form factors given below. Four helicity amplitudes are possible, but the only non-vanishing ones are

$$\begin{aligned} \mathcal{A}_i(+1, +1) &\simeq \sqrt{m_t^2 - M_H^2} F_{1i} \\ \mathcal{A}_i(-1, -1) &\simeq \sqrt{m_t^2 - M_H^2} F_{2i} \end{aligned} \quad (\text{A.8})$$

Each of the form factors  $F_{1i}$  and  $F_{2i}$  can be written

$$F_{ni} = F_{ni}^{(a)} + F_{ni}^{(b)} + F_{ni}^{(c)} + F_{ni}^{(d)} \quad (\text{A.9})$$

where  $n = 1, 2$  and the superscripts refer to the graphs (a)–(d) shown in Figure 1. These can be written in terms of the Passarino-’tHooft-Veltman functions, defined as Euclidean space integrals

$$\begin{aligned} B_0(m_1, m_2; M) &= \int \frac{d^4 k}{\pi^2} \frac{1}{(k^2 + m_1^2)\{(k+p)^2 + m_2^2\}} \\ p_\mu B_1(m_1, m_2; M) &= \int \frac{d^4 k}{\pi^2} \frac{k_\mu}{(k^2 + m_1^2)\{(k+p)^2 + m_2^2\}} \end{aligned} \quad (\text{A.10})$$

where  $p^2 = -M^2$ . In the  $\overline{\text{MS}}$  scheme, we can write

$$\begin{aligned} B_0(m_1, m_2; M) &= \Delta + \hat{B}_0(m_1, m_2; M) \\ B_1(m_1, m_2; M) &= -\frac{1}{2}\Delta + \hat{B}_1(m_1, m_2; M) \end{aligned} \quad (\text{A.11})$$

where the  $\hat{B}_{0,1}$  are finite. The divergent quantity is  $\Delta = 2/\varepsilon - \gamma + \ln 4\pi$  where  $\varepsilon \rightarrow 0$  and  $\gamma$  is the Euler-Mascheroni constant. We also have

$$\begin{aligned} C_0(m_1, m_2, m_3; M_1, M_2, M_3) &= \int \frac{d^4 k}{\pi^2} \frac{1}{(k^2 + m_1^2)\{(k+p_2)^2 + m_2^2\}\{(k+p_2+p_3)^2 + m_3^2\}} \\ C_{11}p_{2\mu} + C_{12}p_{3\mu} &= \int \frac{d^4 k}{\pi^2} \frac{k_\mu}{(k^2 + m_1^2)\{(k+p_2)^2 + m_2^2\}\{(k+p_2+p_3)^2 + m_3^2\}} \end{aligned} \quad (\text{A.12})$$

where  $p_1 = p_2 + p_3$  and  $p_i^2 = -M_i^2$  for  $i = 1, 2, 3$  and the  $C_0, C_{11}$  and  $C_{12}$  are naturally finite. In fact, the GIM cancellation ensures that all the form factors are finite and hence, we keep only the finite parts of the  $B$  and  $C$  functions. In terms of these, we can now compute the  $F_1$  form factors

$$\begin{aligned} F_{1i}^{(a)} &= -\frac{\xi\eta^2}{16\pi^2} m_c C_{12}^{(a)} \\ F_{1i}^{(b)} &= \frac{y_i m_i \eta^2}{16\pi^2} m_t \{2(C_{11}^{(b)} - C_{12}^{(b)}) + C_0^{(b)}\} \\ F_{1i}^{(c)} &= \frac{y_c \eta^2 m_t}{16\pi^2(m_t^2 - m_c^2)} m_t \tilde{B}_1(m_i, M_\omega; m_t) \\ F_{1i}^{(d)} &= -\frac{y_t \eta^2 m_c}{16\pi^2(m_t^2 - m_c^2)} m_c \tilde{B}_1(m_i, M_\omega; m_c) \end{aligned} \quad (\text{A.13})$$

and the  $F_2$  form factors

$$\begin{aligned} F_{2i}^{(a)} &= -\frac{\xi\eta^2}{16\pi^2} m_t (C_{11}^{(a)} - C_{12}^{(a)}) \\ F_{2i}^{(b)} &= \frac{y_i m_i \eta^2}{16\pi^2} m_c (C_0^{(b)} + 2C_{12}^{(b)}) \\ F_{2i}^{(c)} &= \frac{y_c \eta^2 m_t}{16\pi^2(m_t^2 - m_c^2)} m_c \tilde{B}_1(m_i, M_\omega; m_t) \\ F_{2i}^{(d)} &= -\frac{y_t \eta^2 m_c}{16\pi^2(m_t^2 - m_c^2)} m_t \tilde{B}_1(m_i, M_\omega; m_c) \end{aligned} \quad (\text{A.14})$$

where

$$\begin{aligned} C_X^{(a)} &= C_X(m_i, M_\omega, M_\omega; m_c, m_t, M_H) \\ C_X^{(b)} &= C_X(M_\omega, m_i, m_i; m_c, m_t, M_H) \end{aligned} \quad (\text{A.15})$$

for  $X = 0, 11, 12, 22$ . These are evaluated using the public domain software FF [27].

The Yukawa couplings  $y$  are the SM ones, i.e.

$$y_i = \frac{gm_i}{2M_\omega} \quad y_t = \frac{gm_t}{2M_\omega} \quad y_c = \frac{gm_c}{2M_\omega} . \quad (\text{A.16})$$

The above form factors can be used to evaluate the total form factors appearing in Eqn. (A.9), which then enables us to compute the helicity amplitudes in Eqn. (A.8). These are then convoluted with the  $\lambda$  factors in Eqn. (2.3) and used to generate the squared and spin-summed/averaged matrix element in Eqn. (2.4). Plugging this into Eqn. (2.5) then produces the desired result.

## A.2 The decay $t \rightarrow c + Z$

We now consider the decay  $t(k) \rightarrow c(p) + Z(q)$ . The kinematics is similar to the previous case, with  $M_Z$  in place of  $M_H$ . Accordingly, the helicity spinor for the  $c$ -quark, in the approximation  $m_c \ll m_t, M_Z$ , is

$$u(p, h_c) \simeq \sqrt{\frac{m_t^2 - M_Z^2}{8m_t}} \begin{pmatrix} 1 + h_c & 1 - h_c & 1 + h_c & -1 + h_c \end{pmatrix}^T \quad (\text{A.17})$$

while the helicity spinor for the  $t$ -quark is identical with that in Eqn. (A.1). In this case, we also have to consider the polarisation vector of the  $Z$  boson, which, for the three helicity choices  $h_Z = 0, \pm 1$ , has the form

$$\varepsilon(q, h_Z) = \begin{pmatrix} -\frac{(1-|h_Z|)|\vec{p}|}{M_Z} & \mp \frac{h_Z}{\sqrt{2}} & -\frac{i|h_Z|}{\sqrt{2}} & \frac{(1-|h_Z|)E_Z}{M_Z} \end{pmatrix} \quad (\text{A.18})$$

where, as in Eqn. (A.3),

$$|\vec{p}| \simeq E_c \simeq \frac{m_t^2 - M_Z^2}{2m_t} \quad E_Z \simeq \frac{m_t^2 + M_Z^2}{2m_t} \quad (\text{A.19})$$

The helicity amplitudes  $\mathcal{M}(h_Z; h_c, h_t)$  now have the explicit form

$$\mathcal{M}(h_Z; h_c, h_t) = \sum_{i=1}^3 \lambda_i \mathcal{A}_i(h_Z; h_c, h_t) \quad (\text{A.20})$$

where  $i$  runs over the three  $d$ -type quarks in the loop,  $\lambda_i = V_{2i}V_{3i}^*$ , and we parametrise

$$\begin{aligned} \mathcal{A}_i(h_Z; h_c, h_t) &= \bar{u}(p, h_c) i\Gamma^\mu u(k, h_t) \varepsilon_\mu^*(q) \\ \Gamma^\mu &= F_{1i}\gamma^\mu P_L + F_{2i}\gamma^\mu P_R + iF_{3i}\sigma^{\mu\nu} q_\nu P_L + iF_{4i}\sigma^{\mu\nu} q_\nu P_R \end{aligned} \quad (\text{A.21})$$

Of the 12 possible helicity amplitudes, the only nonvanishing ones are

$$\begin{aligned}
\mathcal{A}_i(+1; -1, +1) &= -\sqrt{2(m_t^2 - M_Z^2)} [F_{1i} - F_{4i}(E_Z + |\vec{p}|)] \\
\mathcal{A}_i(-1; +1, -1) &= -\sqrt{2(m_t^2 - M_Z^2)} [F_{2i} - F_{3i}(E_Z + |\vec{p}|)] \\
\mathcal{A}_i(0; +1, +1) &= -\sqrt{m_t^2 - M_Z^2} \left[ F_{2i} \sqrt{\frac{E_Z + |\vec{p}|}{E_Z - |\vec{p}|}} - F_{3i} M_Z \right] \\
\mathcal{A}_i(0; -1, -1) &= -\sqrt{m_t^2 - M_Z^2} \left[ F_{1i} \sqrt{\frac{E_Z + |\vec{p}|}{E_Z - |\vec{p}|}} - F_{4i} M_Z \right]
\end{aligned} \tag{A.22}$$

Each of the form factors can be written

$$F_{ni} = F_{ni}^{(a)} + F_{ni}^{(b)} + F_{ni}^{(c)} + F_{ni}^{(d)} \tag{A.23}$$

where  $n = 1, 2, 3, 4$  and the superscripts refer to the graphs (a)–(d) shown in Figure 1 (with  $H$  replaced by  $Z$ ). These can be written, as before, in terms of the Passarino-'tHooft-Veltman functions. We thus obtain the  $F_1$  form factors

$$\begin{aligned}
F_{1i}^{(a)} &= \frac{\xi \eta^2}{16\pi^2} [m_t^2(C_{11}^{(a)} - C_{12}^{(a)} + C_{21}^{(a)} - C_{23}^{(a)}) + m_c m_t (C_{12}^{(a)} + C_{23}^{(a)}) - C_{24}^{(a)}] \\
F_{1i}^{(b)} &= \frac{\eta^2}{16\pi^2} [\alpha_i m_i^2 C_0^{(b)} + \beta_i (B_0 - M_\omega^2 C_0^{(b)} + m_t^2 (C_{21}^{(b)} - C_{23}^{(b)}) - m_c^2 C_{12}^{(b)} - 2C_{24}^{(b)}) \\
&\quad + \beta_i m_c m_t \left( \frac{3}{2} (C_0^{(b)} + C_{11}^{(b)}) + C_{12}^{(b)} + C_{23}^{(b)} \right)] \\
F_{1i}^{(c)} &= -\frac{\eta^2}{16\pi^2 (m_t^2 - m_c^2)} [\alpha m_c^2 B_1(m_i, M_\omega; m_c) + \beta m_c m_t B_1(m_i, M_\omega; m_c)] \\
F_{1i}^{(d)} &= \frac{\eta^2}{16\pi^2 (m_t^2 - m_c^2)} [\alpha m_t^2 B_1(m_i, M_\omega; m_t) + \beta m_c m_t B_1(m_i, M_\omega; m_t)]
\end{aligned} \tag{A.24}$$

the  $F_2$  form factors

$$\begin{aligned}
F_{2i}^{(a)} &= -\frac{\xi \eta^2}{16\pi^2} [m_t^2 (C_{11}^{(a)} - C_{12}^{(a)} + C_{21}^{(a)} - C_{23}^{(a)}) - m_c m_t (C_{12}^{(a)} + C_{23}^{(a)}) - C_{24}^{(a)}] \\
F_{2i}^{(b)} &= -\frac{\eta^2}{16\pi^2} [\alpha_i m_i^2 C_0^{(b)} + \beta_i (B_0 - M_\omega^2 C_0^{(b)} + m_t^2 (C_{21}^{(b)} - C_{23}^{(b)}) - m_c^2 C_{12}^{(b)} - 2C_{24}^{(b)}) \\
&\quad - \beta_i m_c m_t \left( \frac{3}{2} (C_0^{(b)} + C_{11}^{(b)}) + C_{12}^{(b)} + C_{23}^{(b)} \right)] \\
F_{2i}^{(c)} &= \frac{\eta^2}{16\pi^2 (m_t^2 - m_c^2)} [\alpha m_c^2 B_1(m_i, M_\omega; m_c) - \beta m_c m_t B_1(m_i, M_\omega; m_c)] \\
F_{2i}^{(d)} &= -\frac{\eta^2}{16\pi^2 (m_t^2 - m_c^2)} [\alpha m_t^2 B_1(m_i, M_\omega; m_t) - \beta m_c m_t B_1(m_i, M_\omega; m_t)]
\end{aligned} \tag{A.25}$$

the nonvanishing  $F_3$  form factors

$$\begin{aligned}
F_{3i}^{(a)} &= -\frac{\xi \eta^2}{16\pi^2} [m_t (C_{11}^{(a)} - C_{12}^{(a)} + C_{21}^{(a)} - C_{23}^{(a)}) + m_c (C_{12}^{(a)} + C_{23}^{(a)})] \\
F_{3i}^{(b)} &= -\frac{\eta^2}{16\pi^2} \beta_i [m_t (C_{11}^{(b)} - C_{12}^{(b)} + C_{21}^{(b)} - C_{23}^{(b)}) + m_c \left( \frac{1}{2} (C_0^{(b)} + C_{11}^{(b)}) + C_{12}^{(b)} + C_{23}^{(b)} \right)]
\end{aligned} \tag{A.26}$$

and the nonvanishing  $F_4$  form factors

$$\begin{aligned}
F_{4i}^{(a)} &= -\frac{\xi \eta^2}{16\pi^2} [m_t (C_{11}^{(a)} - C_{12}^{(a)} + C_{21}^{(a)} - C_{23}^{(a)}) - m_c (C_{12}^{(a)} + C_{23}^{(a)})] \\
F_{4i}^{(b)} &= -\frac{\eta^2}{16\pi^2} \beta_i [m_t (C_{11}^{(b)} - C_{12}^{(b)} + C_{21}^{(b)} - C_{23}^{(b)}) - m_c \left( \frac{1}{2} (C_0^{(b)} + C_{11}^{(b)}) + C_{12}^{(b)} + C_{23}^{(b)} \right)]
\end{aligned} \tag{A.27}$$

In the above,

$$\begin{aligned}
B_0 &= B_0(m_i, m_i; M_Z) \\
C_X^{(a)} &= C_X(m_i, M_\omega, M_\omega; m_c, m_t, M_Z) \\
C_X^{(b)} &= C_X(M_\omega, m_i, m_i; m_c, m_t, M_Z)
\end{aligned}$$

where  $X = 0, 11, 12, 21, 23, 24$ . The  $Zd_i\bar{d}_i$  couplings are  $\alpha = -\frac{1}{2} - 2Q\sin^2\theta_W$  and  $\beta = \frac{1}{2}$  where  $Q = -1/3$  is the charge of the down-type quark.

Once we have these form factors, we sum them up using Eqn. (A.23) and use them to calculate the helicity amplitudes in Eqn. (A.23). These are then convoluted with the  $\lambda_i$  factors in Eqn. (2.13) and used to calculate the squared spin-summed/ averaged matrix element in Eqn. (2.14). Finally this is used in Eqn. (2.15) to produce the partial width.

## Appendix B SM and cMSSM amplitudes

### B.1 The decay $t \rightarrow c + H$

In the Standard Model, as in the toy model, the decay  $t \rightarrow c + H$  can be parametrised in terms of the two nonvanishing helicity amplitudes of Eqn. (A.8). The calculation follows the lines of the toy model, except that the diagrams are those of Figure 4 instead of Figure 1. Thus, in this Appendix, we only require to list the form factors, diagram-wise.

It is convenient, in evaluating these diagrams, to define a set of general vertices:

$$\begin{aligned}
\bar{u}_i u_i h &: ig(A_{ui}^h P_L + B_{ui}^h P_R) \\
\bar{d}_i d_i h &: ig(A_{di}^h P_L + B_{di}^h P_R) \\
h(-q)\phi^+(p)W_\mu^- &: ig\alpha_\phi^h(p+q)_\mu \\
h\phi^+\phi'^- &: igM_W\beta_{\phi\phi'}^h \\
hW_\mu^+W_\nu^- &: igM_W\omega_h g_{\mu\nu} \\
\bar{u}_i d_j \phi^+ &: ig\left(X_{ij}^\phi P_L + Y_{ij}^\phi P_R\right)
\end{aligned}$$

in terms of a set of coupling constants  $A_{ui}^h, B_{ui}^h, A_{di}^h, B_{di}^h, \alpha_\phi^h, \beta_{\phi\phi'}^h, \omega_h, X_{ij}^\phi$  and  $Y_{ij}^\phi$ . In order to obtain numerical values in the SM, we need to substitute the coupling constants according to the table given below.

coupling:	$A_{ui}^h$	$B_{ui}^h$	$A_{di}^h$	$B_{di}^h$	$\alpha_\phi^h$	$\beta_{\phi\phi'}^h$	$\omega_h$	$X_{ij}^\phi$	$Y_{ij}^\phi$
SM value :	$\frac{m_i}{2M_W}$	$\frac{m_i}{2M_W}$	$\frac{m_i}{2M_W}$	$\frac{m_i}{2M_W}$	$-\frac{1}{2}$	$-\frac{m_h^2}{M_W^2}$	1	$\frac{m_i}{\sqrt{2}M_W}$	$-\frac{m_j}{\sqrt{2}M_W}$

In terms of these, the form factors of type  $F_1$  are

$$\begin{aligned}
F_{1i}^{(a)} &= \frac{ig^3 M_W \omega_h}{16\pi^2} m_c C_{12}^{(a)} \\
F_{1i}^{(b)} &= \frac{ig^3 \alpha_{G+}^h}{16\sqrt{2}\pi^2} \left[ X_{ci}^G \left( (m_t^2 - 2M_h^2)(C_{11}^{(b)} - C_{12}^{(b)}) - B_0(2,3) + m_t^2 C_0^{(b)} + 2m_c^2 C_{11}^{(b)} \right) - m_i m_c Y_{ci}^G (C_{12}^{(b)} + 2C_0^{(b)}) \right] \\
F_{1i}^{(c)} &= \frac{ig^3 \alpha_{G+}^h}{16\sqrt{2}\pi^2} \left[ X_{ti}^G \left( 2m_t^2 C_{11}^{(c)} - 2m_s^2 C_{12}^{(c)} + m_c^2 C_{12}^{(c)} - B_0(2,3) + m_t^2 C_0^{(c)} \right) - m_i m_t Y_{ti}^G (C_{11}^{(c)} - C_{12}^{(c)} + 2C_0^{(c)}) \right] \\
F_{1i}^{(d)} &= -\frac{ig^3 M_W \beta_{GG}^h}{16\pi^2} \left[ m_t X_{ci}^G X_{ti}^G (C_{11}^{(d)} - C_{12}^{(d)}) - m_i X_{ci}^G Y_{ti}^G C_0^{(d)} + m_c Y_{ci}^G Y_{ti}^G C_{12}^{(d)} \right] \\
F_{1i}^{(e)} &= \frac{ig^3 m_i}{16\pi^2} m_c \left[ (A_{di}^h + B_{di}^h) C_{12}^{(e)} + B_{di}^h C_0^{(e)} \right] \\
F_{1i}^{(f)} &= -\frac{ig^3}{16\pi^2} \left[ z_1 \left( B_0(2,3) - M_W^2 C_0^{(f)} \right) - z_3 C_0^{(f)} - m_t z_5 \frac{X_{ti}^G}{Y_{ti}^G} (C_{11}^{(f)} - C_{12}^{(f)}) - m_c z_2 C_{12}^{(f)} \right] Y_{ti}^G \\
F_{1i}^{(g)} &= \frac{ig^3}{16\pi^2 (m_t^2 - m_c^2)} m_t^2 A_{uc}^h B_1^{(g)} \\
F_{1i}^{(h)} &= \frac{ig^3}{16\pi^2 (m_t^2 - m_c^2)} \left[ m_t \left( m_t A_{uc}^h Y_{ci}^G + m_c A_{uc}^h \frac{X_{ti}^G}{Y_{ti}^G} X_{ci}^G \right) B_1^{(h)} - m_i \left( m_t A_{uc}^h Y_{ci}^G \frac{X_{ti}^G}{Y_{ti}^G} + m_c A_{uc}^h X_{ci}^G \right) B_0^{(h)} \right] Y_{ti}^G \\
F_{1i}^{(i)} &= -\frac{ig^3}{16\pi^2 (m_t^2 - m_c^2)} m_c m_t A_{ut}^h B_1^{(i)} \\
F_{1i}^{(j)} &= -\frac{ig^3}{16\pi^2 (m_t^2 - m_c^2)} \left[ m_c X_{ti}^G (m_c X_{ci}^G B_1^{(j)} - m_i Y_{ci}^G B_0^{(j)}) + m_t Y_{ti}^G (m_c Y_{ci}^G B_1^{(j)} - m_i X_{ci}^G B_0^{(j)}) \right] A_{ut}^h \quad (B.1)
\end{aligned}$$

and the form factors of type  $F_2$  are

$$\begin{aligned}
F_{2i}^{(a)} &= \frac{ig^3 M_W \omega_h}{16\pi^2} m_t (C_{11}^{(a)} - C_{12}^{(a)}) \\
F_{2i}^{(b)} &= \frac{ig^3 \alpha_{G+}^h}{16\sqrt{2}\pi^2} \left[ X_{ci}^G m_c m_t (C_{12}^{(b)} - 2C_{11}^{(b)}) + Y_{ci}^G m_i m_t (C_0^{(b)} - C_{11}^{(b)} + C_{12}^{(b)}) \right] \\
F_{2i}^{(c)} &= \frac{-ig^3 \alpha_{G+}^h}{16\sqrt{2}\pi^2} \left[ X_{ti}^G m_c m_t (C_{12}^{(c)} - 2C_{11}^{(c)}) + Y_{ti}^G m_i m_t (C_0^{(c)} - C_{11}^{(c)} + C_{12}^{(c)}) \right] \\
F_{2i}^{(d)} &= -\frac{ig^3 M_W \beta_{GG}^h}{16\pi^2} \left[ m_t Y_{ci}^G Y_{ti}^G (C_{11}^{(d)} - C_{12}^{(d)}) - m_i X_{ti}^G Y_{ci}^G C_0^{(d)} + m_c X_{ci}^G X_{ti}^G C_{12}^{(d)} \right] \\
F_{2i}^{(e)} &= \frac{ig^3 m_i}{16\pi^2} m_t \left[ (A_{di}^h + B_{di}^h) (C_{11}^{(e)} - C_{12}^{(e)}) + A_{di}^h C_0^{(e)} \right] \\
F_{2i}^{(f)} &= -\frac{ig^3}{16\pi^2} \left[ z_4 \left( B_0(2,3) - M_W^2 C_0^{(f)} \right) - z_6 C_0^{(f)} - m_t z_2 \frac{Y_{ti}^G}{X_{ti}^G} (C_{11}^{(f)} - C_{12}^{(f)}) - m_c z_5 C_{12}^{(f)} \right] X_{ti}^G \\
F_{2i}^{(g)} &= \frac{ig^3}{16\pi^2 (m_t^2 - m_c^2)} m_c m_t B_{uc}^h B_1^{(g)} \\
F_{2i}^{(h)} &= \frac{ig^3}{16\pi^2 (m_t^2 - m_c^2)} \left[ m_t \left( m_t B_{uc}^h X_{ci}^G + m_c B_{uc}^h \frac{Y_{ti}^G}{X_{ti}^G} Y_{ci}^G \right) B_1^{(h)} - m_i \left( m_t B_{uc}^h X_{ci}^G \frac{Y_{ti}^G}{X_{ti}^G} + m_c B_{uc}^h Y_{ci}^G \right) B_0^{(h)} \right] X_{ti}^G \\
F_{2i}^{(i)} &= -\frac{ig^3}{16\pi^2 (m_t^2 - m_c^2)} m_c^2 B_{ut}^h B_1^{(i)} \\
F_{2i}^{(j)} &= -\frac{ig^3}{16\pi^2 (m_t^2 - m_c^2)} \left[ m_c Y_{ti}^G (m_c Y_{ci}^G B_1^{(j)} - m_i X_{ci}^G B_0^{(j)}) + m_t X_{ti}^G (m_c X_{ci}^G B_1^{(j)} - m_i Y_{ci}^G B_0^{(j)}) \right] B_{ut}^h \quad (B.2)
\end{aligned}$$

As in the previous section, the superscripts refer to the diagrams marked (a)–(j) in Figure 4.



In the above, we have used the functions

$$\begin{aligned}
C_X^{(a)} &= C_X(m_i, M_W, M_W; m_c, m_t, M_h) & B_1^{(g)} &= B_1(m_i, M_W; m_t) \\
C_X^{(b)} &= C_X(m_i, M_W, M_W; m_c, m_t, M_h) & B_1^{(h)} &= B_1(m_i, M_W; m_t) \\
C_X^{(c)} &= C_X(m_i, M_W, M_W; m_c, m_t, M_h) & B_0^{(h)} &= B_0(m_i, M_W; m_t) \\
C_X^{(d)} &= C_X(m_i, M_W, M_W; m_c, m_t, M_h) & B_1^{(i)} &= B_1(m_i, M_W; m_c) \\
C_X^{(e)} &= C_X(M_W, m_i, m_i; m_c, m_t, M_h) & B_1^{(j)} &= B_1(m_i, M_W; m_c) \\
C_X^{(f)} &= C_X(M_W, m_i, m_i; m_c, m_t, M_h) & B_0^{(j)} &= B_0(m_i, M_W; m_c)
\end{aligned} \tag{B.3}$$

where  $X = 0, 11, 12, 21, 23, 24$ , as before, and defined a set of effective couplings

$$\begin{aligned}
z_1 &= X_{ci}^G B_{di}^h \\
z_2 &= m_t Y_{ci}^G \frac{X_{ti}^G}{Y_{ti}^G} A_{di}^h + m_c X_{ci}^G B_{di}^h + m_i Y_{ci}^G B_{di}^h + m_i Y_{ci}^G A_{di}^h \\
z_3 &= m_t \frac{X_{ti}^G}{Y_{ti}^G} A_{di}^h (m_i X_{ci}^G + m_c Y_{ci}^G) + m_i^2 A_{di}^h X_{ci}^G + m_i m_c A_{di}^h Y_{ci}^G \\
z_4 &= Y_{ci}^G A_{di}^h \\
z_5 &= m_t X_{ci}^G \frac{Y_{ti}^G}{X_{ti}^G} B_{di}^h + m_c Y_{ci}^G A_{di}^h + m_i X_{ci}^G A_{di}^h + m_i X_{ci}^G B_{di}^h \\
z_6 &= m_t \frac{Y_{ti}^G}{X_{ti}^G} B_{di}^h (m_i Y_{ci}^G + m_c X_{ci}^G) + m_i^2 B_{di}^h Y_{ci}^G + m_i m_c B_{di}^h X_{ci}^G
\end{aligned} \tag{B.4}$$

These form factors can now be combined, using  $F_{ni} = \sum_{A=a}^j F_{ni}^A$  for  $n = 1, 2$  and the results substituted into Eqn. (A.8) as before.

When we come to consider the cMSSM, the SM contributions will not only involve modifications of the SM couplings given above, but will also be enhanced by contributions from the additional eight diagrams in Figure 5, which involve superparticles in the loops. These involve some additional couplings which are parametrised in a general way as

$$\begin{aligned}
\chi_i^+ \chi_j^- h &: ig \left( A_{ij}^h P_L + B_{ij}^h P_R \right) \\
\chi_i^+ \chi_j^- Z^\mu &: ig \gamma^\mu \left( A_{ij}^Z P_L + B_{ij}^Z P_R \right) \\
\tilde{d}^* \tilde{d} h &: ig M_W \beta_{\tilde{d}\tilde{d}}^h \\
\tilde{d}(p) \tilde{d}^*(q) Z^\mu &: ig \alpha_{\tilde{d}}^{\tilde{d}} (p + q)^\mu \\
\tilde{d}_i^* \bar{u}_k \chi_j^+ &: ig \left( X_{kj}^i P_L + Y_{kj}^i P_R \right)
\end{aligned}$$

in terms of an additional set of coupling constants  $A_{ij}^h, B_{ij}^h, A_{ij}^Z, B_{ij}^Z, \beta_{\tilde{d}\tilde{d}}^h, \alpha_{\tilde{d}}^{\tilde{d}}, X_{kj}^i, Y_{kj}^i$ . For a numerical analysis, we require to take the full set of coupling constants as given in the table below.

coupling :	$A_{ui}^h$	$B_{ui}^h$	$A_{di}^h$	$B_{di}^h$
cMSSM :	$-\frac{m_i \cos \alpha}{2M_W \sin \beta}$	$-\frac{m_i \cos \alpha}{2M_W \sin \beta}$	$\frac{m_i \sin \alpha}{2M_W \cos \beta}$	$\frac{m_i \sin \alpha}{2M_W \cos \beta}$
coupling:	$\alpha_{G^+}^h$	$\alpha_{h^+}^h$	$\beta_{G^+G^-}^h$	$\beta_{G^+h^+}^h$
cMSSM :	$-\frac{1}{2} \sin(\beta - \alpha)$	$-\frac{1}{2} \cos(\beta - \alpha)$	$\frac{\cos 2\beta \sin(\alpha + \beta)}{2 \cos^2 \theta_W}$	$\frac{\cos(\beta - \alpha)(m_{h^+}^2 - m_{h^0}^2)}{2M_W^2}$
coupling:	$\beta_{h^+h^-}^h$	$\omega_h$	$X_{ij}^{G^+}$	$Y_{ij}^{G^+}$
cMSSM value :	$-\sin(\beta - \alpha)$ $-\frac{\cos 2\beta \sin(\alpha + \beta)}{2 \cos^2 \theta_W}$	$\sin(\beta - \alpha)$	$\frac{m_i}{\sqrt{2}M_W}$	$-\frac{m_j}{\sqrt{2}M_W}$
coupling:	$X_{ij}^{h^+}$	$Y_{ij}^{h^+}$		
cMSSM value :	$\frac{m_i \cot \beta}{\sqrt{2}M_W}$	$\frac{m_j \tan \beta}{\sqrt{2}M_W}$		
coupling:	$A_{ij}^h$	$B_{ij}^h$	$A_{ij}^Z$	$B_{ij}^Z$
cMSSM value :	$Q_{ij}^* \sin \alpha - S_{ij}^* \cos \alpha$	$Q_{ji} \sin \alpha - S_{ji} \cos \alpha$	$Q_{ij}^V$	$Q_{ij}^U$
coupling:	$\beta_{d\bar{d}}^h$	$\alpha_{\bar{d}}^{\tilde{d}}$	$X_{kj}^i$	$Y_{kj}^i$
cMSSM value :	$-\left(\frac{1}{2} - \frac{\sin^2 \theta_W}{3}\right)$ $+\frac{\sin(\alpha + \beta)}{\cos^2 \theta_W}$	$\frac{1 - \frac{2}{3} \sin^2 \theta_W}{2 \cos \theta_W}$	0	$U_{j1}$

where, in terms of the chargino mixing matrices  $U$  and  $V$ ,

$$Q_{ij} = \frac{1}{\sqrt{2}} U_{i2} V_{j1}; \quad S_{ij} = \frac{1}{\sqrt{2}} U_{i1} V_{j2}$$

$$Q_{ij}^U = -U_{i1} U_{j1}^* - \frac{1}{2} U_{i2} U_{j2}^* + \delta_{ij} \sin^2 \theta_W; \quad Q_{ij}^V = -V_{i1} V_{j1}^* - \frac{1}{2} V_{i2} V_{j2}^* + \delta_{ij} \sin^2 \theta_W$$

Evaluating the Feynman diagrams of Figs. 4 and 5 now leads to the  $F_1$  form factors

$$F_{1i}^{(k)} = \frac{ig^3 \alpha_{h^+}^h}{16\sqrt{2}\pi^2} \left[ X_{ci}^{h^+} \left( (m_t^2 - 2M_{h^+}^2)(C_{11}^{(k)} - C_{12}^{(k)}) - B_0(2, 3) + m_i^2 C_0^{(k)} + 2m_c^2 C_{11}^{(k)} \right) - m_i m_c Y_{ci}^{h^+} (C_{12}^{(k)} + 2C_0^{(k)}) \right]$$

$$F_{1i}^{(l)} = \frac{ig^3 \alpha_{h^+}^h}{16\sqrt{2}\pi^2} \left[ X_{ti}^{h^+} \left( 2m_t^2 C_{11}^{(l)} - 2M_{h^+}^2 C_{12}^{(l)} + m_c^2 C_{12}^{(l)} - B_0(2, 3) + m_i^2 C_0^{(l)} \right) - m_i m_t Y_{ti}^{h^+} (C_{11}^{(l)} - C_{12}^{(l)} + 2C_0^{(l)}) \right]$$

$$F_{1i}^{(m)} = -\frac{ig^3 M_W \beta_{h^+h^-}^h}{16\pi^2} \left[ m_t X_{ci}^{h^+} X_{ti}^{h^+} (C_{11}^{(m)} - C_{12}^{(m)}) - m_i X_{ci}^{h^+} Y_{ti}^{h^+} C_0^{(m)} + m_c Y_{ci}^{h^+} Y_{ti}^{h^+} C_{12}^{(m)} \right]$$

$$F_{1i}^{(n)} = -\frac{ig^3 M_W \beta_{G^+h^-}^h}{16\pi^2} \left[ m_t X_{ci}^G X_{ti}^{h^+} (C_{11}^{(n)} - C_{12}^{(n)}) - m_i X_{ci}^G Y_{ti}^{h^+} C_0^{(n)} + m_c Y_{ci}^G Y_{ti}^{h^+} C_{12}^{(n)} \right]$$

$$F_{1i}^{(o)} = -\frac{ig^3 M_W \beta_{G^+h^-}^S}{16\pi^2} \left[ m_t X_{ci}^{h^+} X_{ti}^G (C_{11}^{(o)} - C_{12}^{(o)}) - m_i X_{ci}^{h^+} Y_{ti}^G C_0^{(o)} + m_c Y_{ci}^{h^+} Y_{ti}^G C_{12}^{(o)} \right]$$

$$F_{1i}^{(p)} = -\frac{ig^3}{16\pi^2} \left[ z_1 (B_0^{(p)} - M_{h^+}^2 C_0^{(p)}) - z_3 C_0^{(p)} - m_t z_5 \frac{X_{ti}^{h^+}}{Y_{ti}^{h^+}} (C_{11}^{(p)} - C_{12}^{(p)}) - m_c z_2 C_{12}^{(p)} \right] Y_{ti}^{h^+}$$

$$F_{1i}^{(q)} = -\frac{ig^3 M_W \beta_{d\bar{d}}^h}{16\pi^2} \left[ m_t X_{cj}^i X_{tj}^i (C_{11}^{(q)} - C_{12}^{(q)}) - m_i X_{cj}^i Y_{tj}^i C_0^{(q)} + m_c Y_{cj}^i Y_{tj}^i C_{12}^{(q)} \right]$$

$$\begin{aligned}
F_{1i}^{(r)} &= -\frac{ig^3}{16\pi^2} \left[ z_1 \left( B_0^{(r)} - M_{di}^2 C_0^{(r)} \right) - z_3 C_0^{(r)} - m_t z_5 \frac{X_{tj}^i}{Y_{tj}^i} (C_{11}^{(r)} - C_{12}^{(r)}) - m_c z_2 C_{12}^{(r)} \right] Y_{tj}^i \\
F_{1i}^{(s)} &= \frac{ig^3}{16\pi^2(m_t^2 - m_c^2)} \left[ m_t \left( m_t A_{uc}^h Y_{ci}^{h+} + m_c A_{uc}^h \frac{X_{ti}^{h+}}{Y_{ti}^{h+}} X_{ci}^{h+} \right) B_1^{(s)} \right. \\
&\quad \left. - m_i \left( m_t A_{uc}^h Y_{ci}^{h+} \frac{X_{ti}^{h+}}{Y_{ti}^{h+}} + m_c A_{uc}^h X_{ci}^{h+} \right) B_0^{(s)} \right] Y_{ti}^{h+} \\
F_{1i}^{(t)} &= \frac{ig^3}{16\pi^2(m_t^2 - m_c^2)} \left[ m_t \left( m_t A_{uc}^h Y_{cj}^i + m_c A_{uc}^h \frac{X_{ti}^{h+}}{Y_{ti}^{h+}} X_{cj}^i \right) B_1^{(t)} - m_i \left( m_t A_{uc}^h Y_{cj}^i \frac{X_{ti}^{h+}}{Y_{ti}^{h+}} + m_c A_{uc}^h X_{cj}^i \right) B_0^{(t)} \right] Y_{ti}^{h+} \\
F_{1i}^{(u)} &= -\frac{ig^3}{16\pi^2(m_t^2 - m_c^2)} \left[ m_c X_{ti}^{h+} \left( m_c X_{ci}^{h+} B_1^{(u)} - m_i Y_{ci}^{h+} B_0^{(u)} \right) + m_t Y_{ti}^{h+} \left( m_c Y_{ci}^{h+} B_1^{(u)} - m_i X_{ci}^{h+} B_0^{(u)} \right) \right] A_{ut}^h \\
F_{1i}^{(v)} &= -\frac{ig^3}{16\pi^2(m_t^2 - m_c^2)} \left[ m_c X_{tj}^i \left( m_c X_{cj}^i B_1^{(v)} - m_i Y_{cj}^i B_0^{(v)} \right) + m_t Y_{tj}^i \left( m_c Y_{cj}^i B_1^{(v)} - m_i X_{cj}^i B_0^{(v)} \right) \right] A_{ut}^h \quad (B.5)
\end{aligned}$$

and the  $F_2$  form factors

$$\begin{aligned}
F_{2i}^{(k)} &= \frac{ig^3 \alpha_{h+}^h}{16\sqrt{2}\pi^2} \left[ X_{ci}^{h+} m_c m_t (C_{12}^{(k)} - 2C_{11}^{(k)}) + Y_{ci}^{h+} m_i m_t (C_0^{(k)} - C_{11}^{(k)} + C_{12}^{(k)}) \right] \\
F_{2i}^{(l)} &= \frac{-ig^3 \alpha_{h+}^h}{16\sqrt{2}\pi^2} \left[ X_{ti}^{h+} m_c m_t (C_{12}^{(l)} - 2C_{11}^{(l)}) + Y_{ti}^{h+} m_i m_t (C_0^{(l)} - C_{11}^{(l)} + C_{12}^{(l)}) \right] \\
F_{2i}^{(m)} &= -\frac{ig^3 M_W \beta_{h+h-}^h}{16\pi^2} \left[ m_t Y_{ci}^{h+} Y_{ti}^{h+} (C_{11}^{(m)} - C_{12}^{(m)}) - m_i X_{ti}^{h+} Y_{ci}^{h+} C_0^{(m)} + m_c X_{ci}^{h+} X_{ti}^{h+} C_{12}^{(m)} \right] \\
F_{2i}^{(n)} &= -\frac{ig^3 M_W \beta_{G+h-}^h}{16\pi^2} \left[ m_t Y_{ci}^G Y_{ti}^{h+} (C_{11}^{(n)} - C_{12}^{(n)}) - m_i X_{ti}^{h+} Y_{ci}^G C_0^{(n)} + m_c X_{ci}^G X_{ti}^{h+} C_{12}^{(n)} \right] \\
F_{2i}^{(o)} &= -\frac{ig^3 M_W \beta_{G+h-}^S}{16\pi^2} \left[ m_t Y_{ci}^{h+} Y_{ti}^G (C_{11}^{(o)} - C_{12}^{(o)}) - m_i X_{ti}^G Y_{ci}^{h+} C_0^{(o)} + m_c X_{ci}^{h+} X_{ti}^G C_{12}^{(o)} \right] \\
F_{2i}^{(p)} &= -\frac{ig^3}{16\pi^2} \left[ z_4 \left( B_0^{(p)} - M_{h+}^2 C_0^{(p)} \right) - z_6 C_0^{(p)} - m_t z_2 \frac{Y_{ti}^{h+}}{X_{ti}^{h+}} (C_{11}^{(p)} - C_{12}^{(p)}) - m_c z_5 C_{12}^{(p)} \right] X_{ti}^{h+} \\
F_{2i}^{(q)} &= -\frac{ig^3 M_W \beta_{dd}^h}{16\pi^2} \left[ m_t Y_{cj}^i Y_{tj}^i (C_{11}^{(q)} - C_{12}^{(q)}) - m_i X_{tj}^i Y_{cj}^i C_0^{(q)} + m_c X_{cj}^i X_{tj}^i C_{12}^{(q)} \right] \\
F_{2i}^{(r)} &= -\frac{ig^3}{16\pi^2} \left[ z_4 \left( B_0^{(r)} - M_{di}^2 C_0^{(r)} \right) - z_6 C_0^{(r)} - m_t z_2 \frac{Y_{tj}^i}{X_{tj}^i} (C_{11}^{(r)} - C_{12}^{(r)}) - m_c z_5 C_{12}^{(r)} \right] X_{tj}^i \quad (B.6)
\end{aligned}$$

$$\begin{aligned}
F_{2i}^{(s)} &= \frac{ig^3}{16\pi^2(m_t^2 - m_c^2)} \left[ m_t \left( m_t B_{uc}^h X_{ci}^{h+} + m_c B_{uc}^h \frac{Y_{ti}^{h+}}{X_{ti}^{h+}} Y_{ci}^{h+} \right) B_1^{(s)} \right. \\
&\quad \left. - m_i \left( m_t B_{uc}^h X_{ci}^{h+} \frac{Y_{ti}^{h+}}{X_{ti}^{h+}} + m_c B_{uc}^h Y_{ci}^{h+} \right) B_0^{(s)} \right] X_{ti}^{h+} \\
F_{2i}^{(t)} &= \frac{ig^3}{16\pi^2(m_t^2 - m_c^2)} \left[ m_t \left( m_t B_{uc}^h X_{cj}^i + m_c B_{uc}^h \frac{Y_{ti}^{h+}}{X_{ti}^{h+}} Y_{cj}^i \right) B_1^{(t)} - m_i \left( m_t B_{uc}^h X_{cj}^i \frac{Y_{ti}^{h+}}{X_{ti}^{h+}} + m_c B_{uc}^h Y_{cj}^i \right) B_0^{(t)} \right] X_{ti}^{h+} \\
F_{2i}^{(u)} &= -\frac{ig^3}{16\pi^2(m_t^2 - m_c^2)} \left[ m_c Y_{ti}^{h+} \left( m_c Y_{ci}^{h+} B_1^{(u)} - m_i X_{ci}^{h+} B_0^{(u)} \right) + m_t X_{ti}^{h+} \left( m_c X_{ci}^{h+} B_1^{(u)} - m_i Y_{ci}^{h+} B_0^{(u)} \right) \right] B_{ut}^h \\
F_{2i}^{(v)} &= -\frac{ig^3}{16\pi^2(m_t^2 - m_c^2)} \left[ m_c Y_{tj}^i \left( m_c Y_{cj}^i B_1^{(v)} - m_i X_{cj}^i B_0^{(v)} \right) + m_t X_{tj}^i \left( m_c X_{cj}^i B_1^{(v)} - m_i Y_{cj}^i B_0^{(v)} \right) \right] B_{ut}^h \quad (B.7)
\end{aligned}$$

where

$$\begin{aligned}
C_X^{(k)} &= C_X(m_i, M_W, M_{h^+}; m_c, m_t, M_h) & B_X^{(s)} &= B_X(m_{\tilde{\chi}_i^+}, M_{\tilde{d}_j}; m_t) \\
C_X^{(l)} &= C_X(m_i, M_{h^+}, M_W; m_c, m_t, M_h) & B_X^{(t)} &= B_X(m_i, M_{h^+}; m_t) \\
C_X^{(m)} &= C_X(m_i, M_{h^+}, M_{h^+}; m_c, m_t, M_h) & B_X^{(u)} &= B_X(m_{\tilde{\chi}_i^+}, M_{\tilde{d}_j}; m_c) \\
C_X^{(n)} &= C_X(m_i, M_{h^+}, M_W; m_c, m_t, M_h) & B_X^{(v)} &= B_X(m_i, M_{h^+}; m_c) \\
C_X^{(o)} &= C_X(m_i, M_W, M_{h^+}; m_c, m_t, M_h) & C_X^{(p)} &= C_X(M_{h^+}, m_i, m_i; m_c, m_t, M_h) \\
C_X^{(q)} &= C_X(m_{\tilde{\chi}_i^+}, M_{\tilde{d}_j}, M_{\tilde{d}_j}; m_c, m_t, M_h) & C_X^{(r)} &= C_X(M_{\tilde{d}_j}, m_{\tilde{\chi}_i^+}, m_{\tilde{\chi}_i^+}; m_c, m_t, M_h)
\end{aligned} \tag{B.8}$$

where  $X = 0, 11, 12, 21, 23, 24$ , as before, and defined two sets of effective couplings

$$\begin{aligned}
z_1^{(p)} &= X_{ci}^h B_{di}^h \\
z_2^{(p)} &= m_t Y_{ci}^h \frac{X_{ti}^h}{Y_{ti}^h} A_{di}^h + m_c X_{ci}^h B_{di}^h + m_i Y_{ci}^h B_{di}^h + m_i Y_{ci}^h A_{di}^h \\
z_3^{(p)} &= m_t \frac{X_{ti}^h}{Y_{ti}^h} A_{di}^h (m_i X_{ci}^h + m_c Y_{ci}^h) + m_i^2 A_{di}^h X_{ci}^h + m_i m_c A_{di}^h Y_{ci}^h \\
z_4^{(p)} &= Y_{ci}^h A_{di}^h \\
z_5^{(p)} &= m_t X_{ci}^h \frac{Y_{ti}^h}{X_{ti}^h} B_{di}^h + m_c Y_{ci}^h A_{di}^h + m_i X_{ci}^h A_{di}^h + m_i X_{ci}^h B_{di}^h \\
z_6^{(p)} &= m_t \frac{Y_{ti}^h}{X_{ti}^h} B_{di}^h (m_i Y_{ci}^h + m_c X_{ci}^h) + m_i^2 B_{di}^h Y_{ci}^h + m_i m_c B_{di}^h X_{ci}^h
\end{aligned} \tag{B.9}$$

and

$$\begin{aligned}
z_1^{(r)} &= X_{cj}^i B_{ij}^h \\
z_2^{(r)} &= m_t Y_{cj}^i \frac{X_{tj}^i}{Y_{tj}^i} A_{ij}^h + m_c X_{cj}^i B_{ij}^h + m_i Y_{cj}^i B_{ij}^h + m_i Y_{cj}^i A_{ij}^h \\
z_3^{(r)} &= m_t \frac{X_{tj}^i}{Y_{tj}^i} A_{ij}^h (m_i X_{cj}^i + m_c Y_{cj}^i) + m_i^2 A_{ij}^h X_{cj}^i + m_i m_c A_{ij}^h Y_{cj}^i \\
z_4^{(r)} &= Y_{cj}^i A_{ij}^h \\
z_5^{(r)} &= m_t X_{cj}^i \frac{Y_{tj}^i}{X_{tj}^i} B_{ij}^h + m_c Y_{cj}^i A_{ij}^h + m_i X_{cj}^i A_{ij}^h + m_i X_{cj}^i B_{ij}^h \\
z_6^{(r)} &= m_t \frac{Y_{tj}^i}{X_{tj}^i} B_{ij}^h (m_i Y_{cj}^i + m_c X_{cj}^i) + m_i^2 B_{ij}^h Y_{cj}^i + m_i m_c B_{ij}^h X_{cj}^i
\end{aligned} \tag{B.10}$$

As before, these form factors can now be combined, using  $F_{ni} = \sum_{A=a}^j F_{ni}^A$  for  $n = 1, 2$  and the results substituted into Eqn. (A.8) to get the final amplitude.

## B.2 The decay $t \rightarrow c + Z$

When we turn to the decay process  $t \rightarrow c + Z$ , then, as in the toy model, we have to calculate four helicity amplitudes in terms of four form factors  $F_1$ ,  $F_2$ ,  $F_3$  and  $F_4$ . For the Standard

Model, we then evaluate the diagrams of Figure 4, replacing the  $H$  everywhere by a  $Z$ . In order to do this, we set up the following general vertices.

$$\begin{aligned}
\bar{u}_i u_i Z^\mu & : ig\gamma^\mu (A_{ui}^Z P_L + B_{ui}^Z P_R) \\
\bar{d}_i d_i Z^\mu & : ig\gamma^\mu (A_{di}^Z P_L + B_{di}^Z P_R) \\
W^{\mu+} Z^\nu \phi^- & : ig\omega_{WZ}^\phi g^{\mu\nu} \\
Z^\mu \phi(p)^+ \phi'(q)^- & : ig\alpha_{\phi'}^\phi (p+q)^\mu \\
\bar{u}_i d_j \phi^+ & : ig \left( X_{ij}^\phi P_L + Y_{ij}^\phi P_R \right)
\end{aligned}$$

in terms of a set of coupling constants  $A_{ui}^Z, B_{ui}^Z, A_{di}^Z, B_{di}^Z, \omega_{WZ}^\phi, \alpha_{\phi'}^\phi, X_{ij}^\phi$  and  $Y_{ij}^\phi$ . In the SM, these have values given in the table below.

coupling :	$A_{ui}^Z$	$B_{ui}^Z$	$A_{di}^Z$	$B_{di}^Z$
SM :	$-\frac{g_L^u}{\cos \theta_W}$	$-\frac{g_R^u}{\cos \theta_W}$	$-\frac{g_L^u}{\cos \theta_W}$	$-\frac{g_R^u}{\cos \theta_W}$
coupling :	$\omega_{WZ}^\phi$	$\alpha_{\phi'}^\phi$	$X_{ij}^\phi$	$Y_{ij}^\phi$
SM :	$-M_Z \sin^2 \theta_W$	$-\frac{\cos 2\theta_W}{2 \cos \theta_W}$	$\frac{m_i}{\sqrt{2}M_W}$	$-\frac{m_j}{\sqrt{2}M_W}$

where

$$\begin{aligned}
g_L^u &= \frac{1}{2} - \frac{2}{3} \sin^2 \theta_W & g_R^u &= -\frac{2}{3} \sin^2 \theta_W \\
g_L^d &= -\frac{1}{2} + \frac{1}{3} \sin^2 \theta_W & g_R^d &= \frac{1}{3} \sin^2 \theta_W
\end{aligned} \tag{B.11}$$

As in the previous cases, we can now compute, using the diagrams of Figure 4 (with  $h^0 \rightarrow Z$ ) a set of forms factors. The set of  $F_1$  form factors are

$$\begin{aligned}
F_{1i}^{(a)} &= \frac{g^3 \cos \theta_W}{16\pi^2} \left[ 2m_t^2 (C_{21}^{(a)} - C_{23}^{(a)}) - 2C_{24}^{(a)} + (m_t^2 + m_c^2 - M_Z^2) C_{11}^{(a)} - m_c^2 C_{12}^{(a)} - (B_0^{(a)} - m_i^2 C_0^{(a)}) \right] \\
F_{1i}^{(b)} &= -\frac{g^3 \omega_{WZ}^{G+}}{16\sqrt{2}\pi^2} \left[ m_t X_{ti}^G (C_{11}^{(b)} - C_{12}^{(b)}) - m_i Y_{ti}^G C_0^{(b)} \right] \\
F_{1i}^{(c)} &= -\frac{g^3 \omega_{WZ}^{G+}}{16\sqrt{2}\pi^2} \left[ m_c X_{ci}^G C_{12}^{(c)} - 2m_i Y_{ci}^G C_0^{(c)} + 2m_t X_{ci}^G (C_{11}^{(c)} - C_{12}^{(c)}) \right] \\
F_{1i}^{(d)} &= -\frac{g^3 \alpha_{G-}^{G+}}{16\sqrt{2}\pi^2} \left[ m_t^2 Y_{ci}^G Y_{ti}^G (C_{21}^{(d)} - C_{23}^{(d)}) + m_c m_t X_{ci}^G X_{ti}^G C_{23}^{(d)} - 2Y_{ci}^G Y_{ti}^G C_{24}^{(d)} - m_i m_t Y_{ti}^G X_{ci}^G (C_0^{(d)} + C_{11}^{(d)}) \right] \\
F_{1i}^{(e)} &= \frac{g^3}{32\pi^2} \left[ A_{di}^Z \left\{ 2(m_c^2 + m_t^2 - M_Z^2 + m_c m_t) (C_0^{(e)} + C_{11}^{(e)}) + 2m_t^2 (C_{11}^{(e)} - C_{12}^{(e)}) + m_c^2 C_{12}^{(e)} + 2C_{24}^{(e)} \right. \right. \\
&\quad \left. \left. + 2m_i m_t (C_0^{(e)} + C_{11}^{(e)}) - B_0^{(e)} + M_W^2 C_0^{(e)} \right\} + 2m_i B_{di}^Z \left\{ m_t (C_0^{(e)} + C_{11}^{(e)}) - m_i C_0^{(e)} \right\} \right]
\end{aligned}$$

$$\begin{aligned}
F_{1i}^{(f)} &= -\frac{g^3}{16\pi^2} \left[ X_{ci}^G \left\{ \left( m_i + m_t \frac{Y_{ci}^G}{X_{ci}^G} \right) A_{di}^Z \left( m_c X_{ci}^G (C_0^{(f)} + C_{12}^{(f)}) + m_i Y_{ci}^G C_0^{(f)} \right) \right. \right. \\
&\quad \left. \left. - B_{di}^Z \left( m_c (m_i X_{ci}^G + m_c Y_{ci}^G) C_{12}^{(f)} - Y_{ci}^G (B_0^{(f)} - M_W^2 C_0^{(f)}) - m_t Y_{ci}^G (m_t C_{21}^{(f)} + m_c C_{23}^{(f)}) - 2C_{24}^{(f)} \right) \right\} \right. \\
&\quad \left. - m_t Y_{ci}^G A_{di}^Z (m_c X_{ci}^G + m_i Y_{ci}^G) C_{11}^{(f)} \right] \\
F_{1i}^{(g)} &= -\frac{g^3}{16\pi^2 (m_t^2 - m_c^2)} m_c^2 A_{ci}^Z B_1^{(g)} \\
F_{1i}^{(h)} &= -\frac{g^3}{16\pi^2 (m_t^2 - m_c^2)} A_{ti}^Z \left[ m_t X_{ti}^G \left( m_c X_{ci}^G B_1^{(h)} - m_i Y_{ci}^G B_0^{(h)} \right) + m_c Y_{ti}^G \left( Y_{ci}^G m_c B_1^{(h)} - m_i X_{ci}^G B_0^{(h)} \right) \right] \\
F_{1i}^{(i)} &= \frac{g^3}{32\pi^2 (m_t^2 - m_c^2)} m_t \left( m_t A_{ti}^Z + m_c B_{ti}^Z \right) B_1^{(i)} \\
F_{1i}^{(j)} &= \frac{g^3}{16\pi^2 (m_t^2 - m_c^2)} A_{ti}^Z Y_{ti}^G \left[ m_t Y_{ci}^G \left( m_t + m_c \frac{X_{ti}^G X_{ci}^G}{Y_{ti}^G Y_{ci}^G} \right) B_1^{(j)} - m_i X_{ci}^G \left( m_t \frac{Y_{ci}^G X_{ti}^G}{X_{ci}^G Y_{ti}^G} + m_c \right) B_0^{(j)} \right]
\end{aligned} \tag{B.12}$$

The nonvanishing  $F_2$  form factors are

$$\begin{aligned}
F_{2i}^{(a)} &= \frac{g^3 \cos \theta_W}{16\pi^2} m_c m_t (C_{11}^{(a)} - C_{12}^{(a)}) \\
F_{2i}^{(b)} &= -\frac{g^3 \omega_{WZ}^{G+}}{16\sqrt{2}\pi^2} (m_t - m_c) X_{ti}^G C_{12}^{(b)} \\
F_{2i}^{(c)} &= \frac{g^3 \omega_{WZ}^{G+}}{16\sqrt{2}\pi^2} m_t X_{ci}^G (C_{11}^{(c)} - C_{12}^{(c)}) \\
F_{2i}^{(d)} &= -\frac{g^3 \alpha_{G-}^{G+}}{16\sqrt{2}\pi^2} \left[ m_t^2 X_{ci}^G X_{ti}^G (C_{21}^{(d)} - C_{23}^{(d)}) + m_c m_t Y_{ci}^G Y_{ti}^G C_{23}^{(d)} - 2X_{ci}^G X_{ti}^G C_{24}^{(d)} - m_i m_t X_{ti}^G Y_{ci}^G (C_0^{(d)} + C_{11}^{(d)}) \right] \\
F_{2i}^{(e)} &= -\frac{g^3}{32\pi^2} A_{di}^Z \left[ m_t (m_t + m_c) (C_0^{(e)} + C_{11}^{(e)}) + m_t^2 (C_{11}^{(e)} - C_{12}^{(e)}) + m_c m_t C_{12}^{(e)} - m_t^2 C_{21}^{(e)} - m_t (m_t - m_c) C_{23}^{(e)} \right] \\
F_{2i}^{(f)} &= -\frac{g^3}{16\pi^2} \left[ Y_{ci}^G \left\{ \left( m_i + m_t \frac{X_{ci}^G}{Y_{ci}^G} \right) B_{di}^Z \left( m_c Y_{ci}^G (C_0^{(f)} + C_{12}^{(f)}) + m_i X_{ci}^G C_0^{(f)} \right) \right. \right. \\
&\quad \left. \left. - A_{di}^Z \left( m_c (m_i Y_{ci}^G + m_c X_{ci}^G) C_{12}^{(f)} - X_{ci}^G (B_0^{(f)} - M_W^2 C_0^{(f)}) - m_t Y_{ci}^G (m_t C_{21}^{(f)} + m_c C_{23}^{(f)}) - 2C_{24}^{(f)} \right) \right\} \right. \\
&\quad \left. - m_t X_{ci}^G B_{di}^Z (m_c Y_{ci}^G + m_i X_{ci}^G) C_{11}^{(f)} \right] \\
F_{2i}^{(g)} &= -\frac{g^3}{16\pi^2 (m_t^2 - m_c^2)} m_c m_t B_{ci}^Z B_1^{(g)} \\
F_{2i}^{(h)} &= -\frac{g^3}{16\pi^2 (m_t^2 - m_c^2)} B_{ti}^Z \left[ m_t Y_{ti}^G \left( m_c Y_{ci}^G B_1^{(h)} - m_i X_{ci}^G B_0^{(h)} \right) + m_c X_{ti}^G \left( m_c X_{ci}^G B_1^{(h)} - m_i Y_{ci}^G B_0^{(h)} \right) \right] \\
F_{2i}^{(j)} &= \frac{g^3}{16\pi^2 (m_t^2 - m_c^2)} B_{ti}^Z X_{ti}^G \left[ m_t X_{ci}^G \left( m_t + m_c \frac{Y_{ti}^G Y_{ci}^G}{X_{ti}^G X_{ci}^G} \right) B_1^{(j)} - m_i Y_{ci}^G \left( m_t \frac{X_{ci}^G Y_{ti}^G}{Y_{ci}^G X_{ti}^G} + m_c \right) B_0^{(j)} \right]
\end{aligned} \tag{B.13}$$

The nonvanishing  $F_3$  form factors are

$$\begin{aligned}
F_{3i}^{(a)} &= -\frac{g^3 \cos \theta_W}{32\pi^2} m_c \left[ C_{11}^{(a)} + 2C_{12}^{(a)} \right] \\
F_{3i}^{(c)} &= \frac{g^3 \omega_{WZ}^{G+}}{16\sqrt{2}\pi^2} X_{ci}^G (C_{11}^{(c)} - C_{12}^{(c)}) \\
F_{3i}^{(d)} &= \frac{g^3 \alpha_{G-}^{G+}}{16\sqrt{2}\pi^2} \left[ m_t X_{ci}^G X_{ti}^G (C_{21}^{(d)} - C_{23}^{(d)}) - m_c Y_{ci}^G Y_{ti}^G C_{23}^{(d)} + m_i Y_{ti}^G X_{ci}^G (C_0^{(d)} + C_{11}^{(d)}) \right] \\
F_{3i}^{(e)} &= \frac{g^3}{32\pi^2} A_{di}^Z \left[ (m_t + m_c) (C_0^{(e)} + C_{11}^{(e)}) + m_t (C_{11}^{(e)} - C_{12}^{(e)}) + m_c C_{12}^{(e)} - m_t C_{21}^{(e)} - (m_t - m_c) C_{23}^{(e)} \right] \\
F_{3i}^{(f)} &= \frac{g^3}{16\pi^2} X_{ci}^G \left[ A_{di}^Z \left( m_i + m_t \frac{Y_{ci}^G}{X_{ci}^G} \right) X_{ci}^G (C_{11}^{(f)} - C_{12}^{(f)}) \right. \\
&\quad \left. - B_{di}^Z \left\{ \left( m_i X_{ci}^G + m_c Y_{ci}^G \right) (C_{11}^{(f)} - C_{12}^{(f)}) + (m_i X_{ci}^G + m_c Y_{ci}^G) C_{11}^{(f)} + Y_{ci}^G (m_t C_{21}^{(f)} + m_c C_{23}^{(f)}) \right\} \right]
\end{aligned} \tag{B.14}$$

The nonvanishing  $F_4$  form factors are

$$\begin{aligned}
F_{4i}^{(a)} &= \frac{g^3 \cos \theta_W}{16\pi^2} m_t \{2(C_{11}^{(a)} - C_{12}^{(a)}) - (C_{21}^{(a)} - C_{23}^{(a)})\} \\
F_{4i}^{(b)} &= -\frac{g^3 \omega_{WZ}^{G+}}{16\sqrt{2}\pi^2} X_{ti}^G C_{12}^{(b)} \\
F_{4i}^{(d)} &= \frac{g^3 \alpha_{G-}^{G+}}{16\sqrt{2}\pi^2} \left[ m_t Y_{ci}^G Y_{ti}^G (C_{21}^{(d)} - C_{23}^{(d)}) - m_c X_{ci}^G X_{ti}^G C_{23}^{(d)} + m_i X_{ti}^G Y_{ci}^G (C_0^{(d)} + C_{11}^{(d)}) \right] \\
F_{4i}^{(e)} &= -\frac{g^3}{16\pi^2} m_i (A_{di}^Z + B_{di}^Z) (C_0^{(e)} + C_{11}^{(e)}) \\
F_{4i}^{(f)} &= \frac{g^3}{16\pi^2} Y_{ci}^G \left[ B_{di}^Z \left( m_i + m_t \frac{X_{ci}^G}{Y_{ci}^G} \right) Y_{ci}^G (C_{11}^{(f)} - C_{12}^{(f)}) \right. \\
&\quad \left. - A_{di}^Z \left\{ (m_i Y_{ci}^G + m_c X_{ci}^G) (C_{11}^{(f)} - C_{12}^{(f)}) + (m_i Y_{ci}^G + m_c X_{ci}^G) C_{11}^{(f)} + X_{ci}^G (m_t C_{21}^{(f)} + m_c C_{23}^{(f)}) \right\} \right]
\end{aligned} \tag{B.15}$$

where

$$\begin{aligned}
C_X^{(a)} &= C_X(m_i, M_W, M_W; m_c, m_t, M_Z) & B_0^{(e)} &= B_0(M_W, m_i; M_Z) \\
C_X^{(b)} &= C_X(m_i, M_W, M_W; m_c, m_t, M_Z) & B_1^{(g)} &= B_1(m_i, M_W; m_t) \\
C_X^{(c)} &= C_X(m_i, M_W, M_W; m_c, m_t, M_Z) & B_1^{(h)} &= B_1(m_i, M_W; m_t) \\
C_X^{(d)} &= C_X(m_i, M_W, M_W; m_c, m_t, M_Z) & B_0^{(h)} &= B_0(m_i, M_W; m_t) \\
C_X^{(e)} &= C_X(M_W, m_i, m_i; m_c, m_t, M_Z) & B_1^{(i)} &= B_1(m_i, M_W; m_c) \\
C_X^{(f)} &= C_X(M_W, m_i, m_i; m_c, m_t, M_Z) & B_1^{(j)} &= B_1(m_i, M_W; m_c) \\
B_0^{(a)} &= B_0(M_W, M_W; M_Z) & B_0^{(j)} &= B_0(m_i, M_W; m_c)
\end{aligned} \tag{B.16}$$

where  $X = 0, 11, 12, 21, 23, 24$ , as usual. We then calculate the total form factors using  $F_{ni} = \sum_{A=a}^j F_{ni}^A$  for  $n = 1, 2, 3, 4$  and substitute the results into Eqn. (A.23) to get the final SM amplitude.

In the cMSSM, we require to evaluate all the diagrams which contribute in the SM, i.e. those which are listed in Figure 4. This will involve all the vertices we have defined for the SM, but the coupling constants will be somewhat different. These are listed in the table below.

coupling :	$A_{ui}^Z$	$B_{ui}^Z$	$A_{di}^Z$	$B_{di}^Z$
SM :	$-\frac{g_L^u}{\cos \theta_W}$	$-\frac{g_R^u}{\cos \theta_W}$	$-\frac{g_L^u}{\cos \theta_W}$	$-\frac{g_R^u}{\cos \theta_W}$
coupling :	$\omega_{WZ}^{G+}$	$\alpha_{G-}^{G+}$	$X_{ij}^{H+}$	$Y_{ij}^{H+}$
SM :	$-M_Z \sin^2 \theta_W$	$-\frac{\cos 2\theta_W}{2 \cos \theta_W}$	$\frac{m_i \cot \beta}{\sqrt{2} M_W}$	$\frac{m_j \tan \beta}{\sqrt{2} M_W}$

Due to the absence of a  $W^\pm H^\mp Z$  vertex (whereas there is a  $W^\pm H^\mp h^0$  vertex, the list of additional diagrams in the cMSSM can be obtained by changing the  $H$  lines in Figure 5 to  $Z$  lines, provided we discard the diagrams marked  $(k)$ ,  $(\ell)$ ,  $(n)$  and  $(o)$ . Evaluating the remaining

ones we get the  $F_1$  form factors

$$\begin{aligned}
F_{1i}^{(m)} &= -\frac{g^3 \alpha_{h+}^{\bar{h}}}{16\sqrt{2}\pi^2} \left[ m_t^2 (C_{21}^{(m)} - C_{23}^{(m)}) Y_{ci}^h Y_{ti}^h + m_c m_t C_{23}^{(m)} X_{ci}^h X_{ti}^h - 2C_{24}^{(m)} Y_{ci}^h Y_{ti}^h - m_i m_t (C_0^{(m)} + C_{11}^{(m)}) Y_{ti}^h X_{ci}^h \right] \\
F_{1i}^{(p)} &= -\frac{g^3}{16\pi^2} \left[ X_{ci}^h \left\{ \left( m_i + m_t \frac{Y_{ci}^h}{X_{ci}^h} \right) A_{di}^Z \left( X_{ci}^h m_c (C_0^{(p)} + C_{12}^{(p)}) + m_i Y_{ci}^h C_0^{(p)} \right) \right. \right. \\
&\quad \left. \left. - B_{di}^Z \left( (m_i X_{ci}^h + m_c Y_{ci}^h) m_c C_{12}^{(p)} - Y_{ci}^h (B_0^{(p)} - M_{h+}^2 + C_0^{(p)}) - m_t Y_{ci}^h (m_t C_{21}^{(p)} + m_c C_{23}^{(p)}) - 2C_{24}^{(p)} \right) \right\} \right. \\
&\quad \left. - m_t A_{di}^Z Y_{ci}^h (m_i Y_{ci}^h + m_c X_{ci}^h) C_{11}^{(p)} \right] \\
F_{1i}^{(q)} &= -\frac{g^3 \alpha_d^{\bar{d}}}{16\sqrt{2}\pi^2} \left[ m_t^2 Y_{ci}^j Y_{ti}^j (C_{21}^{(q)} - C_{23}^{(q)}) + m_c m_t X_{ci}^j X_{ti}^j C_{23}^{(q)} - 2Y_{ci}^j Y_{ti}^j C_{24}^{(q)} - m_i m_t Y_{ti}^j X_{ci}^j (C_0^{(m)} + C_{11}^{(q)}) \right] \\
F_{1i}^{(r)} &= -\frac{g^3}{16\pi^2} \left[ X_{ci}^j \left\{ \left( m_i + m_t \frac{Y_{ci}^j}{X_{ci}^j} \right) A_{di}^Z \left( X_{ci}^j m_c (C_0^{(r)} + C_{12}^{(r)}) + m_i Y_{ci}^j C_0^{(r)} \right) \right. \right. \\
&\quad \left. \left. - B_{di}^Z \left( (m_i X_{ci}^j + m_c Y_{ci}^j) m_c C_{12}^{(r)} - Y_{ci}^j (B_0^{(r)} - M_{dj}^2 + C_0^{(r)}) - Y_{ci}^j (m_t C_{21}^{(r)} + m_c C_{23}^{(r)}) m_t - 2C_{24}^{(r)} \right) \right\} \right. \\
&\quad \left. - m_t A_{di}^Z Y_{ci}^j (m_i Y_{ci}^j + m_c X_{ci}^j) C_{11}^{(r)} \right] \\
F_{1i}^{(s)} &= \frac{g^3}{16\pi^2 (m_t^2 - m_c^2)} A_{ci}^Z Y_{ti}^h \left[ m_t Y_{ci}^h \left( m_t + m_c \frac{X_{ti}^h X_{ci}^h}{Y_{ti}^h Y_{ci}^h} \right) B_1^{(s)} - m_i X_{ci}^h \left( m_t \frac{Y_{ci}^h X_{ti}^h}{X_{ci}^h Y_{ti}^h} + m_c \right) B_0^{(s)} \right] \\
F_{1i}^{(t)} &= \frac{g^3}{16\pi^2 (m_t^2 - m_c^2)} A_{ci}^Z Y_{ti}^j \left[ m_t Y_{ci}^j \left( m_t + m_c \frac{X_{ti}^j X_{ci}^j}{Y_{ti}^j Y_{ci}^j} \right) B_1^{(t)} - m_i X_{ci}^j \left( m_t \frac{Y_{ci}^j X_{ti}^j}{X_{ci}^j Y_{ti}^j} + m_c \right) B_0^{(t)} \right] \\
F_{1i}^{(u)} &= -\frac{g^3}{16\pi^2 (m_t^2 - m_c^2)} A_{ti}^Z \left[ m_c Y_{ti}^h (m_c Y_{ci}^h B_1^{(u)} - m_i X_{ci}^h B_0^{(u)}) + m_t X_{ti}^h (m_c X_{ci}^h B_1^{(u)} - m_i Y_{ci}^h B_0^{(u)}) \right] \\
F_{1i}^{(v)} &= -\frac{g^3}{16\pi^2 (m_t^2 - m_c^2)} A_{ti}^Z \left[ m_c Y_{ti}^j (m_c Y_{ci}^j B_1^{(r)} - m_i X_{ci}^j B_0^{(r)}) + m_t X_{ti}^j (m_c X_{ci}^j B_1^{(r)} - m_i Y_{ci}^j B_0^{(r)}) \right] \quad (B.17)
\end{aligned}$$

The  $F_2$  form factors are

$$\begin{aligned}
F_{2i}^{(m)} &= -\frac{g^3 \alpha_{h+}^{\bar{h}}}{16\sqrt{2}\pi^2} \left[ m_t^2 X_{ci}^h X_{ti}^h (C_{21}^{(m)} - C_{23}^{(m)}) + m_c m_t Y_{ci}^h Y_{ti}^h C_{23}^{(m)} - 2X_{ci}^h X_{ti}^h C_{24}^{(m)} - m_i m_t X_{ti}^h Y_{ci}^h (C_0^{(m)} + C_{11}^{(m)}) \right] \\
F_{2i}^{(p)} &= -\frac{g^3}{16\pi^2} \left[ Y_{ci}^h \left\{ \left( m_i + m_t \frac{X_{ci}^h}{Y_{ci}^h} \right) B_{di}^Z \left( Y_{ci}^h m_c (C_0^{(p)} + C_{12}^{(p)}) + m_i X_{ci}^h C_0^{(p)} \right) \right. \right. \\
&\quad \left. \left. - A_{di}^Z \left( (m_i Y_{ci}^h + m_c X_{ci}^h) m_c C_{12}^{(p)} - X_{ci}^h (B_0^{(p)} - M_{h+}^2 + C_0^{(p)}) - m_t X_{ci}^h (m_t C_{21}^{(p)} + m_c C_{23}^{(p)}) - 2C_{24}^{(p)} \right) \right\} \right. \\
&\quad \left. - m_t B_{di}^Z X_{ci}^h (m_i X_{ci}^h + m_c Y_{ci}^h) C_{11}^{(p)} \right] \\
F_{2i}^{(q)} &= -\frac{g^3 \alpha_d^{\bar{d}}}{16\sqrt{2}\pi^2} \left[ m_t^2 X_{ci}^j X_{ti}^j (C_{21}^{(q)} - C_{23}^{(q)}) + m_c m_t Y_{ci}^j Y_{ti}^j C_{23}^{(q)} - 2X_{ci}^j X_{ti}^j C_{24}^{(q)} - m_i m_t Y_{ti}^j X_{ci}^j (C_0^{(m)} + C_{11}^{(q)}) \right] \\
F_{2i}^{(r)} &= -\frac{g^3}{16\pi^2} \left[ Y_{ci}^j \left\{ \left( m_i + m_t \frac{X_{ci}^j}{Y_{ci}^j} \right) B_{di}^Z \left( Y_{ci}^j m_c (C_0^{(r)} + C_{12}^{(r)}) + m_i X_{ci}^j C_0^{(r)} \right) \right. \right. \\
&\quad \left. \left. - B_{di}^Z \left( (m_i Y_{ci}^j + m_c X_{ci}^j) m_c C_{12}^{(r)} - X_{ci}^j (B_0^{(r)} - M_{dj}^2 + C_0^{(r)}) - X_{ci}^j (m_t C_{21}^{(r)} + m_c C_{23}^{(r)}) m_t - 2C_{24}^{(r)} \right) \right\} \right. \\
&\quad \left. - m_t B_{di}^Z X_{ci}^j (m_i X_{ci}^j + m_c Y_{ci}^j) C_{11}^{(r)} \right] \\
F_{2i}^{(s)} &= \frac{g^3}{16\pi^2 (m_t^2 - m_c^2)} B_{ci}^Z X_{ti}^h \left[ m_t X_{ci}^h \left( m_t + m_c \frac{Y_{ti}^h Y_{ci}^h}{X_{ti}^h X_{ci}^h} \right) B_1^{(s)} - m_i Y_{ci}^h \left( m_t \frac{X_{ci}^h Y_{ti}^h}{Y_{ci}^h X_{ti}^h} + m_c \right) B_0^{(s)} \right] \\
F_{2i}^{(t)} &= \frac{g^3}{16\pi^2 (m_t^2 - m_c^2)} B_{ci}^Z X_{ti}^j \left[ m_t X_{ci}^j \left( m_t + m_c \frac{Y_{ti}^j Y_{ci}^j}{X_{ti}^j X_{ci}^j} \right) B_1^{(t)} - m_i Y_{ci}^j \left( m_t \frac{X_{ci}^j Y_{ti}^j}{Y_{ci}^j X_{ti}^j} + m_c \right) B_0^{(t)} \right] \\
F_{2i}^{(u)} &= -\frac{g^3}{16\pi^2 (m_t^2 - m_c^2)} B_{ti}^Z \left[ m_c X_{ti}^h (m_c X_{ci}^h B_1^{(u)} - m_i Y_{ci}^h B_0^{(u)}) + m_t Y_{ti}^h (m_c Y_{ci}^h B_1^{(u)} - m_i X_{ci}^h B_0^{(u)}) \right] \\
F_{2i}^{(v)} &= -\frac{g^3}{16\pi^2 (m_t^2 - m_c^2)} B_{ti}^Z \left[ m_c X_{ti}^j (m_c X_{ci}^j B_1^{(r)} - m_i Y_{ci}^j B_0^{(r)}) + m_t Y_{ti}^j (m_c Y_{ci}^j B_1^{(r)} - m_i X_{ci}^j B_0^{(r)}) \right] \quad (B.18)
\end{aligned}$$



The nonvanishing  $F_3$  form factors are

$$\begin{aligned}
F_{3i}^{(m)} &= \frac{g^3 \alpha_{h+}^-}{16\sqrt{2}\pi^2} \left[ m_t X_{ci}^h X_{ti}^h (C_{21}^{(m)} - C_{23}^{(m)}) - m_c Y_{ci}^h Y_{ti}^h C_{23}^{(m)} + m_i Y_{ti}^h X_{ci}^h (C_0^{(m)} + C_{11}^{(m)}) \right] \\
F_{3i}^{(p)} &= \frac{g^3}{16\pi^2} X_{ci}^h \left[ A_{di}^Z \left( m_i + m_t \frac{Y_{ci}^h}{X_{ci}^h} \right) X_{ci}^h (C_{11}^{(p)} - C_{12}^{(p)}) \right. \\
&\quad \left. - B_{di}^Z \left\{ (m_i X_{ci}^h + m_c Y_{ci}^h) (C_{11}^{(p)} - C_{12}^{(p)}) + (m_i X_{ci}^h + m_c Y_{ci}^h) C_{11}^{(p)} + Y_{ci}^h (m_t C_{21}^{(p)} + m_c C_{23}^{(p)}) \right\} \right] \\
F_{3i}^{(q)} &= \frac{g^3 \alpha_d^j}{16\sqrt{2}\pi^2} \left[ m_t X_{ci}^j X_{ti}^j (C_{21}^{(q)} - C_{23}^{(q)}) - m_c Y_{ci}^j Y_{ti}^j C_{23}^{(q)} + m_i Y_{ti}^j X_{ci}^j (C_0^{(m)} + C_{11}^{(q)}) \right] \\
F_{3i}^{(r)} &= \frac{g^3}{16\pi^2} X_{ci}^j \left[ A_{di}^Z \left( m_i + m_t \frac{Y_{ci}^j}{X_{ci}^j} \right) X_{ci}^j (C_{11}^{(r)} - C_{12}^{(r)}) \right. \\
&\quad \left. - B_{di}^Z \left\{ (m_i X_{ci}^j + m_c Y_{ci}^j) (C_{11}^{(r)} - C_{12}^{(r)}) + (m_i X_{ci}^j + m_c Y_{ci}^j) C_{11}^{(r)} + Y_{ci}^j (m_t C_{21}^{(r)} + m_c C_{23}^{(r)}) \right\} \right] \tag{B.19}
\end{aligned}$$

Finally, the nonvanishing  $F_4$  form factors are

$$\begin{aligned}
F_{4i}^{(m)} &= \frac{g^3 \alpha_{h+}^-}{16\sqrt{2}\pi^2} \left[ m_t Y_{ci}^h Y_{ti}^h (C_{21}^{(m)} - C_{23}^{(m)}) - m_c X_{ci}^h X_{ti}^h C_{23}^{(m)} + m_i X_{ti}^h Y_{ci}^h (C_0 + C_{11}^{(m)}) \right] \\
F_{4i}^{(p)} &= \frac{g^3}{16\pi^2} X_{ci}^h \left[ B_{di}^Z \left( m_i + m_t \frac{X_{ci}^h}{Y_{ci}^h} \right) Y_{ci}^h (C_{11}^{(p)} - C_{12}^{(p)}) \right. \\
&\quad \left. - A_{di}^Z \left\{ (m_i Y_{ci}^h + m_c X_{ci}^h) (C_{11}^{(p)} - C_{12}^{(p)}) + (m_i Y_{ci}^h + m_c X_{ci}^h) C_{11}^{(p)} + X_{ci}^h (m_t C_{21}^{(p)} + m_c C_{23}^{(p)}) \right\} \right] \\
F_{4i}^{(q)} &= \frac{g^3 \alpha_d^j}{16\sqrt{2}\pi^2} \left[ m_t Y_{ci}^j Y_{ti}^j (C_{21}^{(q)} - C_{23}^{(q)}) - m_c X_{ci}^j X_{ti}^j C_{23}^{(q)} + m_i X_{ti}^j Y_{ci}^j (C_0 + C_{11}^{(q)}) \right] \\
F_{4i}^{(r)} &= \frac{g^3}{16\pi^2} X_{ci}^j \left[ B_{di}^Z \left( m_i + m_t \frac{X_{ci}^j}{Y_{ci}^j} \right) Y_{ci}^j (C_{11}^{(r)} - C_{12}^{(r)}) \right. \\
&\quad \left. - A_{di}^Z \left\{ (m_i Y_{ci}^j + m_c X_{ci}^j) (C_{11}^{(r)} - C_{12}^{(r)}) + (m_i Y_{ci}^j + m_c X_{ci}^j) C_{11}^{(r)} + X_{ci}^j (m_t C_{21}^{(r)} + m_c C_{23}^{(r)}) \right\} \right] \tag{B.20}
\end{aligned}$$

where we have used

$$\begin{aligned}
C_X^{(m)} &= C_X(m_i, M_{h+}, M_{h+}; m_c, m_t, M_Z) & B_0^{(m)} &= B_0(M_{h+}, M_{h+}; M_Z) \\
C_X^{(p)} &= C_X(M_{h+}, m_i, m_i; m_c, m_t, M_Z) & B_0^{(q)} &= B_X(M_{\tilde{d}_j}, M_{\tilde{d}_j}; M_Z) \\
C_X^{(q)} &= C_X(m_{\tilde{\chi}_i^+}, M_{\tilde{d}_j}, M_{\tilde{d}_j}; m_c, m_t, M_Z) & B_X^{(s)} &= B_X(m_i, M_{h+}; m_t) \\
C_X^{(r)} &= C_X(M_{\tilde{d}_j}, m_{\tilde{\chi}_i^+}, m_{\tilde{\chi}_i^+}; m_c, m_t, M_Z) & B_X^{(t)} &= B_X(m_{\tilde{\chi}_i^+}, M_{\tilde{d}_j}; m_t) \\
B_X^{(u)} &= B_X(m_i, M_{h+}; m_t) & B_X^{(v)} &= B_X(m_{\tilde{\chi}_i^+}, M_{\tilde{d}_j}; m_c) \tag{B.21}
\end{aligned}$$

for  $X = 0, 11, 12, 21, 23, 24$ , as usual. It is now a simple matter to calculate the total form factors using  $F_{ni} = \sum_{A=a}^j F_{ni}^A$  for  $n = 1, 2, 3, 4$  and substitute the results into Eqn. (A.23) to get the final cMSSM amplitude.

## Appendix C RPV-MSSM amplitudes

### C.1 The decay $t \rightarrow c + H$

Since the RPV-MSSM is merely an extension of the MSSM, it will contain all the diagrams of Figures 4 and 5. However, as we have seen in the text, these contributions are small, and

the  $R$ -parity violating contributions can be much larger. It is sensible, therefore, to calculate these alone. To have a unified picture, we include both  $\lambda'_{ijk}$  and  $\lambda''_{ijk}$  couplings when listing the diagrams in Figure 7, though only one set at a time can contribute. In terms of these, the  $F_1$  form factors are

$$\begin{aligned}
F_{1ik}^{1a} &= gM_W \beta_{\bar{e}_i \bar{e}_i}^h \frac{\lambda'_{i2k} \lambda'_{i3k}}{16\pi^2} m_c C_{12}^{(a)} \\
F_{1ik}^{1b} &= \frac{y_{d_k} \lambda'_{i2k} \lambda'_{i3k}}{16\pi^2} m_c M_{\tilde{d}_k} \left[ C_0^{(b)} + 2C_{12}^{(b)} \right] \\
F_{1ik}^{1c} &= gM_W \beta_{\tilde{d}_k \tilde{d}_k}^h \frac{\lambda'_{i2k} \lambda'_{i3k}}{16\pi^2} m_c C_{12}^{(c)} \\
F_{1ik}^{1d} &= \frac{y_{l_i} \lambda'_{i2k} \lambda'_{i3k}}{16\pi^2} m_c m_{l_i} \left[ C_0^{(d)} + 2C_{12}^{(d)} \right] \\
F_{1ik}^{1e} &= -\frac{y_t \lambda'_{i2k} \lambda'_{i3k}}{16\pi^2 (m_t^2 - m_c^2)} m_c m_t B_1^{(e)} \\
F_{1ik}^{1f} &= \frac{y_c \lambda'_{i2k} \lambda'_{i3k}}{16\pi^2 (m_t^2 - m_c^2)} m_t (m_t + m_c) B_1^{(f)} \\
F_{1jk}^{1g} &= gM_W \beta_{\tilde{d}_k \tilde{d}_k}^h \frac{\lambda''_{2jk} \lambda''_{3jk}}{16\pi^2} m_t \left[ C_{11}^{(g)} - C_{12}^{(g)} \right] \\
F_{1jk}^{1h} &= \frac{y_{d_k} \lambda''_{2jk} \lambda''_{3jk}}{16\pi^2} m_t m_{d_i} \left[ C_0^{(h)} + 2 \left( C_{11}^{(h)} - C_{12}^{(h)} \right) \right] \\
F_{1jk}^{1i} &= \frac{y_t \lambda''_{2jk} \lambda''_{3jk}}{16\pi^2 (m_t^2 - m_c^2)} m_c m_t B_1^{(i)} \\
F_{1jk}^{1j} &= -\frac{y_c \lambda''_{2jk} \lambda''_{3jk}}{16\pi^2 (m_t^2 - m_c^2)} m_t (m_t + m_c) B_1^{(j)} \tag{C.1}
\end{aligned}$$

and the  $F_2$  form factors are

$$\begin{aligned}
F_{1ik}^{2a} &= gM_W \beta_{\bar{e}_i \bar{e}_i}^h \frac{\lambda'_{i2k} \lambda'_{i3k}}{16\pi^2} m_t \left[ C_{11}^{(a)} - C_{12}^{(a)} \right] \\
F_{1ik}^{2b} &= \frac{y_{d_k} \lambda'_{i2k} \lambda'_{i3k}}{16\pi^2} m_t m_{d_k} \left[ C_0^{(b)} + 2(C_{11}^{(b)} - C_{12}^{(b)}) \right] \\
F_{1ik}^{2c} &= gM_W \beta_{\tilde{d}_k \tilde{d}_k}^h \frac{\lambda'_{i2k} \lambda'_{i3k}}{16\pi^2} m_t \left[ C_{11}^{(c)} - C_{12}^{(c)} \right] \\
F_{1ik}^{2d} &= \frac{y_{l_i} \lambda'_{i2k} \lambda'_{i3k}}{16\pi^2} m_t m_{l_i} \left[ C_0^{(d)} + 2 \left( C_{11}^{(d)} - C_{12}^{(d)} \right) \right] \\
F_{1ik}^{2e} &= -\frac{y_t \lambda'_{i2k} \lambda'_{i3k}}{16\pi^2 (m_t^2 - m_c^2)} m_c^2 B_1^{(e)} \\
F_{1jk}^{2g} &= gM_W \beta_{\tilde{d}_k \tilde{d}_k}^h \frac{\lambda''_{2jk} \lambda''_{3jk}}{16\pi^2} m_c C_{12}^{(g)} \\
F_{1jk}^{2h} &= \frac{y_{d_k} \lambda''_{2jk} \lambda''_{3jk}}{16\pi^2} m_c M_{\tilde{d}_k} \left[ C_0^{(h)} + 2C_{12}^{(h)} \right] \\
F_{1jk}^{2i} &= \frac{y_t \lambda''_{2jk} \lambda''_{3jk}}{16\pi^2 (m_t^2 - m_c^2)} m_c^2 B_1^{(i)} \tag{C.2}
\end{aligned}$$

in terms of

$$\begin{aligned}
C_X^{(a)} &= C_X(m_k, M_{\tilde{e}_i}, M_{\tilde{e}_i}; m_c, m_t, M_h) & B_1^{(e)} &= B_1(m_k, M_{\tilde{e}_i}; m_c) \\
C_X^{(b)} &= C_X(M_{\tilde{e}_i}, m_k, m_k; m_c, m_t, M_h) & B_1^{(f)} &= B_1(m_k, M_{\tilde{e}_i}; m_c) \\
C_X^{(c)} &= C_X(m_i, M_{\tilde{d}_k}, M_{\tilde{d}_k}; m_c, m_t, M_h) & B_1^{(i)} &= B_1(m_j, M_{\tilde{d}_k}; m_t) \\
C_X^{(d)} &= C_X(M_{\tilde{d}_k}, m_{e_i}, m_{e_i}; m_c, m_t, M_h) & B_1^{(j)} &= B_1(m_j, M_{\tilde{d}_k}; m_t) \\
C_X^{(g)} &= C_X(m_j, M_{\tilde{d}_k}, M_{\tilde{d}_k}; m_c, m_t, M_h) & C_X^{(h)} &= C_X(M_{\tilde{d}_k}, m_j, m_j; m_c, m_t, M_h)
\end{aligned} \tag{C.3}$$

where, as usual,  $X = 0, 11, 12, 21, 23, 24$ . As before, we go on to compute total form factors using  $F_{ni} = \sum_{A=a}^j F_{ni}^A$  for  $n = 1, 2$  and substitute the results into Eqn. (A.8) to get the amplitude in the RPV-MSSM.

## C.2 The decay $t \rightarrow c + Z$

The Feynman diagrams for the decay  $t \rightarrow c + Z$  are the same as those in Figure 7, with  $h^0 \rightarrow Z$ , as we have seen before. As before, we present the amplitudes for the  $\lambda'$  and  $\lambda''$  couplings together, though either one or the other must be zero.

The  $F_1$  form factors are

$$\begin{aligned}
F_{1ik}^{1a} &= \frac{g_{Ze} \lambda'_{i2k} \lambda'_{i3k}}{16\pi^2} \left[ m_t^2 (C_{11}^{(a)} - C_{12}^{(a)} + C_{21}^{(a)} - C_{23}^{(a)}) - 2C_{24}^{(a)} \right] \\
F_{1ik}^{1b} &= \frac{\lambda'_{i2k} \lambda'_{i3k}}{16\pi^2} \left[ g_{dR} (m_t^2 (C_{21}^{(b)} - C_{23}^{(b)}) - 2C_{24}^{(b)} + B_0^{(b)} - M_{\tilde{e}_i}^2 C_0^{(b)}) + g_{dL} m_k^2 C_0^{(b)} \right] \\
F_{1ik}^{1c} &= \frac{g_{Ze} \lambda'_{i2k} \lambda'_{i3k}}{16\pi^2} \left[ m_t^2 (C_{11}^{(c)} - C_{12}^{(c)} + C_{21}^{(c)} - C_{23}^{(c)}) - 2C_{24}^{(c)} \right] \\
F_{1ik}^{1d} &= \frac{\lambda'_{i2k} \lambda'_{i3k}}{16\pi^2} \left[ g_{eR} (m_t^2 (C_{21}^{(d)} - C_{23}^{(d)}) - 2C_{24}^{(d)} + B_0^{(d)} - M_{\tilde{d}_k}^2 C_0^{(d)}) + g_{eL} m_i^2 C_0^{(d)} \right] \\
F_{1ik}^{1e} &= -\frac{\lambda'_{i2k} \lambda'_{i3k}}{16\pi^2 (m_t^2 - m_c^2)} g_{uL} m_t^2 B_1^{(e)} \\
F_{1ik}^{1f} &= \frac{\lambda'_{i2k} \lambda'_{i3k}}{16\pi^2 (m_t^2 - m_c^2)} g_{uL} m_c^2 B_1^{(f)} \\
F_{1jk}^{1g} &= \frac{g_{Ze} \lambda''_{2jk} \lambda''_{3jk}}{16\pi^2} m_t m_c (C_{12}^{(g)} + C_{23}^{(g)}) \\
F_{1jk}^{1h} &= \frac{\lambda''_{2jk} \lambda''_{3jk}}{16\pi^2} g_{dL} \left[ m_c m_t C_{23}^{(h)} + m_t (m_t (C_{11}^{(h)} - C_{12}^{(h)}) + m_c C_{12}^{(h)}) + m_c m_t C_{11}^{(h)} \right] \\
F_{1jk}^{1i} &= -\frac{\lambda''_{2jk} \lambda''_{3jk}}{16\pi^2 (m_t^2 - m_c^2)} g_{uL} m_c m_t B_1^{(i)} \\
F_{1jk}^{1j} &= \frac{\lambda''_{2jk} \lambda''_{3jk}}{16\pi^2 (m_t^2 - m_c^2)} g_{uL} m_c m_t B_1^{(j)}
\end{aligned} \tag{C.4}$$

The  $F_2$  form factors are

$$\begin{aligned}
F_{1ik}^{2a} &= \frac{gZe\lambda'_{i2k}\lambda'_{i3k}}{16\pi^2}m_tm_c\left(C_{12}^{(a)}+C_{23}^{(a)}\right) \\
F_{1ik}^{2b} &= \frac{\lambda'_{i2k}\lambda'_{i3k}}{16\pi^2}g_{dR}\left(m_t^2(C_{11}^{(b)}-C_{12}^{(b)})+m_cm_t(C_{11}^{(b)}+C_{12}^{(b)}+C_{23}^{(b)})\right) \\
F_{1ik}^{2c} &= \frac{gZd\lambda'_{i2k}\lambda'_{i3k}}{16\pi^2}m_tm_c\left(C_{12}^{(c)}+C_{23}^{(c)}\right) \\
F_{1ik}^{2d} &= \frac{\lambda'_{i2k}\lambda'_{i3k}}{16\pi^2}g_{eR}\left[m_cm_tC_{23}^{(d)}+m_t\left(m_t(C_{11}^{(d)}-C_{12}^{(d)})+m_cC_{12}^{(d)}\right)+m_cm_tC_{11}^{(d)}\right] \\
F_{1ik}^{2e} &= -\frac{\lambda'_{i2k}\lambda'_{i3k}}{16\pi^2(m_t^2-m_c^2)}g_{uR}m_cm_tB_1^{(e)} \\
F_{1ik}^{2f} &= \frac{\lambda'_{i2k}\lambda'_{i3k}}{16\pi^2(m_t^2-m_c^2)}g_{uR}m_cm_tB_1^{(f)} \\
F_{1jk}^{2g} &= \frac{gZd\lambda''_{2jk}\lambda''_{3jk}}{16\pi^2}\left[m_t^2\left(C_{11}^{(g)}-C_{12}^{(g)}+C_{21}^{(g)}-C_{23}^{(g)}\right)-2C_{24}^{(g)}\right] \\
F_{1jk}^{2h} &= \frac{\lambda''_{2jk}\lambda''_{3jk}}{16\pi^2}\left[g_{dL}\left(m_t^2(C_{21}^{(h)}-C_{23}^{(h)})-2C_{24}^{(h)}+B_0^{(h)}-M_{\tilde{d}_k}^2C_0^{(h)}\right)+g_{dR}m_j^2C_0^{(h)}\right] \\
F_{1jk}^{2i} &= -\frac{\lambda''_{2jk}\lambda''_{3jk}}{16\pi^2(m_t^2-m_c^2)}g_{uR}m_t^2B_1^{(i)} \\
F_{1jk}^{2j} &= \frac{\lambda''_{2jk}\lambda''_{3jk}}{16\pi^2(m_t^2-m_c^2)}g_{uR}m_c^2B_1^{(j)} \tag{C.5}
\end{aligned}$$

The  $F_3$  form factors are

$$\begin{aligned}
F_{1ik}^{3a} &= -\frac{gZe\lambda'_{i2k}\lambda'_{i3k}}{16\pi^2}m_c\left(C_{12}^{(a)}+C_{23}^{(a)}\right) \\
F_{1ik}^{3b} &= -\frac{\lambda'_{i2k}\lambda'_{i3k}}{16\pi^2}g_{dL}m_c\left(C_{11}^{(b)}+C_{23}^{(b)}\right) \\
F_{1ik}^{3c} &= -\frac{gZd\lambda'_{i2k}\lambda'_{i3k}}{16\pi^2}m_c\left(C_{12}^{(c)}+C_{23}^{(c)}\right) \\
F_{1ik}^{3d} &= -\frac{\lambda'_{i2k}\lambda'_{i3k}}{16\pi^2}g_{eL}m_c\left(C_{11}^{(d)}+C_{23}^{(d)}\right) \\
F_{1jk}^{3g} &= -\frac{gZd\lambda''_{2jk}\lambda''_{3jk}}{16\pi^2}m_t\left(C_{11}^{(g)}-C_{12}^{(g)}+C_{21}^{(g)}-C_{23}^{(g)}\right) \\
F_{1jk}^{3h} &= -\frac{\lambda''_{2jk}\lambda''_{3jk}}{16\pi^2}g_{dL}m_t\left(C_{21}^{(h)}-C_{23}^{(h)}\right) \tag{C.6}
\end{aligned}$$

and, finally the  $F_4$  form factors are

$$\begin{aligned}
F_{1ik}^{4a} &= -\frac{gZe\lambda'_{i2k}\lambda'_{i3k}}{16\pi^2}m_t\left(C_{11}^{(a)}-C_{12}^{(a)}+C_{21}^{(a)}-C_{23}^{(a)}\right) \\
F_{1ik}^{4b} &= \frac{\lambda'_{i2k}\lambda'_{i3k}}{16\pi^2}g_{dR}m_c\left(C_{21}^{(b)}-C_{23}^{(b)}\right) \\
F_{1ik}^{4c} &= -\frac{gZd\lambda'_{i2k}\lambda'_{i3k}}{16\pi^2}m_t\left(C_{11}^{(c)}-C_{12}^{(c)}+C_{21}^{(c)}-C_{23}^{(c)}\right) \\
F_{1ik}^{4d} &= -\frac{\lambda'_{i2k}\lambda'_{i3k}}{16\pi^2}g_{eR}m_t\left(C_{21}^{(d)}-C_{23}^{(d)}\right) \\
F_{1jk}^{4g} &= -\frac{gZd\lambda''_{2jk}\lambda''_{3jk}}{16\pi^2}m_c\left(C_{12}^{(g)}+C_{23}^{(g)}\right) \\
F_{1jk}^{4h} &= -\frac{\lambda''_{2jk}\lambda''_{3jk}}{16\pi^2}g_{dR}m_c\left(C_{11}^{(h)}+C_{23}^{(h)}\right) \tag{C.7}
\end{aligned}$$

where

$$\begin{aligned}
C_X^{(a)} &= C_X(m_k, M_{\tilde{e}_i}, M_{\tilde{e}_i}; m_c, m_t, M_Z) & B_0^{(b)} &= B_0(m_k, m_k; M_Z) \\
C_X^{(b)} &= C_X(M_{\tilde{e}_i}, m_k, m_k; m_c, m_t, M_Z) & B_0^{(d)} &= B_0(m_i, m_i; M_Z) \\
C_X^{(c)} &= C_X(m_i, M_{\tilde{d}_k}, M_{\tilde{d}_k}; m_c, m_t, M_Z) & B_1^{(e)} &= B_1(m_k, M_{\tilde{e}_i}; m_c) \\
C_X^{(d)} &= C_X(M_{\tilde{d}_k}, m_i, m_i; m_c, m_t, M_Z) & B_1^{(f)} &= B_1(m_k, M_{\tilde{e}_i}; m_t) \\
C_X^{(g)} &= C_X(m_i, M_{\tilde{d}_k}, M_{\tilde{d}_k}; m_c, m_t, M_Z) & B_0^{(h)} &= B_0(m_j, m_j; M_Z) \\
C_X^{(h)} &= C_X(M_{\tilde{d}_k}, m_j, m_j; m_c, m_t, M_Z) & B_1^{(i)} &= B_1(m_j, M_{\tilde{d}_k}; m_c) \\
B_1^{(j)} &= B_1(m_j, M_{\tilde{d}_k}; m_t) & & 
\end{aligned} \tag{C.8}$$

and we have defined effective couplings

$$\begin{aligned}
g_{Zd} &= -\frac{\sin^2 \theta_W}{6 \cos \theta_W} & g_{Ze} &= \frac{1 - 2 \sin^2 \theta_W}{2 \cos \theta_W} \\
g_{uL} &= -\frac{1 - 2q_u \sin^2 \theta_W}{2 \cos \theta_W} & g_{uR} &= \frac{q_u \sin^2 \theta_W}{\cos \theta_W} \\
g_{dL} &= \frac{1 + 2q_d \sin^2 \theta_W}{2 \cos \theta_W} & g_{dR} &= \frac{q_d \sin^2 \theta_W}{\cos \theta_W} \\
g_{eL} &= \frac{1 - 2 \sin^2 \theta_W}{2 \cos \theta_W} & g_{eR} &= -\frac{\sin^2 \theta_W}{\cos \theta_W}
\end{aligned} \tag{C.9}$$

It is now a straightforward matter to calculate the total form factors using  $F_{ni} = \sum_{A=a}^j F_{ni}^A$  for  $n = 1, 2, 3, 4$  and substitute the results into Eqn. (A.23) to get the final RPV-MSSM amplitude.

## References

- [1] G. Aad *et al.* [ATLAS Collaboration], Observation of a new particle in the search for the Standard Model Higgs boson with the ATLAS detector at the LHC, Phys. Lett. B **716**, 1 (2012);  
S. Chatrchyan *et al.* [CMS Collaboration], Observation of a new boson at a mass of 125 GeV with the CMS experiment at the LHC, Phys. Lett. B **716**, 30 (2012)
- [2] R. Aaij *et al.*, Observation of  $J/\psi p$  Resonances Consistent with Pentaquark States in  $\Lambda_b^0 \rightarrow J/K^- p$  Decays, [LHCb Collaboration], Phys. Rev. Lett. **115**, 072001 (2015)
- [3] The ATLAS collaboration, Search for resonances decaying to photon pairs in  $3.2 \text{ fb}^{-1}$  of  $pp$  collisions at  $\sqrt{s} = 13 \text{ TeV}$  with the ATLAS detector, ATLAS-CONF-2015-081; CMS Collaboration, Search for new physics in high mass diphoton events in proton-proton collisions at 13TeV, CMS-PAS-EXO-15-004.
- [4] See, for example, D. Castelvecchi in *Nature News*, Hint of new boson at LHC sparks flood of papers, doi: 10.1038/nature.2015.19098, December 2015.
- [5] For a comprehensive discussion, see G. Bertone, J. Silk, B. Moore, J. Diemand, J. Bullock, M. Kaplinghat, L. Strigari and Y. Mellier *et al.*, *Particle Dark Matter: Observations, Models and Searches*, (Cambridge University Press, 2010).
- [6] P. J. E. Peebles and B. Ratra, The cosmological constant and dark energy, Rev. Mod. Phys. **75**, 559 (2003) [astro-ph/0207347].
- [7] K. Greisen, End to the cosmic ray spectrum?, Phys. Rev. Lett. **16**, 748 (1966); G. T. Zatsepin and V. A. Kuzmin, Upper limit of the spectrum of cosmic rays, JETP Lett. **4**, 78 (1966), [Pisma Zh. Eksp. Teor. Fiz. **4**, 114 (1966)].
- [8] D. Speller [SuperCDMS Collaboration], Dark matter direct detection with SuperCDMS Soudan, J. Phys. Conf. Ser. **606**, 012003 (2015);  
R. F. Lang and W. Seidel, Search for Dark Matter with CRESST, New J. Phys. **11**, 105017 (2009); L. Hehn [EDELWEISS Collaboration], The EDELWEISS-III Dark Matter Search: Status and Perspectives, doi:10.3204/DESY-PROC-2014-04/235; H. Kraus *et al.*, EURECA: The European future of cryogenic dark matter searches, J. Phys. Conf. Ser. **39**, 139 (2006).
- [9] D. Y. Akimov *et al.* [ZEPLIN-III Collaboration], Limits on inelastic dark matter from ZEPLIN-III, Phys. Lett. B **692**, 180 (2010);  
D. S. Akerib *et al.* [LUX Collaboration], First results from the LUX dark matter experiment at the Sanford Underground Research Facility, Phys. Rev. Lett. **112**, 091303 (2014);  
X. Xiao *et al.* [PandaX Collaboration], Low-mass dark matter search results from full exposure of the PandaX-I experiment, Phys. Rev. D **92**, 052004 (2015);  
P. Agnes *et al.* [DarkSide Collaboration], First Results from the DarkSide-50 Dark Matter Experiment at Laboratori Nazionali del Gran Sasso, Phys. Lett. B **743**, 456 (2015);

- M. Felizardo *et al.*, Final Analysis and Results of the Phase II SIMPLE Dark Matter Search, Phys. Rev. Lett. **108**, 201302 (2012);  
S. Archambault *et al.* [PICASSO Collaboration], Constraints on Low-Mass WIMP Interactions on  $^{19}\text{F}$  from PICASSO, Phys. Lett. B **711**, 153 (2012).
- [10] M. Ackermann *et al.* [Fermi-LAT Collaboration], Searching for Dark Matter Annihilation from Milky Way Dwarf Spheroidal Galaxies with Six Years of Fermi Large Area Telescope Data, Phys. Rev. Lett. **115**, 231301 (2015);  
AMS Collaboration Collaboration, e. Aguilar, M., First result from the alpha magnetic spectrometer on the international space station: Precision measurement of the positron fraction in primary cosmic rays of 0.5-350 gev, Phys. Rev. Lett. **110** (Apr, 2013) 141102;  
I. Cholis and D. Hooper, Constraining the origin of the rising cosmic ray positron fraction with the boron-to-carbon ratio, Phys. Rev. D **89**, 043013 (2014).
- [11] G. Bertone, D. Hooper and J. Silk, Particle dark matter: Evidence, candidates and constraints, Phys. Rept. **405**, 279 (2005)
- [12] G. Aad *et al.* [ATLAS Collaboration], Summary of the searches for squarks and gluinos using  $\sqrt{s} = 8$  TeV pp collisions with the ATLAS experiment at the LHC, JHEP **1510**, 054 (2015)
- [13] G. Aad *et al.* [ATLAS Collaboration], Search for squarks and gluinos with the ATLAS detector in final states with jets and missing transverse momentum using  $\sqrt{s} = 8$  TeV proton-proton collision data, JHEP **1409**, 176 (2014)
- [14] G. Aad *et al.* [ATLAS Collaboration], Search for direct production of charginos, neutralinos and sleptons in final states with two leptons and missing transverse momentum in  $pp$  collisions at  $\sqrt{s} = 8$  TeV with the ATLAS detector, JHEP **1405**, 071 (2014)
- [15] G. Aad *et al.* [ATLAS Collaboration], Search for direct production of charginos and neutralinos in events with three leptons and missing transverse momentum in  $\sqrt{s} = 8\text{TeV}$   $pp$  collisions with the ATLAS detector, JHEP **1404**, 169 (2014)
- [16] G. Aad *et al.* [ATLAS Collaboration], Search for supersymmetry in events with four or more leptons in  $\sqrt{s} = 8$  TeV pp collisions with the ATLAS detector, Phys. Rev. D **90**, 052001 (2014)
- [17] V. Khachatryan *et al.* [CMS Collaboration], Searches for Supersymmetry using the  $M_{T2}$  Variable in Hadronic Events Produced in pp Collisions at 8 TeV, JHEP **1505**, 078 (2015)
- [18] V. Khachatryan *et al.* [CMS Collaboration], Searches for electroweak production of charginos, neutralinos, and sleptons decaying to leptons and W, Z, an Higgs bosons in pp collisions at 8 TeV, Eur. Phys. J. C **74**, 3036 (2014)
- [19] S. L. Glashow, J. Iliopoulos and L. Maiani, Weak Interactions with Lepton-Hadron Symmetry, Phys. Rev. D **2**, 1285 (1970).

- [20] T. P. Cheng and L. F. Li, Gauge Theory Of Elementary Particle Physics, Oxford, Uk: Clarendon ( 1984) 536 P. ( Oxford Science Publications)
- [21] J. A. Aguilar-Saavedra and B. M. Nobre, Rare top decays  $t \rightarrow c \gamma$ ,  $t \rightarrow c g$  and CKM unitarity, Phys. Lett. B **553**, 251 (2003).
- [22] V. Khachatryan *et al.* [CMS Collaboration], Search for anomalous single top quark production in association with a photon in pp collisions at  $\sqrt{s} = 8$  TeV, JHEP **1604**, 035 (2016).
- [23] K. Agashe *et al.* [Top Quark Working Group Collaboration], arXiv:1311.2028 [hep-ph].
- [24] A. J. Buras, P. Gambino, M. Gorbahn, S. Jager and L. Silvestrini, Universal unitarity triangle and physics beyond the standard model, Phys. Lett. B **500**, 161 (2001); G. D'Ambrosio, G. F. Giudice, G. Isidori and A. Strumia, Minimal flavor violation: An Effective field theory Nucl. Phys. B **645**, 155 (2002).
- [25] G. Passarino and M. J. G. Veltman, One Loop Corrections for  $e^+ e^-$  Annihilation Into  $\mu^+ \mu^-$  in the Weinberg Model, Nucl. Phys. B **160**, 151 (1979).
- [26] K. A. Olive *et al.* [Particle Data Group Collaboration], Review of Particle Physics, Chin. Phys. C **38**, 090001 (2014).
- [27] G. J. van Oldenborgh, FF: A Package to evaluate one loop Feynman diagrams, Comput. Phys. Commun. **66**, 1 (1991).
- [28] See, for example, S. P. Martin, A Supersymmetry primer, Adv. Ser. Direct. High Energy Phys. **21**, 1 (2010) [hep-ph/9709356]; M. Drees, R. Godbole and P. Roy, *Theory and phenomenology of sparticles* (Hackensack, USA: World Scientific, 2004); H. Baer and X. Tata, *Weak scale supersymmetry*, (CUP, Cambridge 2006).
- [29] J. Cao, C. Han, L. Wu, J. M. Yang and M. Zhang, SUSY induced top quark FCNC decay  $t \rightarrow ch$  after Run I of LHC, Eur. Phys. J. C **74**, 3058 (2014)
- [30] A. Djouadi, J. L. Kneur and G. Moultaka, SuSpect: A Fortran code for the supersymmetric and Higgs particle spectrum in the MSSM, Comput. Phys. Commun. **176**, 426 (2007)
- [31] G. Aad *et al.* [ATLAS Collaboration], Search for massive supersymmetric particles decaying to many jets using the ATLAS detector in  $pp$  collisions at  $\sqrt{s} = 8$  TeV, Phys. Rev. D **91**, 112016 (2015).
- [32] F. Mahmoudi, SuperIso v2.3: A Program for calculating flavor physics observables in Supersymmetry, Comput. Phys. Commun. **180**, 1579 (2009).
- [33] R. Aaij *et al.* [LHCb Collaboration], First Evidence for the Decay  $B_s^0 \rightarrow \mu^+ \mu^-$ , Phys. Rev. Lett. **110**, 021801 (2013).



- [34] V. Khachatryan *et al.* [CMS and LHCb Collaborations], Observation of the rare  $B_s^0 \rightarrow \mu^+ \mu^-$  decay from the combined analysis of CMS and LHCb data, *Nature* **522**, 68 (2015).
- [35] J. P. Lees *et al.* [BaBar Collaboration], Exclusive Measurements of  $b \rightarrow s\gamma$  Transition Rate and Photon Energy Spectrum, *Phys. Rev. D* **86**, 052012 (2012)
- [36] D. Ghosh, M. Guchait, S. Raychaudhuri and D. Sengupta, How Constrained is the cMSSM?, *Phys. Rev. D* **86**, 055007 (2012)
- [37] A. Dighe, D. Ghosh, K. M. Patel and S. Raychaudhuri, Testing Times for Supersymmetry: Looking Under the Lamp Post, *Int. J. Mod. Phys. A* **28**, 1350134 (2013)
- [38] J. P. Lees *et al.* [BaBar Collaboration], Evidence of  $B^+ \rightarrow \tau^+ \nu$  decays with hadronic B tags, *Phys. Rev. D* **88**, 031102 (2013)
- [39] B. Bhattacharjee, A. Dighe, D. Ghosh and S. Raychaudhuri, Do new data on  $B^+ \rightarrow \tau^+ \nu_\tau$  decays point to an early discovery of supersymmetry at the LHC?, *Phys. Rev. D* **83**, 094026 (2011)
- [40] F. Ambrosino *et al.* [KLOE Collaboration], Measurement of the absolute branching ratio for the  $K^+ \rightarrow \mu^+ \nu(\gamma)$  decay with the KLOE detector, *Phys. Lett. B* **632**, 76 (2006)
- [41] F. Mahmoudi, Flavour constraints on beyond the Standard Model scenarios, *PoS ICHEP* **2010**, 252 (2010)
- [42] See M. Sher, *Phys. Rept.* **179**, 273 (1989), and references therein, for early work on the subject;  
for more recent work, see J. Ellis, J. R. Espinosa, G. F. Giudice, A. Hoecker and A. Riotto, *Phys. Lett. B* **679**, 369 (2009);  
J. Elias-Miro, J. R. Espinosa, G. F. Giudice, G. Isidori, A. Riotto and A. Strumia, *Phys. Lett. B* **709**, 222 (2012) ;  
G. Degrandi, S. Di Vita, J. Elias-Miro, J. R. Espinosa, G. F. Giudice, G. Isidori and A. Strumia, *JHEP* **1208**, 098 (2012);  
F. Bezrukov, M.Y. Kalmykov, B.A. Kniehl and M. Shaposhnikov, *JHEP* **1210**, 140 (2012);  
M. Holthausen, K.S. Lim and M. Lindner, *JHEP* **1202**, 037 (2012).
- [43] S. Alekhin, A. Djouadi and S. Moch, The top quark and Higgs boson masses and the stability of the electroweak vacuum, *Phys. Lett. B* **716** (2012) 214 [arXiv:1207.0980 [hep-ph]].
- [44] A. Dedes, M. Paraskevas, J. Rosiek, K. Suxho and K. Tamvakis, Rare Top-quark Decays to Higgs boson in MSSM, *JHEP* **1411**, 137 (2014)
- [45] G. Senjanovic, Proton decay and grand unification, *AIP Conf. Proc.* **1200**, 131 (2010)
- [46] C. Macesanu, The Phenomenology of universal extra dimensions at hadron colliders, *Int. J. Mod. Phys. A* **21**, 2259 (2006)

- [47] N. Arkani-Hamed, A. G. Cohen, E. Katz and A. E. Nelson, The Littlest Higgs, JHEP **0207**, 034 (2002);  
T. Han, H. E. Logan, B. McElrath and L. T. Wang, Phenomenology of the little Higgs model, Phys. Rev. D **67**, 095004 (2003);  
M. Perelstein, Little Higgs models and their phenomenology, Prog. Part. Nucl. Phys. **58**, 247 (2007)
- [48] R. Barbier *et al.*, R-parity violating supersymmetry, Phys. Rept. **420**, 1 (2005)
- [49] H. K. Dreiner, An Introduction to explicit R-parity violation, Adv. Ser. Direct. High Energy Phys. **21**, 565 (2010)
- [50] G. Bhattacharyya, R-parity violating supersymmetric Yukawa couplings: A Minireview, Nucl. Phys. Proc. Suppl. **52A**, 83 (1997)
- [51] G. Bhattacharyya, A Brief review of R-parity violating couplings, In \*Tegernsee 1997, Beyond the desert 1997\* 194-201 [hep-ph/9709395].
- [52] C. Csaki, Y. Grossman and B. Heidenreich, MFV SUSY: A Natural Theory for R-Parity Violation, Phys. Rev. D **85**, 095009 (2012)
- [53] Y. Kao and T. Takeuchi, Single-Coupling Bounds on R-parity violating Supersymmetry, an update, arXiv:0910.4980 [hep-ph].
- [54] S. Davidson, M. L. Mangano, S. Perries and V. Sordini, Lepton Flavour Violating top decays at the LHC, Eur. Phys. J. C **75**, 450 (2015).
- [55] G. Eilam, A. Gemintern, T. Han, J. M. Yang and X. Zhang, Top quark rare decay  $t \rightarrow \bar{c} \chi$  in R-parity violating SUSY, Phys. Lett. B **510**, 227 (2001)
- [56] G. Aad *et al.* [ATLAS Collaboration], Search for supersymmetry at  $\sqrt{s}=8$  TeV in final states with jets and two same-sign leptons or three leptons with the ATLAS detector, JHEP **1406**, 035 (2014)
- [57] G. Bhattacharyya, H. V. Klapdor-Kleingrothaus and H. Pas, Neutrino mass and magnetic moment in supersymmetry without R parity in the light of recent data, Phys. Lett. B **463**, 77 (1999);  
S. Rakshit, G. Bhattacharyya and A. Raychaudhuri, R-parity violating trilinear couplings and recent neutrino data, Phys. Rev. D **59**, 091701 (1999).
- [58] G. Aad *et al.* [ATLAS Collaboration], Search for direct third-generation squark pair production in final states with missing transverse momentum and two  $b$ -jets in  $\sqrt{s} = 8$  TeV  $pp$  collisions with the ATLAS detector, JHEP **1310**, 189 (2013).
- [59] G. Aad *et al.* [ATLAS Collaboration], A search for top squarks with R-parity-violating decays to all-hadronic final states with the ATLAS detector in  $\sqrt{s} = 8$  TeV proton-proton collisions, JHEP **1606**, 067 (2016).

- [60] G. Bhattacharyya and D. Choudhury, D and tau decays: Placing new bounds on R-parity violating supersymmetric coupling, *Mod. Phys. Lett. A* **10**, 1699 (1995)
- [61] G. Aad *et al.* [ATLAS Collaboration], Search for a Heavy Neutral Particle Decaying to  $e\mu$ ,  $e\tau$ , or  $\mu\tau$  in  $pp$  Collisions at  $\sqrt{s} = 8$  TeV with the ATLAS Detector, *Phys. Rev. Lett.* **115**, 031801 (2015)
- [62] J. M. Yang, R(b) and R(l) in MSSM without R-parity, *Eur. Phys. J. C* **20**, 553 (2001)
- [63] G. Bhattacharyya, J. R. Ellis and K. Sridhar, New LEP constraints on some supersymmetric Yukawa interactions that violate R-parity, *Mod. Phys. Lett. A* **10**, 1583 (1995)
- [64] B. Brahmachari and P. Roy, Constraints on baryon nonconserving Yukawa couplings in a supersymmetric theory, *Phys. Rev. D* **50**, 39 (1994) [*Phys. Rev. D* **51**, 3974 (1995)]
- [65] M. Sher and J. L. Goity, Bounds on Delta B = 1 couplings in the supersymmetric standard model, [hep-ph/9503472].
- [66] M. Chemtob, Phenomenological constraints on broken R parity symmetry in supersymmetry models, *Prog. Part. Nucl. Phys.* **54**, 71 (2005)
- [67] G. Bhattacharyya, D. Choudhury and K. Sridhar, New LEP bounds on  $B$  violating scalar couplings: R-parity violating supersymmetry or diquarks, *Phys. Lett. B* **355**, 193 (1995)
- [68] CMS Collaboration, Physics Analysis Summary CMS-PAS-HIG-13-034 (2014);  
S. Chatrchyan *et al.* [CMS Collaboration], Search for Flavor-Changing Neutral Currents in Top-Quark Decays  $t \rightarrow Zq$  in  $pp$  Collisions at  $\sqrt{s} = 8$  TeV, *Phys. Rev. Lett.* **112**, 171802 (2014).
- [69] T. J. Gao, T. F. Feng, F. Sun, H. B. Zhang and S. M. Zhao, Top quark decay to a 125 GeV Higgs in the BLMSSM, *Chin. Phys. C* **39**, 073101 (2015)
- [70] J. J. Cao, G. Eilam, M. Frank, K. Hikasa, G. L. Liu, I. Turan and J. M. Yang, SUSY-induced FCNC top-quark processes at the large hadron collider, *Phys. Rev. D* **75**, 075021 (2007)
- [71] B. Mele, Top quark rare decays in the standard model and beyond, hep-ph/0003064.
- [72] S. Bejar, J. Guasch and J. Sola, FCNC top quark decays beyond the standard model, hep-ph/0101294.
- [73] G. Eilam, A. Gemintern, T. Han, J. M. Yang and X. Zhang, Top quark rare decay  $t \rightarrow ch$  in  $R$ -parity violating SUSY, *Phys. Lett. B* **510**, 227 (2001)
- [74] C. x. Yue, H. j. Zong and L. j. Liu, Nonuniversal gauge bosons Z-prime and rare top decays, *Mod. Phys. Lett. A* **18**, 2187 (2003)
- [75] I. Baum, G. Eilam and S. Bar-Shalom, Scalar flavor changing neutral currents and rare top quark decays in a two Higgs doublet model ‘for the top quark’, *Phys. Rev. D* **77**, 113008 (2008)